Non-perturbative solutions to quasi-one-dimensional strongly correlated systems

Submitted for the degree of Doctor of Philosophy

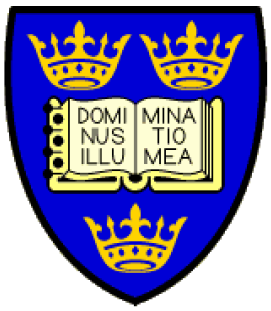

Sam T. Carr

St John's College, University of Oxford

October, 2003

Don't search for the answers, which could not be given to you now, because you would not be able to live them. And the point is, to live everything. Live the questions now. Perhaps then, someday far in the future, you will gradually, without even noticing it, live your way into the answer.

–Rilke

Abstract

In this thesis, we deal with quasi-one-dimensional field theories by which we mean strongly anisotropic higher dimensional models. One way to solve such quasi-one-dimensional models is to split them into a one-dimensional part and a weaker inter-chain perturbation on this. The one-dimensional model can then be solved exactly by techniques such as bosonisation or integrability, and the weak inter-chain part can be treated perturbatively by using the Random Phase Approximation (RPA), or beyond this. This allows us to comment on concepts such as dimensional crossover, and by treating the one-dimensional fluctuations exactly, we access phases not accessible by conventional perturbation theory. In this thesis, we report results for three such models: the first is a model of non-BCS superconductivity where a spin-gap in the one dimensional chains leads to pairing, even for repulsive interactions. We look at the interplay between a superconducting and a charge density wave ground state. The second model is that of a Mott insulator, where we are specifically looking at the effects of a magnetic field on the model. We look at the density of states as the angle of the magnetic field is varied. The third system is the quantum Ising model, a generic model of two-state systems, where we calculate the correlation functions in the ordered phase. All three models are motivated by reference to real materials with a strong structural anisotropy.

Publications

1. **S.T.Carr and A.M.Tsvelik**: *Superconductivity and charge density wave in a quasi-one-dimensional spin gap system*, Phys. Rev. B65, 195121 (2002) [1].

   We consider a model of spin-gapped chains weakly coupled by Josephson and Coulomb interactions. Combining such non-perturbative methods as bosonisation and Bethe ansatz to treat the intra-chain interactions with the Random Phase Approximation for the inter-chain couplings and the first corrections to this, we investigate the phase diagram of this model. The phase diagram shows both charge density wave ordering and superconductivity. These phases are separated by a line of critical points which exhibits an approximate an SU(2) symmetry. We consider the effects of a magnetic field on the system. We apply the theory to the material $Sr_2Ca_{12}Cu_{24}O_{41}$ and suggest further experiments.

2. **S.T.Carr and A.M.Tsvelik**: *Spectrum and correlation functions of a quasi-one-dimensional quantum Ising model*, Phys. Rev. Lett. 90 177206 (2003) [2].

   We consider a model of weakly coupled quantum Ising chains. We describe the phase diagram of such a model and study the dynamical magnetic susceptibility by means of Bethe ansatz and the Random Phase Approximation applied to the inter-chain exchange. We argue that some of the beautiful physics of the quantum Ising chain in a magnetic field survives in the ordered state of the quasi-one-dimensional model and can be observed experimentally by means of neutron scattering.

Acknowledgements

I would like to thank my friend and supervisor Alexei Tsvelik for taking me as a student and unveiling to me the world of physics through his eyes. His intuition in both physical phenomena and mathematical problems as well as his interest in everything under the sun has kept me constantly stimulated throughout my time working with him.

I would also like to thank Ralph Werner, Fabian Essler, Myron Strongin, Tim Kidd, Florian Merz, Nic Shannon and Revaz Ramazashvili for many fruitful discussions as well as all their friendship and support.

The department of theoretical physics, Oxford and department of condensed matter physics, Brookhaven National Laboratory both offered me warm working environments, and for financial support I have to thank both EPSRC and BNL.

Of course, one can't live without friends; and to this end I thank all my friends for keeping me sane during my time as a DPhil student, both in Oxford and New York. In particular David, Laszlo, Zoe, Debbie, Darcy, Ken, Nora, Dan, Alex, Shela, Alison, David, Alison, Joe and Christine.

In times of stress, I could always rely on Mozart to calm me down.

And finally, I have to thank my family: Nancy, Emily, Lemma, mummy and daddy for continuous support and affection. Without you all I wouldn't be here.

Contents

Chapter 1

Introduction

"Begin at the beginning," the King said gravely, "and go on till you come to the end: then stop".

–Lewis Carroll

The topic of strong correlations in condensed matter physics is a fascinating story of mystery and surprise.

To understand strong correlations we must first understand weakly correlated systems, for example Fermi liquid theory [3, 4]. The easiest thing to do as a first approximation in an interacting field theory is to simply ignore the interactions. It turns out in many models of condensed matter physics, this rather drastic looking step is not such a bad thing to do. The effect of 'weak' interactions is merely to renormalize the excitations (quasi-particles) of the non-interacting system. Basically, this means that you map your model of interacting electrons onto a model of free electron like particles, where properties such as mass are a parameter different from the bare (free) electron mass. Because nothing unusual happens, one can calculate these effective parameters from the original theory as a perturbation series; where including more terms gives a more accurate result.

A strongly-correlated system is a system where we can not do this; the interactions change the nature of the ground-state and/or the quantum numbers of the excitation spectrum. It is not possible to obtain the characteristics of the system perturbatively by smoothly switching on the interaction from the free model.

We must then say what it means to 'solve' such a model. This requires in a certain region of parameter space mapping the model onto a weakly-interacting systems, where you can then read off the ground state and excitation spectra and quantum numbers. The residual interactions can be treated perturbatively and do not give any qualitative change to the results. We must stress that in most cases this can only be done in certain localised regions of parameter space. Elsewhere, the spectrum may be (and usually is) completely different.

There are two ways of solving physical problems in condensed matter: a 'top-down' and a 'bottom-up' approach. In the 'bottom-up' approach, one writes down some exact Hamiltonian for the system and then tries to approximately solve it using powerful computation techniques. This is in some sense the most fundamental approach. You start with no assumptions

about your system and you see what you can find out. This can be very satisfying when it gives correct answers for questions such as the band-gap in semiconductors. However, it will often offer very little physical insight into the system. For this, the top-down approach is preferred. You start by looking at your system and making some guess as to what the important physical features of it are. You then construct some simplified Hamiltonian retaining these features which you then hope to be able to solve analytically.

In this thesis, the feature that we concentrate on is a strong structural anisotropy of hopping or interactions meaning that the system is effectively one-dimensional. Our model Hamiltonian is therefore going to be one-dimensional.

There are many interesting features of one dimensional models. Firstly, interaction effects are usually much stronger. This can be understood very naively by simple phase space arguments: two particles in two or more dimensions have to be travelling at a specific angle to 'collide' with each other. In one dimension, merely having different velocities is sufficient to ensure eventual meeting. Secondly, there are a wealth of techniques available to come up with exact solutions of one-dimensional models, so we can accurately say what our model Hamiltonian predicts about the system in question, and then say any discrepancies are due to our model being over-simplified rather than an incorrect or incomplete solution to the model.

Of course, a true one-dimensional model is almost always over-simplified when trying to describe a three dimensional solid. Most importantly, three dimensional crystals show phase transitions, whereas one dimensional ones do not. So for many purposes we need to extend our exactly solvable one-dimensional models to have some weak inter-chain coupling before we can make definite predictions about the system. This is the topic of this thesis.

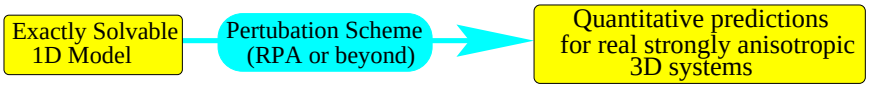

Figure 1.1: An overview of the approach taken in this thesis

In chapter 2 we introduce the mathematical tools available to us in one-dimension. The principle of bosonisation is central to this thesis, so we spend some time discussing this: talking about the Luttinger model, spin-charge separation and gap formation. We then introduce two other techniques that are commonly used to solve one dimensional problems: integrability and conformal field theory. Many results from these techniques will be used, although we derive few new ones so this part of the introduction is meant only to give a flavour and some physical insight into the methods so the reader can understand where the results come from.

In chapter 3, we introduce our first model system: a model of spin-gapped chains weakly coupled together. It turns out that the spin gap promotes superconductivity, we look at the interplay between this ground state and a charge density wave ground state induced by Coulomb interactions between the chains. We then look at the rather interesting effects of a magnetic field on our model of non-BCS superconductivity. Also in this chapter, we introduce our perturbation method to add inter-chain couplings to the one-dimensional solution. Although this

is a perturbation theory, it is not in interaction strength as the one dimensional interactions are treated exactly. In this sense, the method is rather confusingly known as a non-perturbative solution. This allows us to see possibilities not accessible by conventional perturbation theory, and allows us to comment on phenomena such as non-Fermi-liquids and dimensional crossover.

Chapter 4 then goes on to look at a complimentary model, where the one-dimensional chains have a charge-gap rather than a spin-gap, i.e. the chains are Mott Insulators (meaning that the insulating behaviour comes from the electron-electron interactions rather than band structure). It turns out that adding an inter-chain hopping term to this system can drive it to a rather unusual metallic state. The central question in this chapter is what happens to this state in a magnetic field, a question very pertinent to recent experimental results.

Finally, in chapter 5, we look at a quasi-one-dimensional spin-chain model. A large number of interesting results are known about the quantum Ising model in one-dimension, our question here is how robust are some of these results against inter-chain interactions. When we form an ordered phase, it is necessarily three-dimensional, but in this chapter we show that for certain regions of parameter space this ordered phase will show a lot of one dimensional properties, a signature that should be visible in experimental results.

In each chapter, we try to motivate and support the model with reference to real materials to which the model could be at least partially applied. It was the original aim of this work to then fully apply our solutions to these materials to attempt to come up with quantitative predictions about the materials. Unfortunately, the complexity of the materials we talk about in this thesis means that such detailed calculations are outside the scope of this work. However, we believe that a solution of the underlying models is a good starting point for any attempt to accurately describe these materials.

Chapter 2

Techniques in one dimension

> *As far as the laws of mathematics refer to reality, they are not certain, and as far as they are certain, they do not refer to reality.*
>
> –A. Einstein

One dimensional models are the perfect place to explore the effects of strong correlations. Not only are the effects of correlations the strongest, there also exists a wealth of mathematical techniques which facilitate the study of such systems. The three main techniques are as follows:

1. Bosonisation, which comes about from the low energy excitations in a 1D Fermi liquid being limited to the vicinity of the two Fermi points,
2. Exact solutions of integrable models which have the property that the scattering matrix factorises due to strong kinematic constraints in one dimension, and
3. Conformal Field Theory (CFT), which comes from special properties of the conformal group in 1+1D and is useful for critical phenomena.

The first of these points is central to most of the thesis, so we spend some time discussing it. Many results from integrability and CFT will be used although we derive no new ones so we simply give a brief overview of what each of these techniques involves.

2.1 Bosonisation

For one-dimensional field theories of interacting electrons, bosonisation is usually the starting point. We begin by giving some physical intuition why this is a good idea in one dimension, then go on to derive the mathematical relations between an interacting Fermi system and a Bosonic model. This also serves to introduce the notation used throughout much of this thesis.

2.1.1 A heuristic view

In a one dimensional system, the Fermi surface is simply two points. A low energy excitation above the ground state involves taking an electron near one of these points, and exciting it

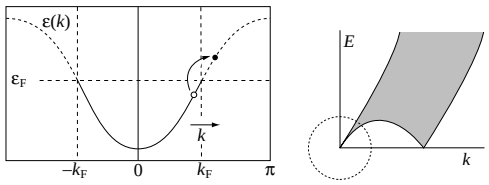

Figure 2.1: Particle/hole excitations in a 1D electron system. Because the Fermi surface is simply two points, the low energy low-momentum excitation spectrum collapses onto a narrow line. The width is related to the curvature of the spectrum at the Fermi-points, so becomes zero if one linearises the spectrum - see the text. After [5].

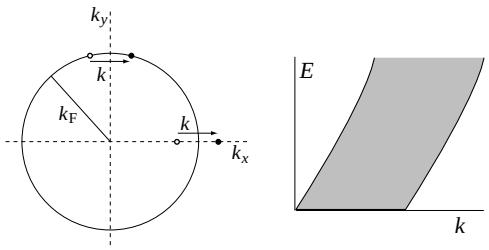

Figure 2.2: Particle-hole excitations in a 2D electron system. k is the momentum in some direction, the full spectrum would be found by rotating the graph about it's origin into the page. Because of the choice of angle for the excitations, there is a continuum of low-energy particle hole excitations, meaning that the particle and hole must be considered as independent excitations. After [5].

to a vacant spot just outside the Fermi surface, leaving a hole. The momentum transfer is $q = k_e - k_h$ and the energy is $\epsilon_q = E_e - E_h$. As shown in figure 2.1, the low energy excitations are then a coherent state of the electron and the hole, and so the excitation can be considered a single bosonic state. In two or three dimensions, there will be a range of ϵ_q to go with any one momentum transfer (figure 2.2), so one must still consider the excitations as independent particles and holes.

The power of bosonisation is that upon adding certain electron-electron (e-e) interactions it turns out that the bosons are robust (naively because the interactions affect the particles and holes in similar ways). Although it is then difficult to say how the excitations are made out of the original electrons, we find they are renormalised bosons rather than renormalised fermions as in Fermi-liquid theory. This is the essence of bosonisation, it is all made rather more concrete in the next section.

As a historical aside, it was realised by Bloch as early as 1934 that hole-electron pairs are bosonic in nature, but it was Tomonaga in 1950 [6] who first showed that these were elementary excitations in one dimension. Luttinger then proposed a one-dimensional model [7] which was solved by a method similar to today's bosonisation procedure by Mattis and Leib [8]. The first modern field-theoretic approach to bosonisation was given by Heidenreich et. al. [9] and gave the solution to the model proposed by Luther and Peschel [10]. Around the same time, the same ideas were being developed starting from the equivalence between the sine-Gordon and massive Thirring models [11, 12]. There are a number of good reviews

of the bosonisation procedure, for example Tsvelik, Nersesyan and Gogolin [13] or Emery [14]. Another good and very complete review is von Delft and Schoeller [15], but the one we follow closest is Senechal [5] who uses the field theory formulation. In this section, we do not attempt to give a proof of the procedure, but merely give the basics with as much physical motivation as possible.

2.1.2 The free boson and the free electron

To show the equivalence between an electronic model and a bosonic model, we first consider the relevant properties of the bosonic Gaussian model defined by the action

$$S = \frac{1}{2}\int d\tau dx \left[\frac{1}{v}(\partial_\tau \Phi)^2 + v(\partial_x \Phi)^2\right], \tag{2.1}$$

where τ is Matsubara time, v is a velocity and Φ is a scaler bosonic field. At $T = 0$, it is relatively simple to show (see eg [16]) that the single particle Green's function is

$$G(z,\bar{z}) = \langle \Phi(z,\bar{z})\Phi(0,0)\rangle = \frac{1}{4\pi}\ln\left(\frac{R^2}{z\bar{z}+a_0^2}\right), \tag{2.2}$$

where $z = x + \mathrm{i}\tau$, R is the system size and a_0 is the lattice spacing which are introduced to regularise the system. Now, defining the correlation functions of bosonic exponents:

$$F(1,2,\ldots,N) = \langle \mathrm{e}^{\mathrm{i}\beta_1\Phi(\xi_1)}\ldots\mathrm{e}^{\mathrm{i}\beta_N\Phi(\xi_N)}\rangle, \tag{2.3}$$

we find that (see [13] for details)

$$F(1,2,\ldots,N) = \prod_{i>j}\left(\frac{z_{ij}\bar{z}_{ij}}{a_0^2}\right)^{\beta_i\beta_j/4\pi}\left(\frac{R}{a_0}\right)^{-(\sum_i\beta_i)^2/4\pi}. \tag{2.4}$$

For an infinite system, $R \to \infty$ and we get the neutrality condition that the correlation function of exponents is only non-zero if

$$\sum_i \beta_i = 0. \tag{2.5}$$

We see that the propagator factorises into independent left and right moving parts, which are functions of z and $\bar{z}$ only respectively. Hence we can define the chiral components of the field

$$\Phi(z,\bar{z}) = \phi(z) + \bar{\phi}(\bar{z}), \tag{2.6}$$

and consider correlation functions of $\mathrm{e}^{\mathrm{i}\beta\phi}$ and $\mathrm{e}^{\mathrm{i}\beta\bar{\phi}}$ separately. We must understand however, that this factorisation is a property of the correlation functions only and not a restriction on Φ in a path integral. We also define the dual field

$$\Theta(z,\bar{z}) = \phi(z) - \bar{\phi}(\bar{z}), \tag{2.7}$$

which satisfies $\partial_z\Phi = \partial_z\Theta$ and $\partial_{\bar{z}}\Phi = -\partial_{\bar{z}}\Theta$, or in other words $\partial_x\Theta = \partial_\tau\Phi$. The equal time commutation relations between the field and the dual field is

$$[\Phi(x), \Theta(x')] = -\mathrm{i}\theta(x - x') \tag{2.8}$$

where the $\theta(x)$ on the right hand side is a step function which demonstrates the non-local relation between Φ and Θ. This leads us naturally to define

$$\Pi(x, \tau) = \partial_x\Theta(x, \tau), \tag{2.9}$$

which is the conjugate momentum to the field Φ satisfying $[\Theta(x), \Phi(x')] = \mathrm{i}\delta(x - x')$.

We now move on to a fermionic model. The continuum Hamiltonian of non-interacting one-dimensional electrons obtained by linearising the spectrum around the two Fermi points (see figure 2.1) is

$$H_F = -\mathrm{i}v_F \int \mathrm{d}x \left(\psi^\dagger\partial_x\psi - \bar{\psi}^\dagger\partial_x\bar{\psi}\right), \tag{2.10}$$

where ψ is the low energy excitations near the right Fermi point, $\bar{\psi}$ is near the left Fermi point and v_F is the Fermi-velocity. The electronic annihilation operator at site x is therefore expanded as

$$\frac{c_x}{\sqrt{a_0}} = \psi(x)e^{\mathrm{i}k_F x} + \bar{\psi}(x)e^{-\mathrm{i}k_F x}. \tag{2.11}$$

Unless the curvature of the spectrum around the Fermi points cannot be ignored, equation 2.10 is a universal model for the low-energy excitations of non-interacting one dimensional fermions. The anti-commutation relations between the fields are

$$\begin{aligned} \left\{\psi(x), \psi^\dagger(x')\right\} &= \delta(x - x'), \\ \left\{\bar{\psi}(x), \bar{\psi}^\dagger(x')\right\} &= \delta(x - x'), \\ \left\{\psi(x), \bar{\psi}^\dagger(x')\right\} &= 0. \end{aligned} \tag{2.12}$$

The propagator is easily calculated

$$\langle\psi^\dagger(z)\psi(z')\rangle = \frac{1}{2\pi}\frac{1}{z - z'} \tag{2.13}$$

The bosonisation gives the equivalence between the two models if

$$\begin{aligned} \psi &= \frac{1}{\sqrt{2\pi}}\mathrm{e}^{-\mathrm{i}\sqrt{4\pi}\phi(z)}, \\ \bar{\psi} &= \frac{1}{\sqrt{2\pi}}\mathrm{e}^{\mathrm{i}\sqrt{4\pi}\bar{\phi}(\bar{z})}, \end{aligned} \tag{2.14}$$

We also define the currents

$$\begin{aligned} J &= \psi^\dagger\psi, \\ \bar{J} &= \bar{\psi}^\dagger\bar{\psi}. \end{aligned} \tag{2.15}$$

	Fermionic representation	Bosonic representation
Action	$\int d\tau dx \left[\psi^\dagger \partial_z \psi + \bar{\psi}^\dagger \partial_{\bar{z}} \bar{\psi}\right]$	$\frac{1}{2}\int d\tau dx \left[\frac{1}{v}(\partial_\tau \Phi)^2 + v(\partial_x \Phi)^2\right]$
Left moving	$\psi(z)$, $\psi^\dagger(z)$	$\frac{1}{\sqrt{2\pi}} \mathrm{e}^{\mp \mathrm{i}\sqrt{4\pi}\phi(z)}$
Right moving	$\bar{\psi}(\bar{z})$, $\bar{\psi}^\dagger(\bar{z})$	$\frac{1}{\sqrt{2\pi}} \mathrm{e}^{\pm \mathrm{i}\sqrt{4\pi}\bar{\phi}(\bar{z})}$
Scattering across FS	$\bar{\psi}^\dagger \psi + \psi^\dagger \bar{\psi}$	$\frac{1}{\pi}\cos\left[\sqrt{4\pi}\Phi(z,\bar{z})\right]$
Left Current	$J = \psi^\dagger \psi$	$\frac{\mathrm{i}}{\sqrt{\pi}}\partial_z \phi$
Right Current	$\bar{J} = \psi^\dagger \psi$	$\frac{-\mathrm{i}}{\sqrt{\pi}}\partial_{\bar{z}} \bar{\phi}$

Table 2.1: A bosonisation dictionary.

Bosonizing these requires a little care. In order to remove divergences from the theory, we must consider the vertex operators $\mathrm{e}^{\mathrm{i}\beta\phi(x)}$ to be normal ordered. The normal ordering then means that to multiply two together, we must use the formula

$$\mathrm{e}^{\mathrm{i}\alpha\phi(z)}\mathrm{e}^{\mathrm{i}\beta\phi(z')} = \mathrm{e}^{\mathrm{i}\alpha\phi(z)+\mathrm{i}\beta\phi(z')}\mathrm{e}^{-\alpha\beta\langle\phi(z)\phi(z')\rangle}, \tag{2.16}$$

which follows from the Baker-Campell-Hausdorff formula. This is explained in detail in [5]. Writing the current as $J = \lim_{\epsilon\to 0}\psi^\dagger(z)\psi(z+\epsilon)$ and using the above formula, one derives the bosonised form of the current operators:

$$\begin{aligned} J &= \frac{\mathrm{i}}{\sqrt{\pi}}\partial_z\phi, \\ \bar{J} &= \frac{-\mathrm{i}}{\sqrt{\pi}}\partial_{\bar{z}}\bar{\phi}. \end{aligned} \tag{2.17}$$

Note that this is not a proof of the equivalence of the two models, merely a demonstration at the level of the correlation functions. For a rigorous proof, see the articles cited in the introduction. Also, at this point, it is not clear why bosonizing the theory is useful. This becomes apparent in the next section when we considering interactions in the one dimensional electron gas. We give a summary of the results of this section in table 2.1.

2.1.3 Spin, interactions and the Luttinger model

When considering real electrons, we add a spin index ψ_σ, $\sigma = \uparrow, \downarrow$. In the bosonisation we must then add additional anti-commuting factors known as Klein factors to ensure the anti-commutation of the different species of fermion. These were introduced into the Bosonisation procedure by Haldane [17, 18]. For many purposes, the Klein factors play very little role, and one can simply project them out, although one must be careful doing so. In this work, it turns out that this is the case so we will not discuss them here.

The boson field may be combined into spin and charge components

$$\begin{aligned} \Phi_c &= \frac{1}{\sqrt{2}}\left(\Phi_\uparrow + \Phi_\downarrow\right), \\ \Phi_s &= \frac{1}{\sqrt{2}}\left(\Phi_\uparrow - \Phi_\downarrow\right). \end{aligned} \tag{2.18}$$

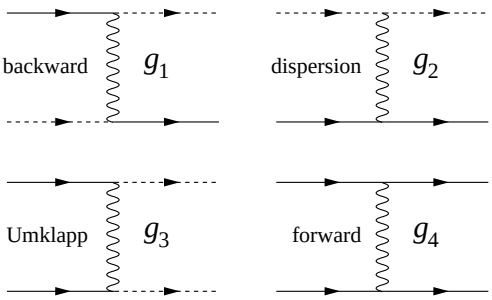

Figure 2.3: The four low energy scattering processes for one dimensional electrons. Continuous lines denote right moving electrons, dashed lines denote left moving electrons. Spin indices are suppressed. After [5]

This will turn out to be a useful parameterisation when we add the interactions. The non-interacting Hamiltonian is simply the sum of the charge and spin sectors $H_0 = H_{c,0} + H_{s,0}$.

In the low energy limit, interactions between electrons are limited to the vicinity of the Fermi points and fall into four different categories - see figure 2.3.

- Back scattering
$$H_1 = v_F g_1 \sum_\sigma \psi^\dagger_\sigma \bar{\psi}_\sigma \bar{\psi}^\dagger_{-\sigma} \psi_{-\sigma}. \tag{2.19}$$

- Dispersion
$$\begin{aligned} H_{2,c} &= v_F g_{2,c} (J_\uparrow + J_\downarrow)(\bar{J}_\uparrow + \bar{J}_\downarrow), \\ H_{2,s} &= v_F g_{2,s} (J_\uparrow - J_\downarrow)(\bar{J}_\uparrow - \bar{J}_\downarrow). \end{aligned} \tag{2.20}$$

- Umklapp (half-filling only because of momentum conservation)
$$H_3 = \frac{1}{2} v_F g_3 \sum_\sigma \psi^\dagger_\sigma \psi^\dagger_{-\sigma} \bar{\psi}_\sigma \bar{\psi}_{-\sigma} + H.C. \tag{2.21}$$

- Forward scattering
$$\begin{aligned} H_{4,c} &= \frac{1}{2} v_F g_{4,c} \left[(J_\uparrow + J_\downarrow)^2 + (\bar{J}_\uparrow + \bar{J}_\downarrow)^2 \right], \\ H_{4,s} &= \frac{1}{2} v_F g_{4,s} \left[(J_\uparrow - J_\downarrow)^2 + (\bar{J}_\uparrow - \bar{J}_\downarrow)^2 \right]. \end{aligned} \tag{2.22}$$

Applying our bosonisation dictionary, 2.1, we will rewrite each of the interactions in terms of the bosonic fields. To begin with, we neglect the scattering across the Fermi points (i.e. the backwards and Umklapp scattering), what we are left with is then known as the Tomonaga-Luttinger model [6, 7]. The beauty of this model is that its bosonised form is still a model of (renormalised) free bosons.

The charge and spin sectors of the interactions decouple, and we can write

$$\mathcal{H}_{\text{T.L.}} = \mathcal{H}_c + \mathcal{H}_s, \tag{2.23}$$

where

$$\begin{aligned}
\mathcal{H}_\mu &= \mathcal{H}_{0,\mu} + \mathcal{H}_{2,\mu} + \mathcal{H}_{4,\mu}, \\
\mathcal{H}_{0,\mu} &= \frac{v_F}{2}\left[\Pi_\mu^2 + (\partial_x \Psi_\mu)^2\right], \\
\mathcal{H}_{2,\mu} &= \frac{-v_F g_{2,\mu}}{2\pi}\left[\Pi_\mu^2 - (\partial_x \Psi_\mu)^2\right], \\
\mathcal{H}_{4,\mu} &= \frac{v_F g_{4,\mu}}{2\pi}\left[\Pi_\mu^2 + (\partial_x \Psi_\mu)^2\right],
\end{aligned} \tag{2.24}$$

with $\mu = \mathrm{c}, \mathrm{s}$. This gives

$$\mathcal{H}_\mu = \frac{v_\mu}{2}\left[K_\mu \Pi_\mu^2 + \frac{1}{K_\mu}(\partial_x \Psi_\mu)^2\right], \tag{2.25}$$

where

$$\begin{aligned}
K_\mu &= \sqrt{\frac{\pi - g_{2,\mu} + g_{4,\mu}}{\pi + g_{2,\mu} + g_{4,\mu}}} \\
v_\mu &= v_F\sqrt{\left(1 + \frac{g_{4,\mu}}{\pi}\right)^2 - \left(\frac{g_{2,\mu}}{\pi}\right)^2}.
\end{aligned} \tag{2.26}$$

The parameter v_μ is the renormalised Fermi velocity and K_μ is called the Luttinger liquid parameter. If the spin sector is to remain SU(2) invariant, we must have $K_s = 1$ as the only term to change this, $g_{2,s}$ is not spin rotation invariant (notice however $g_{4,s}$ is, and this can strongly renormalize the spin velocity). In the charge sector, K_c can take a wide range of values, and this can be seen in experimental systems.

We see that the spin and charge sectors renormalize differently and independently leading to the phenomenon of spin-charge separation. The correlation functions can be obtained by multiplying together the spin and charge components. However, in the presence of interactions across the Fermi surface (i.e. the g_2 term), the left and right bosons become mixed. To show this, we rescale the Hamiltonian 2.25 to put it back into canonical form $\Psi' = \Psi/\sqrt{K}$ which implies the opposite scaling for the conjugate momentum $\Pi' = \Pi\sqrt{K}$. So the left and right parts are not simply rescaled by $\sqrt{K}$, they are mixed:

$$\begin{aligned}
\phi &= \frac{1}{2}(\Psi + \Theta) \to \phi' = \frac{1}{2}\left(\frac{1}{\sqrt{K}}\Psi + \sqrt{K}\Theta\right), \\
\bar{\phi} &= \frac{1}{2}(\Psi - \Theta) \to \bar{\phi}' = \frac{1}{2}\left(\frac{1}{\sqrt{K}}\Psi - \sqrt{K}\Theta\right).
\end{aligned} \tag{2.27}$$

Expressing the old right and left bosons in terms of the new ones gives

$$\begin{aligned}
\phi &= \cosh\xi\ \phi' + \sinh\xi\ \bar{\phi}', \\
\bar{\phi} &= \sinh\xi\ \phi' + \cosh\xi\ \bar{\phi}',
\end{aligned} \tag{2.28}$$

where $K = e^{2\xi}$. This is basically a Bogoliubov transformation in the mode expansion. Hence for example, in the case $K_s = 1$ (spin isotropic system) but $K_c \neq 1$ we have the following expression for the fermionic field operator

$$\begin{aligned}\psi_\uparrow(x,\tau) &= \frac{1}{\sqrt{2\pi}} e^{-\mathrm{i}\sqrt{4\pi}\phi_\uparrow} \\ &= \frac{1}{\sqrt{2\pi}} e^{-\mathrm{i}\sqrt{2\pi}\phi_c} e^{-\mathrm{i}\sqrt{2\pi}\phi_s} \\ &= \frac{1}{\sqrt{2\pi}} e^{-\mathrm{i}\sqrt{2\pi}\cosh\xi\ \phi'_c} e^{-i\sqrt{2\pi}\sinh\xi\ \bar{\phi}'_c} e^{-\mathrm{i}\sqrt{2\pi}\phi_s}. \end{aligned} \tag{2.29}$$

The Luttinger liquid is a critical model with power-law behaviour in correlation functions. The exponents of these power laws depends only on the Luttinger liquid parameter. These correlation functions are easy to write down once we have carried out all the transformations leading to eq. 2.29 because the correlation functions of bosonic exponents are given by 2.4. The propagator for a real electron is of course the sum of our left and right moving parts

$$G_\uparrow(x,\tau) = \langle \psi_\uparrow(x,\tau)\psi^\dagger_\uparrow(0,0)\rangle + \langle \bar{\psi}_\uparrow(x,\tau)\bar{\psi}^\dagger_\uparrow(0,0)\rangle. \tag{2.30}$$

Once more concentrating on the case $K_s = 1$, $K_c \neq 1$, we have

$$\begin{aligned}\langle \psi_\uparrow(x,\tau)\psi^\dagger_\uparrow(0,0)\rangle &= \frac{1}{2\pi}\langle e^{-i\sqrt{2\pi}\cosh\xi\ \phi'_c(z_c)} e^{i\sqrt{2\pi}\cosh\xi\ \phi'_c(0)}\rangle \\ &\quad \times \langle e^{i\sqrt{2\pi}\sinh\xi\ \bar{\phi}'_c(\bar{z}_c)} e^{-i\sqrt{2\pi}\sinh\xi\ \bar{\phi}'_c(0)}\rangle \\ &\quad \times \langle e^{-i\sqrt{2\pi}\phi'_s(z_s)} e^{i\sqrt{2\pi}\phi'_s(0)}\rangle \\ &= \frac{1}{2\pi}\frac{1}{(v_c\tau - ix)^{(1/2)\cosh^2\xi}}\frac{1}{(v_c\tau + ix)^{(1/2)\sinh^2\xi}}\frac{1}{(v_s\tau - ix)^{1/2}} \\ &= \frac{1}{2\pi}\frac{1}{(v_c\tau - ix)^{1/2}}\frac{1}{|v_c\tau - ix|^{\theta_c}}\frac{1}{(v_s\tau - ix)^{1/2}}, \end{aligned} \tag{2.31}$$

where

$$\theta_c = \frac{1}{4}\left(K_c + \frac{1}{K_c} - 2\right). \tag{2.32}$$

Similarly, the left moving sector:

$$\langle \bar{\psi}_\uparrow(x,\tau)\bar{\psi}^\dagger_\uparrow(0,0)\rangle = \frac{1}{2\pi}\frac{1}{(v_c\tau + ix)^{1/2}}\frac{1}{|v_c\tau + ix|^{\theta_c}}\frac{1}{(v_s\tau + ix)^{1/2}}. \tag{2.33}$$

The exponent θ_c turns out to be a very useful parameterisation of K_c, $\theta_c = 0$ corresponds to the non-interacting system $K_c = 1$. Also, by Fourier transforming equation 2.31 (see eg [13]), we see that the single particle density of states behaves as

$$\rho(\omega) \sim |\omega|^{\theta_c}. \tag{2.34}$$

Similarly, the momentum distribution function at the Fermi level

$$n(k) = n(k_F) - \alpha\ \mathrm{sgn}(k - k_F)|k - k_F|^{\theta_c}, \tag{2.35}$$

where α is some constant. In a similar manner, spin-spin and density-density correlation functions can be calculated in this model [5].

Notice that in deriving the Luttinger model, we said very little about the underlying microscopic Hamiltonian. The exact model chosen will put restrictions on the value of the parameters K_s and K_c, but the Luttinger model is universal for many microscopic models. However, the model itself is unstable to many perturbations: for example Umklapp or backwards scattering as we will see in the following section, or some interchain coupling as we will see in section 2.4.

2.1.4 The sine-Gordon model and gap formation

We now go on to bosonise the Umklapp and backwards scattering interactions of figure 2.3. This gives rise to cosine terms in the Hamiltonian which leads to the sine-Gordon model and gap formation. In the spin sector, this can come about for many reasons from the g_1 term. In the charge sector, it requires commensurate filling to have the Umklapp processes. The model still has full spin-charge separation:

$$G(x,\tau) = G_{\text{spin}}(x,\tau)G_{\text{charge}}(x,\tau). \tag{2.36}$$

However, now one or both of $G_{\text{spin,charge}}$ has a gap. If one of the sectors is gapped and the other is critical, then the model is known as the Luther-Emery liquid [19].

In this section, we concentrate on one sector only, and assume it is gapped. The bosonised action in terms of the canonical bosons is

$$S = \frac{1}{2}\int d^2x \left(\partial_\mu \Phi(x)\right)^2 + V\cos\left(\sqrt{8\Pi K}\phi(x)\right). \tag{2.37}$$

where V depends on the g_1 and g_3 terms.

In the sine-Gordon model, the combination $\sqrt{8\pi K}$ is usually written as β and the properties of the model depend very strongly on the value of this β. The sine-Gordon model is integrable for all values of β, hence many exact results are known about it. A number of these are mentioned in section 3.3.3. Many correlation functions are also known, for a full review see [20]. Here, we review the simply state the basic properties of the model. If $\beta^2 > 8\pi$, then it can be shown that the cosine term is irrelevant in an RG sense, however if $\beta^2 < 8\pi$, i.e. $K < 1$ then the model has a gap.

It was shown by Sydney Coleman [11] that model 2.37 can be refermionised as the massive Thirring model

$$\mathcal{H} = i\tilde{v}[\bar{\Psi}^\dagger\partial_x\bar{\Psi} - \Psi^\dagger\partial_x\Psi] + \tilde{\Delta}[\Psi^\dagger\bar{\Psi} + \text{H.c.}] + \tilde{g}\Psi^\dagger\bar{\Psi}^\dagger\bar{\Psi}\Psi, \tag{2.38}$$

where

$$\tilde{v} \;=\; v\left(\frac{1}{4K} + K\right)\;,$$

$$\begin{aligned} \tilde{\Delta} &= \frac{\pi V}{\Lambda}\,, \\ \tilde{g} &= 2\pi v\left(\frac{1}{4K}-K\right)\,. \end{aligned} \tag{2.39}$$

It is very strange indeed that our original interacting *massless* fermions got rewritten first as a bosonic model, then as a model of interacting *massive* fermions.

We see that at the special point $K = 1/2$ i.e. $\beta = \sqrt{4\pi}$ known as the Luther-Emery point, the refermionised model is non-interacting. The relationship between these fermions and the original electrons is very difficult to describe, as we are a) dealing with only one sector of excitations, and b) $K = 1/2$ is a very strongly interacting model; these fermions can be thought of as solitonic excitations of either spin or charge. Once we are away from $K = 1/2$, the fermions are interacting: if $K > 1/2$ the lowest energy excitations are still the solitons however if $K < 1/2$, we have bound states of solitons known as breathers which have a lower energy than the solitons themselves.

2.2 Integrability

Not all one-dimensional models are integrable, but many of the most important are and it is the methods of exact solution of integrable models that perhaps give the most insight into strongly correlated systems, giving solutions unaccessible by conventional perturbation theory.

The basic idea behind integrability is the reduction of the problem to two body dynamics. This is through the factorisation of the scattering matrix, the scattering of N particles can be written as a product of $N(N-1)/2$ two-particle scattering so long as the outcome does not depend on the order in which the particles scatter. This is encompassed within the Yang-Baxter equations (for a review see [21, 22]). It turns out that dynamical systems with such factorisable S-matrices have as a common feature an infinite set of conservation laws. This is rigorously shown in [23]. One can imagine this connection in one-dimension by simply considering the scattering of two identical particles. Energy and momentum conservation imply in one dimension that the incoming two momenta and the outgoing two momenta be identical. This means that the only possible solutions of the equations $p_1 + p_2 = p_1' + p_2'$ and $p_1^2 + p_2^2 = {p'}_1^2 + {p'}_2^2$ is $p_1 = p_1',\ p_2 = p_2'$ or $p_1 = p_2',\ p_2 = p_1'$. In both these cases, we discover we have not only conservation of energy and momentum but conservation of all powers of momenta $p_1^n + p_2^n = {p'}_1^n + {p'}_2^n$. This then raises the obvious question of why aren't all one dimensional models integrable? The answer is that the particles also have internal degrees of freedom, and these internal quantum numbers must also have factorised scattering for the model to be integrable.

The method of building up the S-Matrix from the Yang-Baxter equations is sometimes known as the Quantum Bootstrap approach. Historically, the first way to attack integrable systems was the Coordinate Bethe Ansatz which was first applied to the XXX Heisenberg chain in 1931 [24]. Here, one can write down the exact form of the many-body wave function because of certain factorisation properties from the infinite set of conservation laws. From this

wave-function, one can calculate physical properties of the system. A third method is based on the algebraic structure of the factorisation equations and is known as the Algebraic Bethe Ansatz, or the Quantum Inverse Scattering Method. This is fully reviewed in [25]. All of these methods are equivalent, although each have their advantages and disadvantages in terms of calculation techniques.

2.2.1 The S-matrix

The S-matrix is the heart of an integrable model. It is represented pictorially as

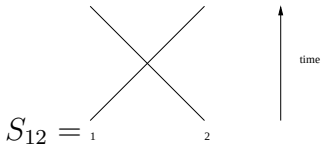

We will mostly be dealing with theories with Lorentz invariance, so we parameterise the energy and momentum by the rapidity θ:

$$\begin{aligned} E &= m\cosh\theta, \\ p &= m\sinh\theta, \end{aligned} \tag{2.40}$$

so scattering between two particles is simply a function of $\theta_{12} = \theta_1 - \theta_2$. We also note here that $\theta \to \theta + \mathrm{i}\pi$ changes $E \to -E$, $p \to p$ so this can be considered as changing a particle into its antiparticle.

The Yang-Baxter factorisation equations are the most important property of the integrable model. They can be represented pictorially as

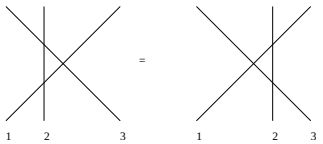

$$S_{12}(\theta_{12})S_{13}(\theta_{13})S_{23}(\theta_{23}) = S_{23}(\theta_{23})S_{13}(\theta_{13})S_{12}(\theta_{12}). \tag{2.41}$$

Basically what this is saying is that if three particles scatter off each other, it doesn't matter which order they do so in.

For a well defined theory, the S-matrix must be unitary:

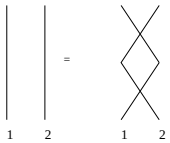

$$1 = S_{12}(\theta_{12})S_{21}(\theta_{21}). \tag{2.42}$$

These conditions are also true for non-relativistic theories if we parameterise the scattering by the momentum transfer rather than the rapidity. The final condition, crossing-symmetry is a purely relativistic effect, which is represented as

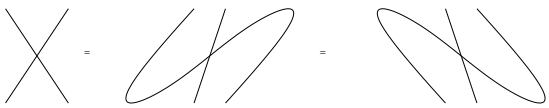

$$S_{12}(\theta_{12}) = S_{\bar{2}1}(\theta_{21} + i\pi) = S_{2\bar{1}}(\theta_{21} - i\pi). \tag{2.43}$$

There are also a number of properties relating to the formation of bound states. A bound state shows up as a pole in the S-matrix, which means that if there are no bound states, then the S-matrix must have no poles in the physical sheet (i.e. $0 < \mathrm{Im}\theta < \pi$. For more information on the bound states, see for example [26].

These properties are enough to exactly determine the S-matrix, which can then be used to determine many observable properties of the system. We give only one extremely simple example which will be used later in this thesis, for the one dimensional Quantum Ising Model (section 5.1).

$$\mathcal{H} = -J \sum_n \left\{ \sigma_n^z \sigma_{n+1}^z + (1+g)\sigma_n^x \right\}. \tag{2.44}$$

In this case, the Jordan-Wigner transformation reduces the model to free fermions. Hence the asymptotic states are free fermions so the scattering matrix is trivial:

$$S = -1. \tag{2.45}$$

2.2.2 Form-factors and correlation functions

Form factors are off-shell scattering amplitudes

$$F^{\mathcal{O}}_{\epsilon_1 \ldots \epsilon_n}(\theta_1, \ldots, \theta_n) = \langle 0|\mathcal{O}|\theta_1, \ldots \theta_n\rangle_{\epsilon_1 \ldots \epsilon_n}, \tag{2.46}$$

where θ_n are the rapidities of some excitations in the system and ϵ_n denotes other internal quantum numbers. These are simply matrix elements of the operator $\mathcal{O}$ with various excited states, however the expression 2.46 is limited to integrable models for the following reason. If one doesn't have factorised scattering, then multi-particle excitations can not be simply written in terms of the rapidities of each excitations, this is an incomplete parameterisation of the state.

The form factors can be calculated in a bootstrap approach similar to the S-matrix [20, 27, 28, 26]. Again the equations come about as consequences of the factorisation of the S-matrix. Firstly, the end result of annihilating the excitations by the operator $\mathcal{O}$ must be the same as if two of them scatter first. This is known as Watson's equation, and can be represented pictorially as:

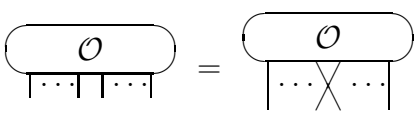

(2.47)

$$F^{\mathcal{O}}_{\ldots ij \ldots}(\ldots, \theta_i, \theta_j, \ldots) = F^{\mathcal{O}}_{\ldots ji \ldots}(\ldots, \theta_j, \theta_i, \ldots)\, S_{ij}(\theta_i - \theta_j). \tag{2.48}$$

Changing particles to anti-particles, we get conditions known as crossing relations which can be represented:

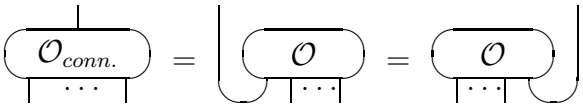

(2.49)

$$
\begin{aligned}
{}_{\bar{\epsilon}_1}\langle\,\theta_1\,|\,\mathcal{O}(0)\,|\,p_2,\ldots,p_n\,\rangle^{in,conn.}_{\epsilon_2\ldots\epsilon_n} &= F^{\mathcal{O}}_{\epsilon_1\epsilon_2\ldots\epsilon_n}(\theta_1+i\pi,\theta_2,\ldots,\theta_n) && (2.50)\\
&= F^{\mathcal{O}}_{\epsilon_2\ldots\epsilon_n\epsilon_1}(\theta_2,\ldots,\theta_n,\theta_1-i\pi). && (2.51)
\end{aligned}
$$

Finally, we can relate form-factors with different numbers of excitations by a recursion relation:

$$\frac{1}{2i}\,\mathrm{Res}_{\theta_{12}=i\pi}$$

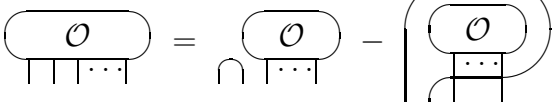

(2.52)

$$\mathrm{Res}_{\theta_{12}=i\pi}F^{\mathcal{O}}_{1\ldots n}(\theta_1,\ldots) = 2i\,\mathbf{C}_{12}\;F^{\mathcal{O}}_{3\ldots n}(\theta_3,\ldots)\,(\mathbf{1}-S_{2n}\ldots S_{23})\,, \qquad (2.53)$$

where $\mathbf{C}_{12}$ is the charge conjugation matrix with elements $C_{\alpha\alpha'}=\delta_{\bar{\alpha}\alpha'}$ which basically ensures charge conservation in the above expression. In words, what this expression is saying is that the particles all being annihilated by the operator $\mathcal{O}$ is equivalent to two of them annihilating each other and the rest being annihilated by $\mathcal{O}$.

Again, there are also a number of relations dealing with bound states which we don't mention here. This set of equations were proposed by Smirnov [20] as generalisations of those in the original articles [29, 30]. After solving these equations, one has to associate which local operators in the original theory correspond to which solution. This is typically done by looking at a perturbation expansion and matching it up to the exact solution.

Using our Ising model example 2.44 with $S=-1$, the above formula's reduce to

$$
\begin{aligned}
F^{(n)}(\theta_2,\theta_1,\theta_3,\ldots,\theta_n) &= -F^{(n)}(\theta_1,\theta_2,\theta_3,\ldots,\theta_n),\\
F^{(n)}(\theta_1-2\mathrm{i}\pi,\theta_2,\ldots,\theta_n) &= F^{(n)}(\theta_1,\theta_2,\ldots,\theta_n),\\
\mathrm{Res}_{\theta_{12}=i\pi}F^{(n)}(\theta_1,\theta_2,\theta_3,\ldots,\theta_n) &= -2F^{(n-2)}(\theta_3,\ldots,\theta_n). \qquad (2.54)
\end{aligned}
$$

Looking at the first two, with the additional requirement that there is no bound state so aside from $\theta_{12}=\mathrm{i}\pi$ (there must be no other poles in the physical sheet $0\le\Im\theta\le\pi$ because there are no bound states), we see that the minimal solution for the two particle form-factor is

$$F(\theta_1,\theta_2)=\tanh\left(\frac{\theta_1-\theta_2}{2}\right). \qquad (2.55)$$

Using the third equation in 2.54 we can build up all the rest of the form factors

$$F^{(n)}(\theta_1,\ldots,\theta_n)=\prod_{i<j}\tanh\left(\frac{\theta_i-\theta_j}{2}\right). \qquad (2.56)$$

It turns out that if n is odd these relate to the spin field and if n is even they relate to the disorder field - see section 5.1

Correlation functions can be calculated in terms of the form factors. This is obtained by inserting a complete set of states:

$$\begin{aligned}\chi^{\mathcal{O}} &= \langle 0|\mathcal{O}(x,t)\mathcal{O}|0\rangle \\ &= \sum_n \frac{1}{n!}\int_{-\infty}^{\infty}\prod_{i=1}^{n}\frac{d\theta_i}{2\pi}\langle 0|\mathcal{O}(x,t)|\theta_1,\ldots,\theta_n\rangle\langle\theta_1,\ldots,\theta_n|\mathcal{O}|0\rangle \\ &= \sum_n \frac{1}{n!}\int_{-\infty}^{\infty}\prod_{i=1}^{n}\frac{d\theta_i}{2\pi}e^{-\mathrm{i}[mt\cosh\theta_i - mx\sinh\theta_i]}|F_{\epsilon_1\ldots\epsilon_n}(\theta_1,\ldots,\theta_n)|^2. \qquad (2.57)\end{aligned}$$

For low-energy excitations in a massive field theory, retaining only the first couple of terms in the expansion can be a very good approximation. There is a similar method that can give finite temperature correlation functions - see [31].

The Fourier transform of the retarded correlation function gives us

$$\begin{aligned}\chi(\omega,k) &= \sum_n \frac{1}{n!}\int_{-\infty}^{\infty}\prod_{i=1}^{n}\frac{d\theta_i}{2\pi}\left\{\frac{\delta(k-m\sum\sinh\theta_j)}{\omega-m\sum\cosh\theta_j+\mathrm{i}\epsilon}-\frac{\delta(k+m\sum\sinh\theta_j)}{\omega+m\sum\cosh\theta_j+\mathrm{i}\epsilon}\right\} \\ &\times |F_{\epsilon_1\ldots\epsilon_n}(\theta_1,\ldots,\theta_n)|^2. \qquad (2.58)\end{aligned}$$

The imaginary part gives the structure factor.

$$\begin{aligned}A(\omega,k) &= \sum_n \frac{1}{n!}\int_{-\infty}^{\infty}\prod_{i=1}^{n}\frac{d\theta_i}{2\pi}\delta(\omega-m\sum_{i=1}^{n}\cosh\theta_i)\delta(k-m\sum_{i=1}^{n}\sinh\theta_i) \\ &\times |F_{\epsilon_1\ldots\epsilon_n}(\theta_1,\ldots,\theta_n)|^2. \qquad (2.59)\end{aligned}$$

The structure factor is a very nice thing to calculate in this way because it turns out if you terminate the expansion after N terms, the expression is exact up to energies $\omega = Nm$[1], and furthermore, the structure factor is directly related to what is measured in the experimental probe Angular Resolved Photoemission Spectroscopy (ARPES).

This ends our brief summary of integrable systems. Basically, the main points are that strong kinematic constraints in one dimension mean that for many models you get factorisation of the S matrix, which can lead to an exact solution of the model. This allows you to calculate many things of physical interest such as thermodynamics or correlation functions.

2.3 Conformal Field Theory

Although conformal field theory will not play a big role in this thesis, some results will be used so we feel it useful to review the basic idea here. For a generic model at arbitrary temperature, there will be at least two length scales in a system, the lattice spacing a_0 and the correlation length ξ. The presence of these lengths means that there is no symmetry of the model under

[1]This can be seen by noting that the minimum value of $m\sum_{i=1}^{n}\cosh\theta_i$ is nm when all the $\theta_i = 0$, and so if ω is less than this, the delta function in equation 2.59 can never be satisfied.

scale transformations. However, at certain critical points (i.e. near a phase transition), ξ can get very large so when looking at correlations on length scales between a_0 and ξ, the system will have an (approximate) scale invariance. In a system with local interactions, an immediate extension to this would be that the system also has a local scale invariance [32], i.e. conformal transformations[2]. Such symmetries occur in all dimensions, however it turns out that only in two dimensions does conformal symmetry alone put huge restrictions on the correlation functions due to a peculiarity of the conformal group in two dimensions.

The group of conformal transformations is a finite group, requiring $d(d+1)/2$ parameters in a $d+1$ dimensional field theory, so it puts relatively few constraints on the form of the correlation functions. The exception is in $1+1$ dimensions where the expression is only for conformal transformations that are well defined everywhere. There are an infinite number of conformal transformations (i.e. any analytic function) that are still equivalent to local dilations, although not regular everywhere. This provides a very powerful tool for calculating correlation functions in a wide class of critical theories in $1+1$ dimensions.

Conformal field theory has grown into a field of its own since the 1984 seminal paper by Belavin, Polyakov and Zamolodchikov [33]. For reviews of the field see [34, 35]. For the purposes of this thesis, we will derive only one result, the correlation functions of bosonic exponents on a torus which is equivalent to the finite temperature correlation functions of a Luttinger liquid.

The analytic function

$$z(\xi) = \sinh(\pi\xi/L) \tag{2.60}$$

transforms the infinite complex plane into a strip of width L in the τ-direction. This therefore maps $T=0$ correlation functions onto finite T correlation functions, where $L = 1/T$. Hence within the Gaussian model 2.1, the zero-temperature correlation function

$$\langle e^{-\mathrm{i}\beta\Phi(x,t)} e^{\mathrm{i}\beta\Phi(0,0)} \rangle = \frac{1}{z^d}\frac{1}{\bar{z}^d} \tag{2.61}$$

will become at finite temperature

$$\langle e^{-\mathrm{i}\beta\Phi(x,t)} e^{\mathrm{i}\beta\Phi(0,0)} \rangle = \left\{ \frac{\pi T}{\sinh[\pi T(x-vt)]} \right\}^d \left\{ \frac{\pi T}{\sinh[\pi T(x+vt)]} \right\}^d \tag{2.62}$$

where $d = \beta^2/8\pi$. This can be Fourier transformed to give

$$\begin{aligned} \chi^{(0)}(q) &= \frac{2}{\Lambda^2} \sin \pi d \left(\frac{2\pi T}{\Lambda} \right)^{-2+2d} \Gamma^2(1-d) \\ &\times \frac{\Gamma(d/2 + i(\omega+vq)/4\pi T)}{\Gamma(1-d/2+i(\omega+vq)/4\pi T)} \frac{\Gamma(d/2+i(\omega-vq)/4\pi T)}{\Gamma(1-d/2+i(\omega-vq)/4\pi T)}, \end{aligned} \tag{2.63}$$

where Λ is the ultra-violet cutoff.

[2] A conformal transformation is a transformation which permits local scale changes and local rotations so long as angles are preserved everywhere.

2.4 From one dimension to quasi one dimension

When considering strongly anisotropic materials, treating them first as strictly one dimensional systems should be a good starting point. However it cannot be the end of the story. True one dimensional systems do not exhibit phase transitions into states with broken symmetry. This was first addressed in 1975 [36] for the case of coupled classical Ising chains. The authors treated the inter-chain interaction in the mean-field and looked for fluctuations around it, a procedure which has since become known as the Random Phase Approximation (RPA). It is only recently that attempts to go beyond this level of approximation have come into the literature [37, 38, 39], showing that the somewhat unjustified looking RPA is in fact the first term in a more general expansion, and that in most of the cases investigated the corrections to this are small.

We postpone a discussion of the RPA and beyond to section 3.3.2 where we can make the derivation more concrete for the particular model we are dealing with. For now, we simply give some brief scaling arguments about what can happen when we add interchain coupling to a one-dimensional model, and when we expect to be able to use perturbation theory.

Consider adding weak interchain electron hopping between Luttinger liquids.

$$\mathcal{H} = \sum_i \mathcal{H}^i_{LL} + \sum_{i,j} \int dx d\tau t_\perp (i-j) \psi^\dagger_i(x) \psi_j(x) \tag{2.64}$$

At large distances, the Green's function of the Luttinger liquid behaves as $|x|^{-1-\alpha}$. Hence each term in the perturbation expansion in $t_\perp$ will have a factor $\omega_\parallel^{\alpha-1}$ which diverges for $\alpha < 1$. We can therefore define a new energy scale $t_{\text{eff}} = t_\perp^{1/(1-\alpha)}$. This characterises for example the crossover temperature above which the effects of $t_\perp$ are covered by temperature and the system behaves as a Luttinger liquid. At temperatures lower than this, the interchain coupling is a strongly relevant operator and will change the ground state, either to a Fermi liquid[3], superconductor, CDW or whatever depending on the nature of the interactions. At these low temperatures, we would be extremely wary of a perturbation expansion in $t_\perp$ about the Luttinger liquid. However, if we consider a one-dimensional model with either a spin or charge gap, the long distance asymptotics in one dimension fall off exponentially and we would expect a perturbation expansion in $t_\perp$ to work well. These are the cases we consider in the following chapters.

[3]It was pointed out by Anderson [40] that in some cases though, one has to be careful applying scaling arguments, and the LL fixed point can sometimes be stable in two dimensions.

Chapter 3

Superconductors

My definition of an intellectual is someone who can listen to the William Tell Overture without thinking of the Lone Ranger.

–Billy Connolly

3.1 Physical motivation

Since the discovery in 1986 of the so called High Temperature superconductors [41] there has been a lot of interest from theorists for non-BCS theories of superconductivity. One of the more interesting models involves a quasi-one dimensional system. The application of such theories to the High-T_c materials is a separate discussion in itself, as these materials have CuO_2 planes which are structurally two-dimensional. However, there is much theoretical and experimental evidence [42] that there are 'stripe' correlations over a wide range of temperatures which make the low-energy electron dynamics in these planes locally one-dimensional. Although a discussion of stripes is beyond the scope of this thesis, this quasi-one dimensional non-BCS model is interesting in its own right as there are many structurally one-dimensional materials such as the Bechgaard salts (organic superconductors).

In certain temperature regimes, the one-dimensional chains are Luttinger liquids so we have spin-charge separation (see section 2.1.3) and we suppose that there is a gap in the spin sector. Single particle hopping between chains must necessarily involve real electrons which are some bound state of both spin and charge excitations. Which means that single particle hopping is strongly suppressed because it requires energies greater than the spin gap, and so the most relevant inter-chain interaction is pair-hopping where we have a pair consisting of both an up and down spin, so it has no net spin. Having these 'pre-formed' pairs is obviously a good start for superconductivity, and it certainly creates an interesting and furthermore solvable example of a non-BCS like transition where the temperature for formation of pairs and that of condensation are not identical. One has to be very careful about the term 'pre-formed pair' however, as you have to remember the excitations with good quantum numbers on the individual chains themselves are still spin-charge separated.

Here we discuss a simple model of a non-BCS superconductor, where the formation of

superconducting pairs on one-dimensional chains is triggered by the formation of a spin gap. The three-dimensional coherence is established through the inter-chain Josephson coupling. This competes with the Coulomb interaction between the chains, which can destroy the superconductivity and establish Charge Density Wave (CDW) ordering. We first introduce our low energy effective model by deriving it from a model of coupled spin-gapped chains - basically what we do is integrate out the spin degrees of freedom. We show that there is a critical line with enhanced symmetry between the two ordered phases, and go on to calculate the critical temperature by combining exact results on the chains with the Random Phase Approximation (RPA) to deal with inter-chain interactions. We also consider the effect of a magnetic field on the phase diagram, which shows some rather interesting behaviour. We calculate corrections to the RPA, and show that they are numerically small for estimating the transition temperature but can help give us more insight into the interplay between the two different ordered states near the critical line. We then show how the single particle spectral function evolves as you go through the phase transition, and discuss how properties of the solution may manifest themselves in experimentally observable features. Finally, we introduce a couple of quasi-one-dimensional spin gapped materials that may lend themselves to such a treatment, although the complexity of these materials means that a detailed application of the theory to the materials is outside the scope of this thesis.

The model we use has been considered in some detail [43] in the context of high-T_c superconductivity. It was assumed that the one-dimensional behaviour came about from the formation of stripes [42]. Since in some stripe pictures, fluctuations of the stripes dephase the CDW coupling [44], only the superconducting inter-chain interaction was considered in [42]. However, more recently [45] the model 3.14 has been considered a good description of a 'caricature of a stripe ordered state' in the Hubbard model. In this chapter, we consider the model as a description of materials that are structurally quasi-one-dimensional, although it is worth remembering that there may be many features of the solution that are relevant for the high-T_c materials also. The scaling properties of the solution have been known as early as 1975 [46] and discussed many times since. However the prefactors, the interplay between the SC and CDW phases, the effects of the magnetic field and the corrections to RPA were all new work in our paper [1].

3.2 The model

The pure one-dimensional part of the Hamiltonian density can be written in its Bosonised form (section 2.1):

$$\mathcal{H}_{\text{chain}} = \mathcal{H}_{\text{charge}} + \mathcal{H}_{\text{spin}}, \tag{3.1}$$

$$\mathcal{H}_\alpha = \frac{v_\alpha}{2}[K_\alpha(\partial_x\Theta_\alpha)^2 + K_\alpha^{-1}(\partial_x\Phi_\alpha)^2] - V_\alpha\cos(\sqrt{8\pi}\Phi_\alpha), \tag{3.2}$$

where $\alpha =$ spin, charge and $[\Theta(x), \Phi(y)] = \mathrm{i}\theta(x-y)$.

We suppose the one dimensional electron gas is sufficiently incommensurate that there is no Umklapp scattering so $V_{\rm charge} = 0$. However, we want to look specifically at the case where a spin-gap Δ_s is present, which means that $V_{\rm spin} \neq 0$ and $K_s \leq 1$. Now, if we are at the SU(2) symmetric point, the sign of $V_{\rm spin}$ is fixed to be positive, and may come, for example from next-nearest neighbour exchange. Ryzhkov and Millis considered another possibility of spin gap formation in a single chain. In their scenario the gap is generated by an Ising anisotropy in the spin sector. In this case $V_{\rm spin}$ is negative. The spectrum of the model is independent of the sign of $V_{\rm spin}$, but the vacuum configuration of $\phi_{\rm spin}$ changes and therefore different operators acquire finite amplitudes. In the case of SU(2) symmetry, the operators which acquire finite amplitudes and whose correlations are enhanced are the singlet superconducting (SSC) and CDW order parameters respectively. However, with the Ising anisotropy, the corresponding operators are the z-component of triplet superconductivity (TSC) and the z-component of Spin Density Wave (SDW). Note that in the latter case, the order parameters will also have Ising anisotropy. In this work, we will not worry too much about the microscopic origins of the spin gap, and will limit ourselves to the case where we are looking at the interplay between SSC and CDW. The alternative case, TSC to SDW was worked out in [47], and we will refer to some of the similarities and differences throughout this chapter.

The spin gap blocks single-particle tunnelling processes between the chains at low energies. Then the virtual multi-particle processes generate pair hopping so the most relevant interchain interaction comes from the Josephson coupling of the superconducting order parameters and the Coulomb backscattering

$$\mathcal{H}_{\rm inter} = V\rho_n^{2k_F}\rho_m^{-2k_F} + J\Delta_n\Delta_m^\dagger, \tag{3.3}$$

where the subscripts refer to chain number. Using our bosonisation dictionary, table 2.1, we see that

$$\begin{aligned}\rho &= \sum_\sigma \left\{\psi_\sigma^\dagger\psi_\sigma + \bar\psi_\sigma^\dagger\bar\psi_\sigma + e^{-2{\rm i}k_F}\left(\bar\psi_\sigma^\dagger\psi_\sigma + \psi_\sigma^\dagger\bar\psi_\sigma\right) + (4k_F{\rm terms})\right\} \\ &= \frac{1}{\sqrt{2\pi}}\partial_x\Phi_c + A\cos(2k_Fx + \sqrt{2\pi}\Phi_c)\cos\sqrt{2\pi}\Phi_s + (4k_F{\rm terms}),\end{aligned} \tag{3.4}$$

and

$$\begin{aligned}\Delta &\sim (\psi_\uparrow\bar\psi_\downarrow + \psi_\downarrow\bar\psi_\uparrow) \\ &= \cos(\sqrt{2\pi}\Theta_c)\cos(\sqrt{2\pi}\Phi_s).\end{aligned} \tag{3.5}$$

We now derive the magnitude of the effective Josephson coupling. We start from a single particle hopping term in our bare Hamiltonian density

$$\mathcal{H}_{\rm hopping} = \frac{t}{2a_0}\sum_{n\neq m}\left\{\psi_n^\dagger(x)\psi_m(x) + \bar\psi_n^\dagger(x)\bar\psi_m(x)\right\}, \tag{3.6}$$

After opening the spin-gap, the effective Hamiltonian density only involves pair hopping as

shown above:

$$\mathcal{H}_{\rm sc} = \frac{1}{2\Delta_s^{-1}} J_{\rm eff} \sum_{n\neq m} :\cos[\sqrt{2\pi}(\Theta_n - \Theta_m)]: . \tag{3.7}$$

These are virtual processes involving an intermediate energy Δ_s, hence the $J_{\rm eff}$ will have a factor t^2/Δ_s. We must also remember that our effective theory has an ultra-violet cut-off determined by the spin-gap, so we must account for the change in cut-off in the normal ordering, and finally we replace anything involving the spin field by its average value $\langle\cos(\sqrt{2\pi}\Phi_s)\rangle \sim (\Delta_s/\Lambda)^{K_s/2}$. Putting this all together gives

$$J_{\rm eff} \sim \left(\frac{\Delta_s}{\Lambda}\right)^{K_s+1/K_c-1} \frac{t^2}{\Delta_s} \tag{3.8}$$

where t is the single particle hopping and Λ is related to the original bandwidth.

Interaction (3.7) has scaling dimension

$$d_{\rm sc} = 1/(2K_c), \tag{3.9}$$

and therefore is relevant even for repulsive interactions in the charge sector provided they are not too strong ($K_c > 1/2$). This is a well known effect of the spin gap; it generates preformed pairs making it easy for them to condense [48].

Now we consider the inter-chain Coulomb coupling. In the bare system, we have a term

$$\mathcal{H}_{\rm coulomb} = \frac{V_0}{a_0} \sum_{n\neq m} \rho_n(x)\rho_m(x), \tag{3.10}$$

with $\rho(x)$ the charge density on each chain, and V_0 is the strength of the inter-chain Coulomb coupling. When we open a spin gap, the uniform part merely changes the chemical potential, so the most relevant operators are the $2k_F$ components of the CDW. Once more, replacing all occurrences of the spin field with its average value and changing the ultraviolet cut-off in the normal ordering, we generate an effective interaction in the charge sector

$$\mathcal{H}_{\rm cdw} = \frac{1}{2}\frac{V_{\rm eff}}{\Delta_s^{-1}} \sum_{n\neq m} :\cos[\sqrt{2\pi}(\Phi_n - \Phi_m)]: \tag{3.11}$$

where

$$V_{\rm eff} \sim \left(\frac{\Delta_s}{\Lambda}\right)^{K_s+K_c-1} V_0. \tag{3.12}$$

The corresponding scaling dimension is

$$d_{\rm cdw} = K_c/2. \tag{3.13}$$

We will also be considering the effect of a magnetic field. We introduce an external magnetic field H directed perpendicular to the chains. This couples to the superconducting

order parameter but doesn't affect the coulomb coupling. In principle, the material will have a Meissner effect, expelling the magnetic field from the inside of the superconductor. However, because of the reduced dimensionality, we would expect the Meissner effect to be very weak (i.e. the materials are strongly type II superconductors), particularly near the phase transition which is the region we are most interested in. Hence we can assume that the magnetic field that couples to the superconducting order parameter is simply the external magnetic field, which will be a good approximation for all but the weakest of applied fields.

The effective action for coupled chains is therefore

$$\begin{aligned}\mathcal{L}_{\text{eff}} = \frac{1}{2K_c}\sum_n (\partial_\mu \Phi_n)^2 \quad &+ \quad \frac{1}{2}\sum_{n\neq m}\{V_{nm} : \cos[\sqrt{2\pi}(\Phi_n - \Phi_m)] : \\ &+ \quad J_{nm} : \cos[\sqrt{2\pi}(\Theta_n - \Theta_m - 2eHb_{nm}x/c)] :\}. \end{aligned} \tag{3.14}$$

where b_{nm} is the projection of the inter-chain lattice vector on the direction perpendicular both to the chains and the magnetic field and the expression has Δ_s as the ultraviolet cut-off. We will be considering nearest-chain interactions only, i.e. $V_{nm} = V, J_{nm} = J$ for neighbouring chains and zero otherwise. In what follows we will be most interested in the case $K_c \approx 1$ when both interactions are important.

Note also that at this point, our effective action deals only with the charge sector, any details of the spin-sector except for the gap have been integrated out. So this model is more universal than its derivation, and can be applied to such cases as when the one-dimensional units are for example ladders rather than chains where they can acquire a Haldane spin-gap [49, 50].

To complete the introduction, we present the hierarchy of energy scales present in the system:

1. The highest energy scale is the spin gap Δ_s. Below Δ_s the system is described by competing CDW and SC fluctuations.

2. There is a transition temperature at which either $\langle \cos\sqrt{2\pi}\Theta\rangle$ or $\langle \cos\sqrt{2\pi}\Phi\rangle$ are formed. According to the mean field calculation, these order parameters cannot be formed simultaneously. Thus we are either in CDW or SC phase, but the temperature of their formation goes smoothly through the point $V = J$.

3. We will see that there is a third energy scale associated with the gap for another mode which becomes soft at the critical point. This mode is not seen in the first order RPA calculations, but its effects can be noted by looking at the first correction to RPA.

3.3 Low temperature phase diagram: Critical temperature and magnetic field effects

We now go further down in temperature where the inter-chain coupling becomes important, and we get dimensional crossover to a three-dimensional ordered phase.

In the case where there are two coupled chains, the model 3.14 was solved by Shelton *et al* [51]. There are two modes; one symmetric in the two chains and the other antisymmetric. In the presence of the inter-chain interactions, the symmetric mode remains gapless and the antisymmetric sector splits into two Majorana fermions with gaps (V + J) and (V - J).

For an infinite number of chains, we expect to see a similar sort of behaviour. The gapless symmetric mode in the the case of two chains will in some sense be the Goldstone mode in our infinite system and we expect to see a range of other modes with gaps ranging from $V - J$ to $V + J$. We will see that within the basic RPA we cannot reproduce this behaviour: the properties will depend only on the stronger of V and J. However when we go beyond the first order term we can start probing the interplay between these two competing interactions.

3.3.1 An Effective theory of the Critical Point

For a general value of K_c the symmetry of the model 3.14 is U(1)×U(1) which corresponds to independent global shifts of Φ and Θ. When $K_c = 1$ and $V = \pm J$ the symmetry increases and becomes SU(2). To see this we use the non-Abelian bosonisation description [13, 52]. At $K_c = 1$ the exponents $\exp[\pm \mathrm{i}\sqrt{2\pi}\Phi], \exp[\pm \mathrm{i}\sqrt{2\pi}\Theta]$ have conformal dimensions (1/4,1/4) and can be understood as matrix elements of the tensor field g_{ab} from the S=1/2 representation - the first primary field of the level $k = 1$ Wess-Zumino-Novikov-Witten (WZNW) model (for a discussion of this model, see e.g. Itzykson and Drouffe[35]):

$$\hat{g} = \begin{pmatrix} \exp[\mathrm{i}\sqrt{2\pi}\Phi] & \exp[\mathrm{i}\sqrt{2\pi}\Theta] \\ \exp[-\mathrm{i}\sqrt{2\pi}\Theta] & \exp[-\mathrm{i}\sqrt{2\pi}\Phi] \end{pmatrix}. \tag{3.15}$$

The Gaussian part of the action becomes the sum of the WZNW actions from individual chains:

$$\frac{1}{2}\sum_n (\partial_\mu \Phi_n)^2 \to \sum_n W[g_n], \tag{3.16}$$

and the interaction term in (3.14) can be written as

$$L_{int} = \sum_{n\neq m} \{(V-J)\sum_{a=1,2} [g_n^{(aa)}][g_m^+]^{(aa)} + (n \to m)] + J\mathrm{Tr}(g_n g_m^+ + g_m g_n^+)\}. \tag{3.17}$$

This description is convenient since it contains only mutually local fields and therefore can be considered as the Ginzburg-Landau theory.

In three spatial dimensions the system undergoes a phase transition into the ordered state

where the matrix g acquires an average value throughout the system. In the long wave limit one can replace the last term in (3.17) by

$$(\partial_y g)(\partial_y g^+), \tag{3.18}$$

and omitting the time dependence of the fields we obtain the following Ginzburg-Landau free energy:

$$F = b_0^{-2} \int \mathrm{d}x\mathrm{d}^2 r \mathrm{Tr}[\frac{va_0}{16\pi}(\partial_x g^+ \partial_x g) + J b_0^2 (\nabla_\perp g^+ \nabla_\perp g)] + F_{anisotropy}, \tag{3.19}$$

where b_0 is the lattice constant in the transverse direction and

$$F_{anisotropy} = (V-J) b_0^{-2} \int \mathrm{d}x\mathrm{d}^2 r \sum_{a=1,2} g^{(aa)} [g^+]^{(aa)}. \tag{3.20}$$

We can now re-parameterise the theory. The order parameter is the SU(2) matrix g. Its relation to the CDW and SC order parameters Θ and Φ are:

$$g = \exp[\mathrm{i}\sigma^3(\Phi+\Theta)/4] \exp[\mathrm{i}\sigma^1\alpha/2] \exp[\mathrm{i}\sigma^3(\Phi-\Theta)/4]. \tag{3.21}$$

The Ginzburg-Landau free energy density is

$$\mathcal{F} = \frac{1}{2}\rho[\cos^2(\alpha/2)(\nabla\Theta)^2 + \sin^2(\alpha/2)(\nabla\Phi)^2] + \frac{1}{2}\rho(\nabla\alpha)^2 + (V-J)\cos\alpha. \tag{3.22}$$

This is interpreted as follows: when $V-J$ is positive, α is pinned at π so that the coefficient in front of $(\nabla\Phi)^2$ is non-zero and hence Φ, the CDW order parameter, is constant throughout the material. When $V-J$ is negative, α is pinned at 0 and hence it is Θ, the superconducting order parameter that acquires an expectation value. When $V-J=0$ we are at the critical point where the free energy of the superconducting and insulating phases becomes equal, and we obtain an extra soft mode. The effects of this $V-J$ mode will be considered when looking more quantitatively at the transition.

In the alternative case of the transition between TSC and SDW, the symmetry at the quantum critical point is enhanced from U(1)×U(1) to $SO(4)$ [47], although this calculation is specifically for the case of a bipartite lattice.

3.3.2 The Random Phase Approximation

To begin with, we will estimate the critical temperature using the RPA. Our effective Lagrangian can be written as the sum of a 1D part and an inter-chain interaction $\mathcal{L}_{\text{eff}} = \mathcal{L}_{1D} + \mathcal{L}_{\text{inter}}$ where

$$\mathcal{L}_{1D} = \frac{1}{2K_c}\sum_n (\partial_\mu \Phi_n)^2$$

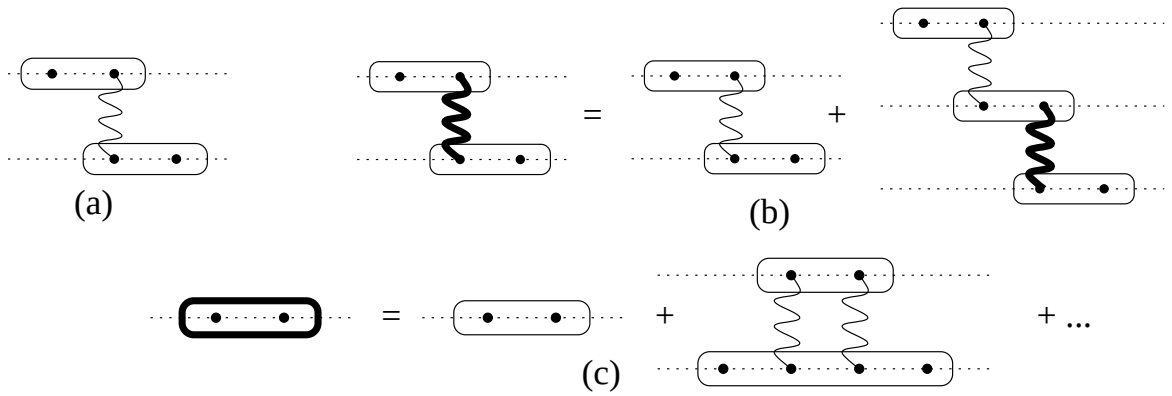

Figure 3.1: (a) The basic RPA diagram, (b) The Dyson series for RPA, (c) The first correction term. In these diagrams, the dashed lines represent the 1D chains, the dots indicate vertex operators of Φ or Θ, the wiggly lines are the inter-chain interactions, and each diagram is an irreducible correlator.

$$\begin{aligned}\mathcal{L}_{\text{inter}} &= \frac{1}{2}\sum_{n\neq m}\{V_{nm} : \cos[\sqrt{2\pi}(\Phi_n - \Phi_m)] : \\ &+ J_{nm} : \cos[\sqrt{2\pi}(\Theta_n - \Theta_m)] :\},\end{aligned} \tag{3.23}$$

where we have ignored the magnetic field for now for simplicity. We are interested in calculating the correlation functions

$$\begin{aligned}\chi_{sc} &= \langle e^{2\pi \mathrm{i}\Phi(\omega,k)} e^{-2\pi \mathrm{i}\Phi(\omega,k)}\rangle, \qquad \text{and} \\ \chi_{cdw} &= \langle e^{2\pi \mathrm{i}\Theta(\omega,k)} e^{-2\pi \mathrm{i}\Theta(\omega,k)}, \rangle\end{aligned} \tag{3.24}$$

as these are the channels in which we may have an instability.

Our starting theory is $\mathcal{L}_{1D}$ and we want a perturbing series in $\mathcal{L}_{\text{inter}}$. Because our starting theory isn't a free theory (in terms of the $e^{2\pi \mathrm{i}\Phi(\omega,k)}$ fields), we don't have Wick's theorem. However, up to the level of RPA, the perturbation expansion is identical with conventional perturbation theory:

$$\begin{aligned}\chi_{sc}(\omega, k_\parallel, k_\perp) &= \frac{\chi^{(0)}_{sc}(\omega, k_\parallel)}{1 - J(k_\perp)\chi^{(0)}_{sc}(\omega, k_\parallel)}, \\ \chi_{cdw}(\omega, k_\parallel, k_\perp) &= \frac{\chi^{(0)}_{cdw}(\omega, k_\parallel)}{1 - V(k_\perp)\chi^{(0)}_{cdw}(\omega, k_\parallel)}.\end{aligned} \tag{3.25}$$

These are shown diagrammatically in figure 3.1 (a) and (b).

To try and get some physical intuition about what this approximation involves, we can demonstrate the terms neglected in the RPA, shown in figure 3.2. These are paths which leave one chain then return to the same chain, thus requiring multi-point correlation functions on that chain. In section 3.4 we will talk about the first corrections to RPA, however we can see from the diagram that higher order terms will be less important by a factor $1/z_\perp$ where $z_\perp$ is the transverse coordination number. Hence one can consider RPA exact in the limit of infinite

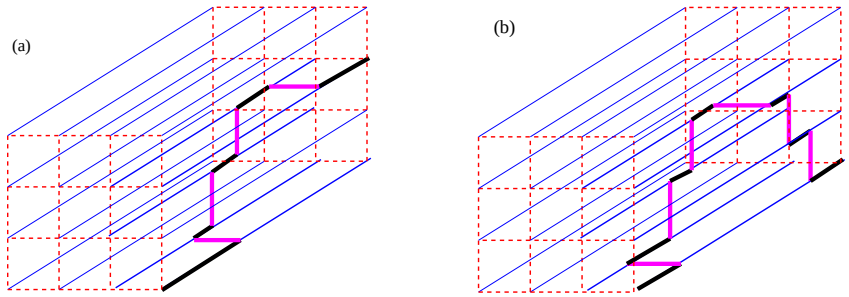

Figure 3.2: A figurative illustration of the paths ignored in the Random Phase Approximation. (a) An example of a path treated correctly, (b) An example of a path incorrectly treated because it returns to the same chain.

connectivity, e.g. a Bethe lattice.

The critical temperature is extracted from these equations by the condition that the susceptibility have an instability at $\omega = 0$, i.e.

$$\begin{aligned} Jz_\perp \chi^{(0)}_{sc}(\omega = 0, k; T) &= 1 \qquad \text{or} \\ Vz_\perp \chi^{(0)}_{cdw}(\omega = 0, k; T) &= 1. \end{aligned} \tag{3.26}$$

Here we have explicitly assumed a nearest-neighbour inter-chain interaction allowing us to write $J(k_\perp = 0) = z_\perp J$. Just to clarify notation, $J(k_\perp)$ as a function is the Fourier transform of the inter-chain hopping, J as a number is the strength of the inter-chain hopping.

When $K_c = 1$ the bare susceptibilities are equal to each other and therefore the instability occurs in that channel where the interchain interaction is stronger. This can be demonstrated explicitly in the mean-field approximation: here we replace the interaction term

$$\begin{aligned} \mathcal{L}_{\text{int}} &= \sum_m \{V \cos[\sqrt{2\pi}(\Phi_n - \Phi_m)] + J \cos[\sqrt{2\pi}(\Theta_n - \Theta_m)]\} \\ &\approx z_\perp V \langle \cos[\sqrt{2\pi}\Phi]\rangle \cos[\sqrt{2\pi}\Phi_n] + z_\perp J \langle \sin[\sqrt{2\pi}\Theta]\rangle \sin[\sqrt{2\pi}\Theta_n]. \end{aligned} \tag{3.27}$$

This can be written as

$$\begin{aligned} \mathcal{L}_{\text{int}} &= \sqrt{A^2 + B^2}\text{Tr}[(\cos\gamma I + \text{i}\sigma^1 \sin\gamma)g + c.c], \\ A &= Vz_\perp \langle \cos[\sqrt{2\pi}\Phi]\rangle, \quad B = Jz_\perp \langle \sin[\sqrt{2\pi}\Theta]\rangle, \quad \tan\gamma = \frac{B}{A}, \end{aligned} \tag{3.28}$$

where g is as defined in 3.15. The constant matrix can be removed by the redefinition of g. After that it becomes evident that the free energy depends only on $R^2 = A^2 + B^2$. The mean field equations are

$$\begin{aligned} A &= -Vz_\perp \frac{\partial F}{\partial A} = -Vz_\perp \frac{A}{R}\frac{\partial F}{\partial R}, \\ B &= -Jz_\perp \frac{\partial F}{\partial B} = -Jz_\perp \frac{B}{R}\frac{\partial F}{\partial R} \end{aligned} \tag{3.29}$$

From this it is clear that the only case where both A and B are simultaneously non-zero is $V = J$.

If $K_c \neq 1$, the instability still occurs in the stronger channel, although this now depends not only on the values of V and J but also on K_c and Δ_s, the crossover point being

$$\left(\frac{t^2}{\Delta_s} v_c\right)^{\frac{1}{2-1/2K_c}} \sim \left(\frac{V}{v_c}\right)^{\frac{1}{2-K_c/2}} . \tag{3.30}$$

For definiteness let us assume that the instability occurs in the superconducting channel which is the most likely case for $K_c > 1$. Note that the duality property of the effective Lagrangian (3.14) under $K \to 1/K$, $V \leftrightarrow J$, $\Theta \leftrightarrow \Phi$ means that all of the results in this and the next section are identical for the CDW channel.

In a Tomonaga-Luttinger liquid with the ultraviolet cut-off Δ_s the static susceptibility for the operator with scaling dimension d was given in section 2.3:

$$\chi^{(0)}(k) = \frac{2}{\Delta_s^2} \sin \pi d \left(\frac{2\pi T}{\Delta_s}\right)^{-2+2d} \Gamma^2(1-d) \left| \frac{\Gamma(d/2 + iv_c k/4\pi T)}{\Gamma(1-d/2 + iv_c k/4\pi T)} \right|^2 . \tag{3.31}$$

In the absence of a magnetic field, the structure of χ means that the instability will occur at $k = 0$.

3.3.3 Zero magnetic field; the critical temperature

Substituting 3.31 with $k = 0$ into equation 3.25 we obtain

$$T_c = \frac{\Delta_s}{2\pi} \left(\frac{2Jz_\perp}{\Delta_s} \sin \pi d \frac{\Gamma^2(d/2)\Gamma^2(1-d)}{\Gamma^2(1-d/2)} \right)^{\frac{1}{2-2d}} . \tag{3.32}$$

Below the transition temperature the long-wavelength fluctuations of superconducting order parameter are three-dimensional. The amplitude fluctuations are however mostly one-dimensional and their spectral weight is concentrated above a certain energy which plays the role of a pseudo-gap. The zero temperature value of the pseudo-gap can be found from the mean-field theory combined with the exact results for the sine-Gordon model. In this approach one approximates the inter-chain interaction

$$J \sum_{<nm>} \cos[\sqrt{2\pi K_c^{-1}}(\Theta_n - \Theta_m)], \tag{3.33}$$

by the one-dimensional (i.e. no chain index) term:

$$2\mu \cos[\sqrt{2\pi K_c^{-1}}\Theta], \tag{3.34}$$

where

$$2\mu = Jz_\perp \Delta_s \langle \cos[\sqrt{2\pi K_c^{-1}}\Theta] \rangle. \tag{3.35}$$

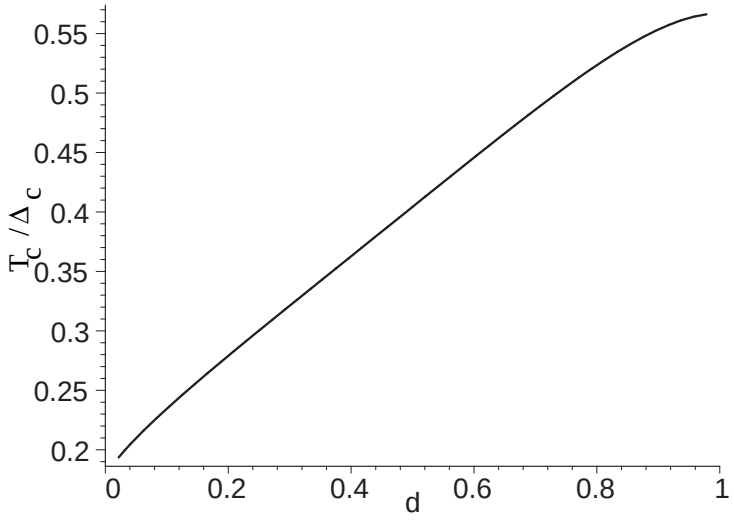

Figure 3.3: A graph of T_c/Δ_c against d. The value $d = 1$ corresponds to the BCS limit, decreasing d corresponds to increasing repulsion.

This expectation value is known exactly [53]:

$$\begin{aligned} & \langle \cos[\sqrt{2\pi K_c^{-1}}\Theta] \rangle \\ = \; & \frac{(1+\xi)\pi\Gamma(1-d/2)}{16\sin\pi\xi\,\Gamma(d/2)} \left(\frac{\Gamma(\frac{1}{2}+\frac{\xi}{2})\Gamma(1-\frac{\xi}{2})}{4\sqrt{\pi}} \right)^{(d-2)} \left(2\sin\frac{\pi\xi}{2} \right)^{d} \left(\frac{\Delta_c}{\Delta_s} \right)^{d}, \end{aligned} \tag{3.36}$$

where the charge gap Δ_c is the soliton mass in the sine-Gordon model, and is related to μ by

$$\mu = \frac{\Gamma(d/2)}{\pi\Gamma(1-d/2)} \left(\frac{2\Gamma(\xi/2)}{\sqrt{\pi}\Gamma(\frac{1}{2}+\frac{\xi}{2})} \right)^{d-2} \left(\frac{\Delta_c}{\Delta_s} \right)^{2-d} \Delta_s^2. \tag{3.37}$$

In all these equations, $d = 1/2K_c$ is the scaling dimension of the field $e^{\mathrm{i}\sqrt{2\pi K_c^{-1}}\Theta}$, and $\xi = 1/(2-d)$. These mean-field relations are solved to give

$$\Delta_c = \Delta_s \left[\frac{Jz_\perp}{\Delta_s} \frac{1}{2(d-2)} \tan\frac{\pi\xi}{2} \right]^{\frac{1}{2-2d}} \left[\frac{\pi\Gamma(1-d/2)}{\Gamma(d/2)} \left(\frac{\Gamma(\frac{1}{2}+\frac{\xi}{2})\sqrt{\pi}}{2\Gamma(\xi/2)} \right)^{(d-2)} \right]^{\frac{1}{1-d}}. \tag{3.38}$$

The ratio T_c/Δ_c which is often considered in the theory of superconductivity is plotted as a function of d in figure 3.3. Its numerical value in certain limits is:

$$\frac{T_c}{\Delta_c}(d=0) = \frac{\sqrt{2}}{8} \approx 0.177, \tag{3.39}$$

$$\frac{T_c}{\Delta_c}(d=1/2) = \frac{3}{16}\frac{\sqrt{3\pi}(\Gamma(2/3)\Gamma(5/6))^3}{\Gamma(3/4)^8} \approx 0.404. \tag{3.40}$$

In the limit $d \to 1$ which corresponds to weak coupling, our expressions for T_c and Δ_c diverge in this approximation. However their ratio can still be evaluated. Writing $x = 1 - d$ and

expanding all the gamma functions as Taylor series in x gives us the BCS value

$$\frac{T_c}{\Delta_c}(d \to 1) = \frac{1}{2\pi} \lim_{x \to 0} [1 + (\ln 2 + \gamma)x]^{\frac{1}{x}} = \frac{1}{\pi} e^{\gamma} \approx 0.567, \tag{3.41}$$

where $\gamma \approx 0.57722$ is Euler's constant.

3.3.4 Phase diagram in a magnetic field

A magnetic field affects the inter-chain interaction in the superconducting channel (3.7). In this case the instability corresponding to the lattice directions **l** should be taken at wave vector $2e(\mathbf{H}[\hat{\mathbf{x}} \times \mathbf{l}])/c$, where $\hat{x}$ is the unit vector along the chains. Therefore the RPA criterion for the transition is by

$$1 = \sum_l J_l \chi_{sc}^{(0)}\{k = 2e(\mathbf{H}[\hat{\mathbf{x}} \times \mathbf{l}])/c\} \tag{3.42}$$

To keep the calculations as simple as possible, let us consider the simplest possible situation when a given chain has four nearest neighbours with Josephson couplings J_z and J_y and the magnetic field lays in the yz plane. Combining equation 3.42 and equation 3.31 we obtain the equation for the critical temperature:

$$C\left(\frac{T_c}{T_c(0)}\right)^{(2-2d)} = J_z \left|\frac{\Gamma(d/2 + i\alpha b_z H_y/T_c)}{\Gamma(1 - d/2 + i\alpha b_z H_y/T_c)}\right|^2 + J_y \left|\frac{\Gamma(d/2 + i\alpha b_y H_z/T_c)}{\Gamma(1 - d/2 + i\alpha b_y H_z/T_c)}\right|^2$$
$$C = (J_z + J_y)\left|\frac{\Gamma(d/2)}{\Gamma(1 - d/2)}\right|^2, \qquad \alpha = ev_c/2\pi c \tag{3.43}$$

We now discuss the solution of this equation which describes several interesting effects.

- A possibility of a re-entrance behaviour.

  Let us consider the case when in-plane interactions are isotropic: $J_z = J_y, b_z = b_y$ and the magnetic field is directed at 45^o angle $H_z = H_y = H$. This gives it the maximal power to suppress T_c. A numerical solution of equation 3.43 is plotted in figure 3.4 (a) for various values of the scaling dimension d. We see that there is a range of magnetic fields for which the superconductivity exists in an intermediate range of temperatures. To study the stability of these solutions one needs to have a good description of the ordered state in magnetic field, which we hope to obtain in the future.

  At $T_c \to 0$ equation 3.43 can be solved analytically which allows us to extract the value of critical field at $T_c = 0$:

$$H_c(0) = \frac{2\pi c}{e}\frac{T_c(0)}{bv}\left(\frac{\Gamma(1 - d/2)}{\Gamma(d/2)}\right)^{1/(1-d)} \tag{3.44}$$

  This is plotted in figure 3.4 (b) along with the numerical solution for H_c^{max}.

- Anisotropy of the phase diagram.

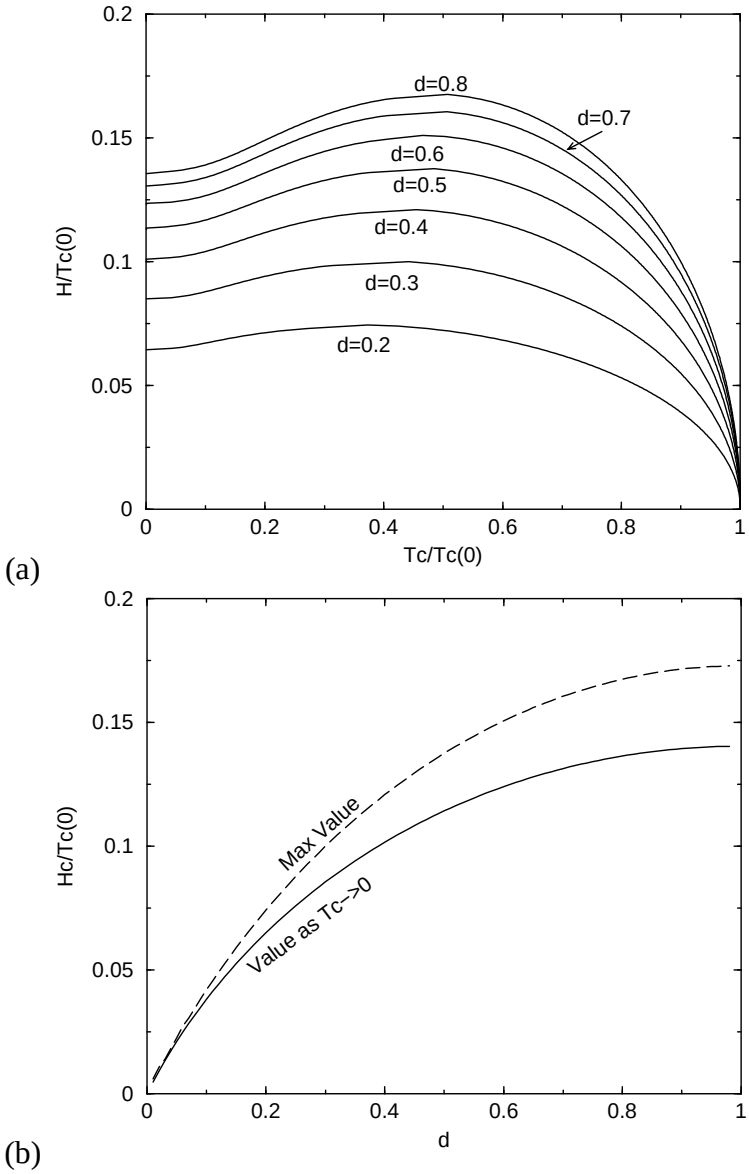

Figure 3.4: (a) The critical temperature as a function of magnetic field for various values of d. (b) The critical magnetic field as a function of d. We plot both the value of H which gives $T_c \to 0$ and the maximum value of H seen in graph (a). The magnetic field is measured in the units of $2e\bar{h}bv/c$.

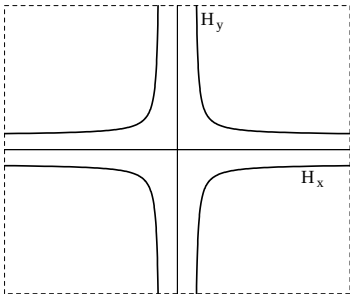

Figure 3.5: Angular dependence of the critical magnetic field. This is plotted for $d = 1/2$. The graph is qualitatively similar for other values of d. In actual fact, the system will be driven to a CDW ground state before the SC transition temperature drops to zero - see the text.

Another prediction following from equation 3.43 is an anisotropy of the phase diagram. This can be illustrated by an analytical solution of the critical field for which $T_c \to 0$. Setting $T_c \to 0$ in equation 3.43 we find

$$\frac{J_z}{(\alpha H_y b_z)^{2(1-d)}} + \frac{J_y}{(\alpha H_z b_y)^{2(1-d)}} = \frac{C}{[T_c(0)]^{2(1-d)}}, \tag{3.45}$$

where α is an unimportant constant factor. This is plotted in figure 3.5. We must be careful to remember however that this is a first order mean field calculation, and further corrections will give a critical flux in all directions, even when the field is pointing directly along one of the crystal axis.

- SC-CDW transition.

  The above calculations are all calculated assuming we are in a parameter range such that the ground state at $H = 0$ is superconducting. However, as we increase the magnetic field and thus reduce the SC transition temperature, we eventually get to a regime where $T_{CDW} > T_{SC}$ as the CDW instability is not affected by the magnetic field. At this point which can happen either by increasing magnetic field (figure 3.4) or by changing the angle of the magnetic field (figure 3.5), we get a first order transition from a superconducting to a CDW state. The latter would be a very unusual effect to observe in a real material.

3.4 Corrections to RPA

The analysis of the previous sections was based on the RPA. In realistic situations the number of nearest neighbours is never large, so it is important to check how robust the RPA is. We will calculate corrections to RPA in the simplest case case of zero magnetic field. We shall also restrict ourselves to $K_c = 1$ ($d = 1/2$ for both interactions).

The basic RPA calculation involves only the stronger of the two interactions - for clarity let us again take this to be J. However as we mentioned before we would expect the presence of

the other competing interaction of the same scaling dimension to also play a role. In particular we expect there to be a mode with a gap of $J - V$, seen in equation 3.22 and in the two chain model. This will be very important around the point $V = J$ as it will become massless thereby increasing fluctuations and decreasing the transition temperature. This can be investigated by looking at the first correction to the RPA formula - figure 3.1(c).

In terms of the fields ϕ and θ, this diagram can be expressed as

$$\begin{aligned}
\delta\chi &= V^2 z_\perp \left[\langle e^{i\sqrt{2\pi}\Theta(a)} e^{i\sqrt{2\pi}\Phi(1)} e^{-i\sqrt{2\pi}\Phi(2)} e^{-i\sqrt{2\pi}\Theta(b)}\rangle - \langle e^{i\sqrt{2\pi}\Theta(a)} e^{-i\sqrt{2\pi}\Theta(b)}\rangle \langle e^{i\sqrt{2\pi}\Phi(1)} e^{-i\sqrt{2\pi}\Phi(2)}\rangle\right] \\
&\qquad \times \langle e^{-i\sqrt{2\pi}\Phi(1)} e^{i\sqrt{2\pi}\Phi(2)}\rangle \\
&+ J^2 z_\perp \left[\langle e^{i\sqrt{2\pi}\Theta(a)} e^{i\sqrt{2\pi}\Theta(1)} e^{-i\sqrt{2\pi}\Theta(2)} e^{-i\sqrt{2\pi}\Theta(b)}\rangle - \langle e^{i\sqrt{2\pi}\Theta(a)} e^{-i\sqrt{2\pi}\Theta(b)}\rangle \langle e^{i\sqrt{2\pi}\Theta(1)} e^{-i\sqrt{2\pi}\Theta(2)}\rangle\right] \\
&\qquad \times \langle e^{-i\sqrt{2\pi}\Theta(1)} e^{i\sqrt{2\pi}\Theta(2)}\rangle, \qquad (3.46)
\end{aligned}$$

where a,b are the start and end points and 1,2 are the intermediate points to be integrated over. Substituting in the expectation values from equation 2.4 and integrating gives the revised RPA equation for the transition temperature:

$$1 = \frac{J z_\perp}{T_c}\left[A_0^J + A_1^J \frac{J^2 z_\perp}{T_c^2} + A_1^V \frac{V^2 z_\perp}{T_c^2}\right] \qquad (3.47)$$

where the coefficients are given by

$$\begin{aligned}
A_0^J &= \frac{1}{\pi}\int_0^\pi d\tau \int_{-\infty}^\infty dx \frac{1}{|\sinh(x+i\tau)|} = \frac{1}{2\pi} B^2(1/4, 1/2), \\
A_1^J &= \frac{1}{\pi^3}\int_0^\pi d\tau_1 d\tau_2 d\tau_b \int_{-\infty}^\infty dx_1 dx_2 dx_b \frac{1}{|\sinh(x_b + i\tau_b)|}\frac{1}{|\sinh(x_{12} + i\tau_{12})|^2} \\
&\qquad \times \left[\frac{|\sinh(x_1 + i\tau_1)||\sinh(x_{b2} + i\tau_{b2})|}{|\sinh(x_2 + i\tau_2)||\sinh(x_{b1} + i\tau_{b1})|} - 1\right], \\
A_1^V &= \frac{1}{\pi^3}\int_0^\pi d\tau_1 d\tau_2 d\tau_b \int_{-\infty}^\infty dx_1 dx_2 dx_b \frac{1}{|\sinh(x_b + i\tau_b)|}\frac{1}{|\sinh(x_{12} + i\tau_{12})|^2} \\
&\times \left[\left(\frac{\sinh(x_1 + i\tau_1)\sinh(x_2 - i\tau_2)\sinh(x_{b2} + i\tau_{b2})\sinh(x_{b1} - i\tau_{b1})}{\sinh(x_1 - i\tau_1)\sinh(x_2 + i\tau_2)\sinh(x_{b2} - i\tau_{b2})\sinh(x_{b1} + i\tau_{b1})}\right)^{1/2} - 1\right] \qquad (3.48)
\end{aligned}$$

with $x_{12} = x_2 - x_1$ and so on. $B(x, y) = \Gamma(x)\Gamma(y)/\Gamma(x + y)$ is a Beta function.

The integrals are evaluated numerically by Monte-Carlo techniques [54] with values calculated over finite volumes then scaled to infinity. The results are

$$\begin{aligned}
A_0^J &= 4.377, \\
A_1^J &= 34.81 \pm 0.02, \\
A_1^V &= -33.01 \pm 0.02. \qquad (3.49)
\end{aligned}$$

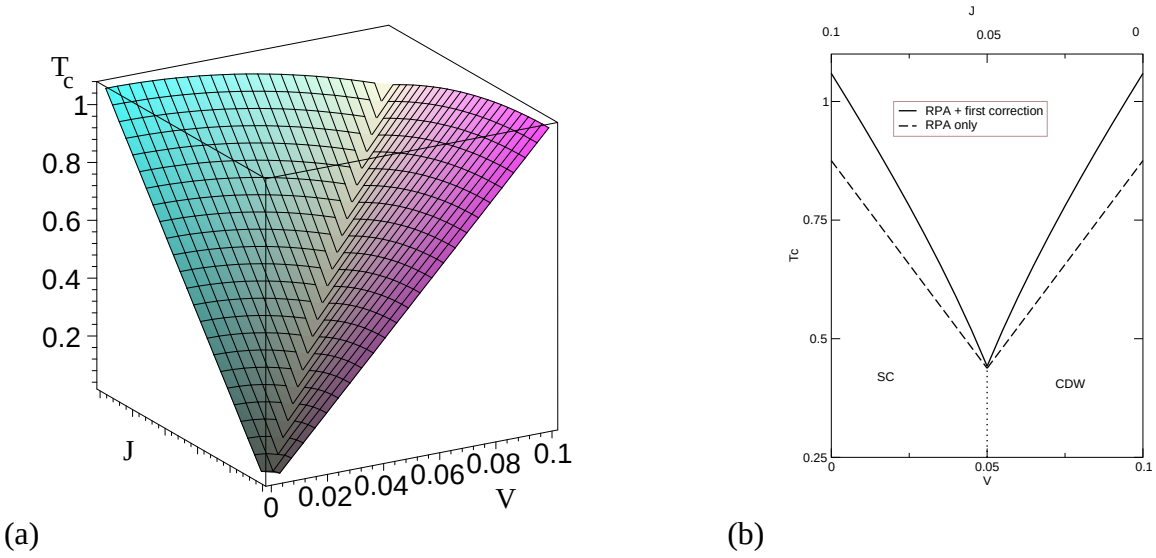

(a) (b)

Figure 3.6: (a) A plot of T_c against V and J, (b) A cross section of T_c against V along the line $V + J = 0.1$. In these plots, we have taken $z_\perp = 2$ to allow these corrections to be clearly seen, although for this approach to be valid, we require $z_\perp \geq 3$.

Hence the correction to the transition temperature is

$$\frac{T_c}{A_0^J J z_\perp} \approx 1 + \frac{1}{z_\perp}\left[0.42 - 0.40\left(\frac{V}{J}\right)^2\right]. \tag{3.50}$$

This expression is valid for $J > V$. If $V > J$, the expression is exactly the same, but with V and J interchanged. This is plotted in figure 3.6 and gives a dip near the critical point as expected.

It is interesting to note that in the absence of the second interaction term, i.e. $V = 0$, these correction raise the transition temperature above the RPA value. This differs from models of coupled spin chains where RPA tends to overestimate the transition temperature [38, 39].

3.5 Single Particle Spectral Function and other experimental signatures

To help relate these results to experiment we will look at the evolution of the spectral functions. These can be seen by Angle Resolved Photoemission Spectroscopy (ARPES) as we go from one phase to the next.

3.5.1 Above the transition temperature

We begin our discussion above the transition temperature where the chains can be considered uncoupled and the system shows one dimensional like behaviour. In this case, our model 3.2 is

simply a Luther-Emery liquid [19]. The correlation functions in the spin-sector can be written as a form-factor expansion [20] but results are only known for $T = 0$, and the first correction for $T << \Delta_s$ in [55]. Although finite temperature results are known in the charge sector, the convolution of this with the spin sector does not admit to easy analytical analysis. However, at the Luther-Emery point, $K_c = 1/2$ (see section 2.1.4) where the spin sector can be rewritten in terms of free fermions, a number of analytic results can be recovered. Details of this are found in [56] and [43], here we limit ourselves here to a discussion of the overall gross features.

At the Luther-Emery point $K_s = 1/2$, the field operators in the refermionised form can be thought of as spin soliton creation and annihilation operators. Hence the spin part of the spectral function can be written as the sum of a coherent one spin soliton part and an incoherent multi-soliton piece

$$A_s(k,\omega) = Z_s(k)\delta[\omega + E_s(k)] + G_s^{(multi)}(k,\omega) \tag{3.51}$$

where the multi-soliton piece at $T = 0$ is zero below the threshold energy $\omega_3 = 3E_s(k/3)$. As the solitons can be written as free fermions, their spectrum is

$$E_s(k) = \sqrt{\Delta_s^2 + (v_s k)^2}. \tag{3.52}$$

Away from the Luther-Emery point for $K_s < 1/2$, soliton-antisoliton bound-states form which will shift the threshold energy slightly.

The convolution with the charge sector ($E_c(k) = v_c|k|$) gives the result

$$\begin{aligned} A(k,\omega;T) &= \frac{c^2}{\pi^3}\frac{\lambda_T^2}{v_c}\left(\frac{a_0}{\lambda_T}\right)^{2\theta_c+\frac{1}{2}}\left(\frac{2v_s}{a_0\Delta_s}\right)^{\frac{3}{8}} \\ &\times \int dq \left[1 - \frac{v_s(k-q)}{E_s(k-q)}\right] h_{\theta_c+\frac{1}{2}}\left[\frac{\omega + E_s(k-q) + v_c q}{2\pi T}\right] \\ &\times h_{\theta_c}\left[\frac{\omega + E_s(k-q) - v_c q}{2\pi T}\right] + \ldots, \end{aligned} \tag{3.53}$$

where the $\ldots$ refer to the 3 spin soliton and higher contributions and $\lambda_T = v_c/\pi T$ is the thermal length. In this expression,

$$h_\theta(k) = \mathrm{Re}\left[(2i)^\theta B\left(\frac{\theta - ik}{2}, 1-\theta\right)\right]. \tag{3.54}$$

Although this is calculated only at the Luther-Emery point, it is expected that the basic features remain the same throughout the spin-gap region (and furthermore in the region $T_c < T < \Delta_s$, even when the spin sector is far more complicated). The shape of the spectral functions is plotted in the way typical in ARPES as various Energy Distribution Curves (EDC's) at constant momenta and momentum distribution curves (MDC's) at constant energy in figure 3.7, showing the effects of a spin-gap.

We see that in the MDC at the Fermi-level, it is hard to distinguish between this sys-

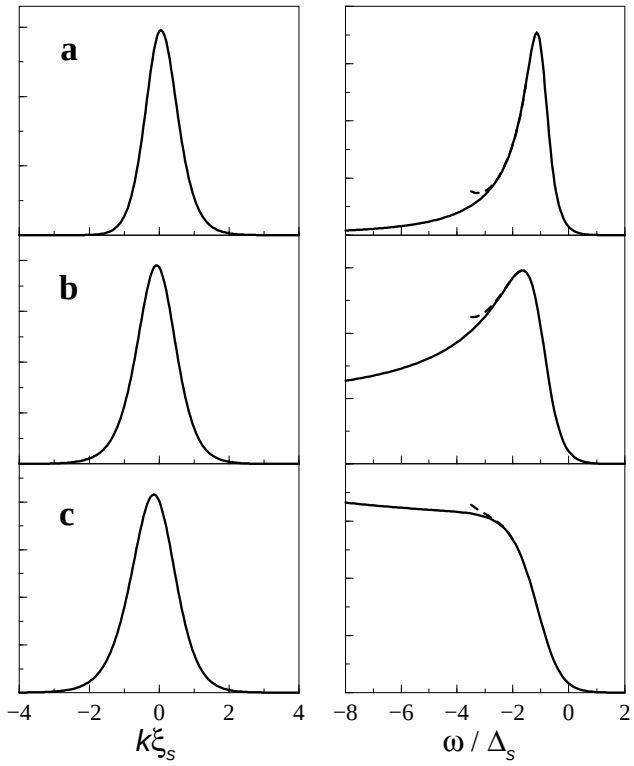

Figure 3.7: The single spin soliton contribution, G_1, to the MDCs at $\omega = 0$ (left) and EDCs at $k = 0$ (right), of a Luther-Emery liquid $(K_s = 1/2)$, with $v_c/v_s = 3$, $\Delta_s/T = 3$ and a) $\theta_c = 0$, b) $\theta_c = 0.2$, and c) $\theta_c = 0.4$. The asymptotic contribution of the three spin soliton piece, to the EDCs, near its zero temperature threshold $\omega = -3\Delta_s$, is indicated by the dashed lines. Taken from [56].

tem and a coherent electron-like peak broadened by temperature. However, in the EDC, the asymmetry and long tails give away that this is a strongly interacting system.

3.5.2 The ordered Phase

The single-particle spectral function requires exciting both a spin and charge excitation within the one dimensional chains. To excite a spin-soliton takes an energy Δ_s. In the three-dimensional ordered phase, this then leaves a term in the Hamiltonian

$$U \cos\left[\sqrt{2\pi/K_c}(\Theta_n^c - \Theta_m^c)\right] \cos\left[\sqrt{2\pi}\Phi_n^s\right] \cos\left[\sqrt{2\pi}\Phi_m^s\right], \tag{3.55}$$

where Φ_n^s has a soliton present. This is shown in figure 3.8. When one looks only at the charge sector, the effect of the soliton is to change the sign of the interaction term on one side of the soliton. This is compensated for by a soliton in the charge sector, which is bound to the spin soliton. This turns out to have an energy[1] $\Delta_c/2$ [57].

[1] As a brief aside, it is interesting to note that if only two chains are coupled, then at $K_c = 1$ a collective mode in both chains has zero energy so the total energy of the excitation is simply Δ_s. Because this involves modes in more than one chain however, it can not be extended to the case of an infinite number of chains.

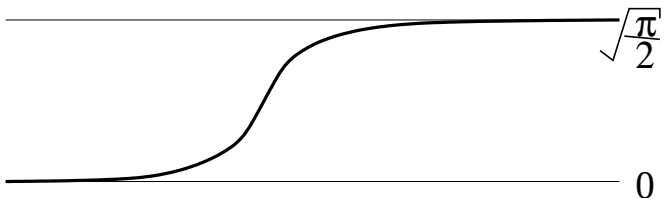

Figure 3.8: A soliton in Φ_n^s.

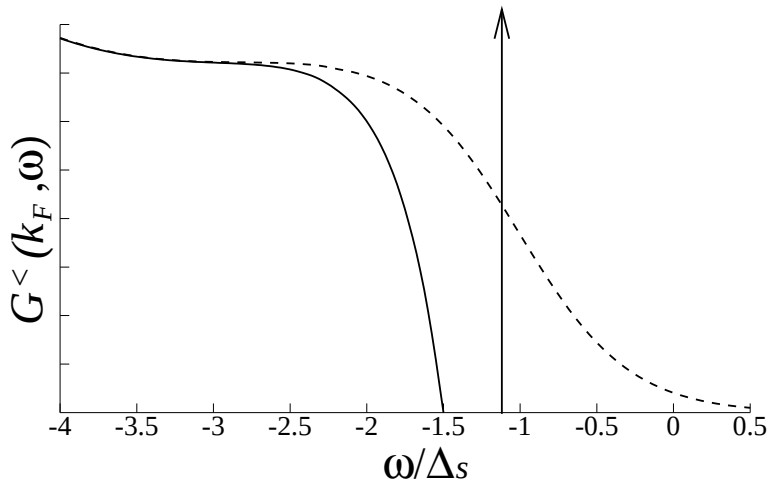

Figure 3.9: The temperature evolution of the spectral function. The dashed line depicts $A(k_F, \omega)$ at temperature $T = \Delta_s/3 > T_c$ for the parameters $\theta_c = 0.3$, $K_s = 1/2$ and $v_s/v_c = 0.2$. The solid line represents the spectral function at zero temperature. A coherent δ-function peak onsets near T_c at energy $\Delta_0 = \Delta_s + \Delta_c(0)/2$. Here we assume $\Delta_s/\Delta_c(0) = 5$. The multi-particle piece starts at a threshold $2\Delta_c(0)$ away from the coherent peak. The exact shape of the incoherent piece at $T = 0$ is schematic. Figure from [43].

Hence, the rest energy of an 'electron' is

$$\Delta_0 = \Delta_s + \Delta_c/2 \approx \Delta_s, \tag{3.56}$$

and this would be the gap seen in single particle spectroscopies, very different from Δ_c which would be seen in Josephson tunnelling. Hence for $T \ll T_c \ll \Delta_s$, the one hole spectral function has a coherent piece and a multiparticle incoherent piece,

$$A(k, \omega) = Z(k)\delta[\omega - E(k)] + G^{(multi)}(k, \omega) \ , \tag{3.57}$$

where

$$E(k) = \sqrt{v_s^2 k^2 + \Delta_0^2} \ . \tag{3.58}$$

This follows from the fact that the bound state of a spin soliton and a charge soliton has the same quantum numbers as a hole. The multiparticle piece has a threshold slightly above the single hole threshold at $\omega = \mathcal{E}(k) + 2\Delta_c$. The evolution of this spectral function as one passes through the phase transition is shown in figure 3.9.

To probe Δ_c, one would have to look at experiments involving pairs of electrons, such

as Andreev tunnelling. In the context of sine-Gordon model, Δ_c is the soliton mass. Solitons correspond to spatial changes in the superconducting phase Θ and hence to vortices. Therefore Δ_c is the minimal energy necessary to create a vortex. It should also be noticed that at $d < 1$ the sine-Gordon model has not only solitons, but bound states which, being neutral, should be interpreted as vortex-antivortex pairs. At $d < 1/2$ the energy of the first bound state is smaller than the soliton.

There are a number of experimental implications of there being two energy scales.

1. The gap seen in single-particle spectroscopies Δ_0 changes only slightly with temperature, and furthermore is unrelated to T_c. Physically, this is saying that it is the onset of phase coherence and not the onset of pairing that is important for superconductivity. This has been talked about experimentally in the context of high-T_c and the pseudo-gap phase for many years now.

2. Experiments involving singlet pairs of electrons such as Andreev tunnelling would see a gap much more related to T_c.

3. The presence of two different correlation lengths implies that different measurements of the order-parameter will be depressed over different distances. For example, near an impurity which locally destroys the superconducting gap, the single particle density of states will recover over a distance ξ_s, and this is what would be seen in for example tunnelling microscopy. However, the magnetic core radius around a vertex as would be seen in μSR would be of order ξ_c.

4. Because the superconducting state comes not from a Fermi-Liquid but from a state with 'pre-formed' pairs, the temperature evolution of the excitation spectrum in the ordered phase will be very different from a conventional superconductor. In BCS theory, the quasi-particle energy is shifted by the opening of the gap so the lifetimes of excitations are strongly temperature dependent below T_c. In our case, the quasi-particles are already there above T_c, so it is only the spectral weight (and not the energies or lifetime) that is strongly temperature dependent.

3.6 A Word about Two Dimensions

In two dimensions the RPA approach in the previous two sections must break down completely, as spontaneous symmetry breaking is forbidden by the Mermin-Wagner theorem. We can see how this comes about by looking at figure 3.1(c). The correction we looked at involved only bare couplings to the bare correlation function. The process of making these lines 'thick' involves much numerical complication and gives rise to only small corrections in three or higher dimensions [38]. However in two dimensions, these corrections have infra-red divergences and drive the transition temperature back down to 0.

Nevertheless we still get a transition in two dimensions: it is of the Kosterlitz-Thouless [58, 59] type. Let's look closer at Coulomb coupling in two dimensions. The Lagrangian for

the coupled chains can be written

$$\mathcal{L} = \sum_i \left\{ \frac{1}{2}(\partial_\mu \phi_i)^2 - \frac{J}{\Delta_s^{-1}} \cos[\beta(\phi_i - \phi_{i+1})] \right\}. \tag{3.59}$$

By making the approximation

$$-\cos\phi = \frac{\phi^2}{2}\langle\cos\phi\rangle, \tag{3.60}$$

which comes from the diagrammatic expansion of the vertex operator, we can write this as

$$\mathcal{L} = \sum_i \left\{ \frac{1}{2}(\partial_\mu \phi_i)^2 + \tilde{J}(\phi_i - \phi_{i+1})^2 \right\}, \tag{3.61}$$

with the self-consistent relation

$$\begin{aligned} \tilde{J} &= J\Delta_s\beta^2\langle\cos\beta(\phi_i - \phi_{i+1})\rangle \\ &= J\Delta_s\beta^2 \exp\left\{ -\beta^2\, T \sum_n \int \frac{dq_\perp}{2\pi}\frac{dq_\parallel}{2\pi} \frac{1-\cos q_\perp}{\omega_n^2 + q_\parallel^2 + 4\tilde{J}\sin^2(q_\perp/2)} \right\}. \end{aligned} \tag{3.62}$$

At $T = 0$ this relation becomes

$$\begin{aligned} \tilde{J} &= J\Delta_s\beta^2 \exp\left(-\frac{\beta^2}{2\pi} \ln \frac{\Delta_s}{\sqrt{2\tilde{J}}} \right) \\ &= J\Delta_s\beta^2 \left(\frac{2\tilde{J}}{\Delta_s^2} \right)^d, \end{aligned} \tag{3.63}$$

where $d = \beta^2/4\pi$ as before. As T increases, the self-consistent value of $\tilde{J}$ will decrease, but for an estimate of the behaviour of the transition temperature this relation will suffice.

The Kosterlitz-Thouless transition temperature [13, 59] $T_{\rm KT} \sim \sqrt{\tilde{J}}$ hence we have

$$T_{\rm KT} \sim \Delta_s \left(\frac{J}{\Delta_s} \right)^{\frac{1}{2-2d}} \tag{3.64}$$

giving the same order of magnitude as the ordering temperature in higher dimensions (3.32).

Hence in two dimensions, although the nature of the transition is different, the energy scales involved are the same as in higher dimensions. The only major difference occurs when approaching the SU(2) critical point where the presence of a non-Abelian symmetry in two dimensions means that the transition temperature will drop to zero at this point. The qualitative phase diagram in two dimensions is shown in figure 3.10.

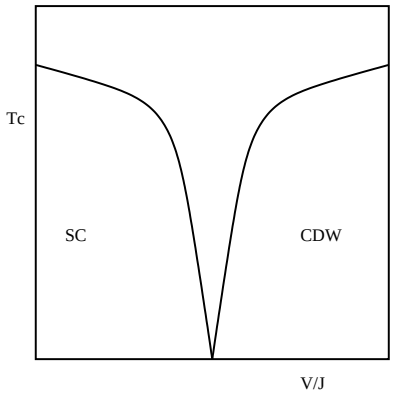

Figure 3.10: The modified phase diagram for our model in two dimensions

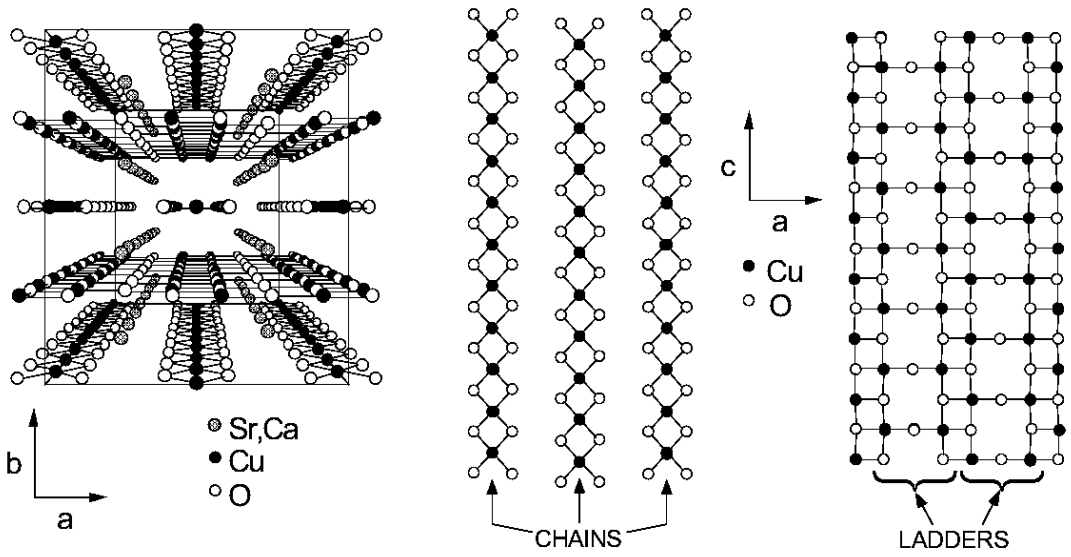

Figure 3.11: Structure of $\mathrm{Sr_{14}Cu_{24}O_{41}}$ after [60]. The compound consists of alternating planes of copper oxide chains and ladders.

3.7 Example experimental systems

3.7.1 The telephone number compound

The class of materials $\mathrm{Sr_{14-x}Ca_xCu_{24}O_{41}}$ are built up from alternating layers of weakly coupled $\mathrm{CuO_2}$ chains and $\mathrm{Cu_2O_3}$ two-leg ladders. The material shows a spin gap in both of these one-dimensional units [61] making it a prime candidate for application of our model. Because our only requirement in the spin-sector was that it was gapped, our theory is still valid even if the superconductivity originates from the ladders.

For $x \geq 11.5$, these materials show superconductivity under pressure [62, 63] and NMR studies [61] also indicate possible charge ordering at low temperature and ambient pressure. Recent measurements of the electrodynamic response [64] have confirmed the presence of CDW in this class of compounds. One of the most interesting measurements however is the DC resistivity [63], which shows a number of features:

- In $\mathrm{Sr_{2.5}Ca_{11.5}Cu_{24}O_{41}}$ below about 4 GPa pressure, the temperature dependence of the resistivity perpendicular and parallel to the ladders is different. This indicates that different mechanisms are governing the transport in these two directions, consistent with the spin-gap concept. Above 4 GPa the temperature dependence of the resistivity anisotropy becomes weak, which indicates that single particle hopping between ladders is now possible, i.e. the spin gap has vanished and we have a crossover to a conventional two-dimensional metallic behaviour. This is consistent with the pressure dependence of the spin gap observed in recent NMR experiments [60].

- At sufficiently high temperatures, coherent inter-ladder charge dynamics is also seen. The temperature where this occurs is consistent with the NMR determinations of the spin gap, so we may conclude that the transport properties of this material are indeed governed by weakly interacting one-dimensional spin-gapped units.

In figure 3.12 a phase diagram of this material is shown [65]. At low calcium doping, there is charge ordering before spin ordering, so our model is inapplicable. However under increased levels of calcium doping or pressure, the spin gap is the largest energy scale in the model meaning that our theory may describe the nature of the transition between the CDW and the SC phases.

In our model, taking $K_c \approx 1$ we have

$$\begin{aligned} J_{\text{eff}} &\sim (\Delta_s/\Lambda)t^2/\Delta_s, \\ V_{\text{eff}} &\sim (\Delta_s/\Lambda)V_0. \end{aligned} \tag{3.65}$$

The size of the spin gap is reasonably constant as we change calcium doping and pressure, however under pressure the hopping t will increase which makes the inter-ladder Josephson coupling stronger until eventually the material becomes a superconductor instead of having

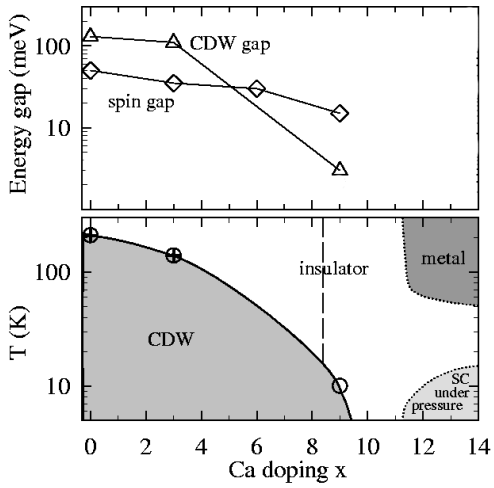

Figure 3.12: Phase diagram for the spin gap and superconducting transition temperature against Ca doping in $\mathrm{Sr_{14}Cu_{24}O_{41}}$. After [65].

.

a CDW ground state. Unfortunately, the complexity of the material as well as having both physical and chemical pressure makes it difficult to say anything more qualitative than this.

It would be interesting for this material to measure the single-particle gap in the superconducting region. This may be achieved via optical conductivity measurements. For the Luttinger liquid parameter $K_c \approx 1$, our model then predicts the ratio T_c/Δ_c to be the non-BCS value of order of 0.4.

Also in this material, T_c is very small in comparison to the Fermi energy v/a_0, so the magnetic field effects on the superconducting state should be strong. This would be an interesting experiment to perform.

3.7.2 β-Sodium Vanadate

The phase diagram (figure 3.14) of the compound β-$\mathrm{Na_{0.33}V_2O_5}$ is remarkably similar to that of $\mathrm{Sr_{14}Cu_{24}O_{41}}$. Structurally, the material is quasi-one-dimensional (figure 3.13) and contains both ladders and chains. At ambient pressure, there is a metal-insulator transition at 134K, and although the low temperature phase is charge ordered, it isn't a simple $2k_F$ charge-density wave [66]. At a lower temperature, T=22K there is a further transition into a canted-anti-ferromagnetic state. It was recently discovered [67] that under pressure, there is a superconducting state with transition temperature $T_c = 8$K. This is very interesting as it is for the stoichiometric compound without any chemical doping, and also it is the first observation of a superconducting state in the Vanadium Oxides.

It is not yet known if there is a spin-gap under high pressures above the superconducting transition temperature, but there is some evidence that this may be the case:

- By simply extrapolating the anti-ferromagnetic ordering temperature in figure 3.14, it will eventually exceed the charge gap.

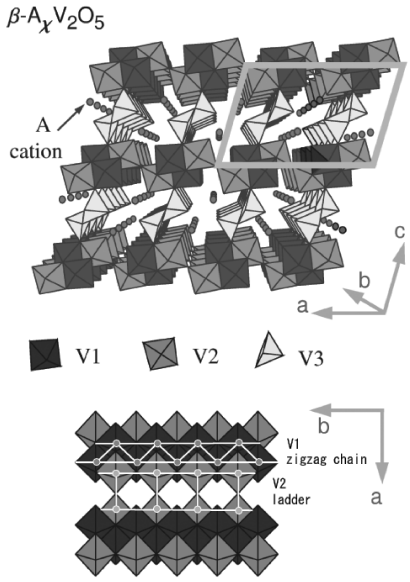

Figure 3.13: Structure of β-$Na_{0.33}V_2O_5$. After [68]. Similar to the previous section, chains and ladders are both present - this time of vanadium oxide.

.

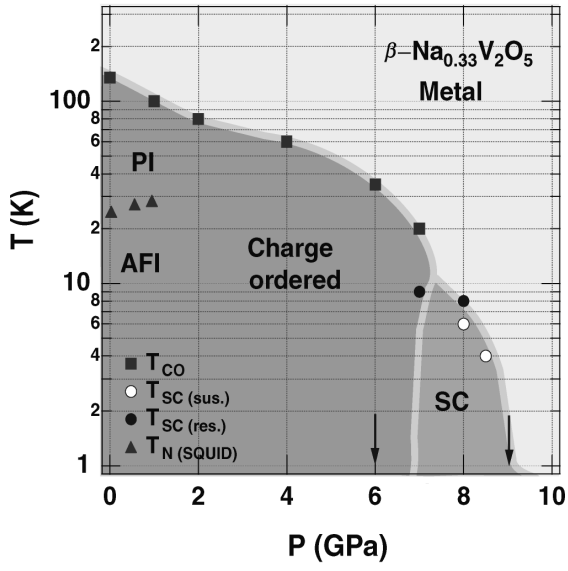

Figure 3.14: Pressure-Temperature Phase Diagram of β-$Na_{0.33}V_2O_5$. After [67]. The triangles obtained from the Neel temperature are indicative of the spin gap in the system, but this has only been measured for low pressure. The squares are the charge-ordering temperature, so representative of the charge gap, and the circles are the boundary of the superconducting phase.

- We additionally have evidence from a number of other materials that the spin gap does not significantly change with external pressure.
- The similarity between the phase diagrams 3.14 and 3.12 suggests that the superconducting state could be described by our theory.

This is a very interesting material to study experimentally, and more data should be available soon.

Chapter 4

Mott Insulators

Wisdom is knowing what to do next; virtue is doing it.

–David Star Jordan

4.1 Physical Motivation

The Bechgaard salts $TMTSF_2X$ and $TMTTF_2X$ were the first organic compounds to show superconductivity, and furthermore have a remarkably rich phase diagram showing all sorts of properties interesting to the theorist, for example metallic non-Fermi-liquids or Mott Insulators. Figure 4.1 shows the structure of the building blocks of these materials, and figure 4.2 shows a unified experimental phase diagram for these properties. For a review of these properties, see [69, 70]. However, the behaviour gets even stranger when a magnetic field is applied. The magnetoresistance in $(TMTSF)_2PF_6$ at low temperatures in its metallic state was measured in 1998 by Chashechkina and Chaikin [71] and revealed some surprising features.

The magnetoresistance showed a striking angular dependence, with large dips at the 'magic-angles' where the the ratio of the flux through two of the crystal planes is a rational number with a small denominator - Figure 4.3. Basically this means that at high fields, the

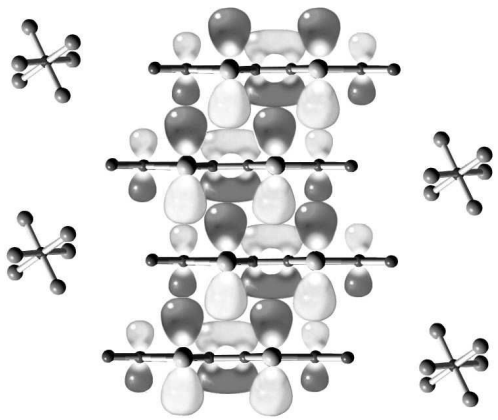

Figure 4.1: Structure (after [69])

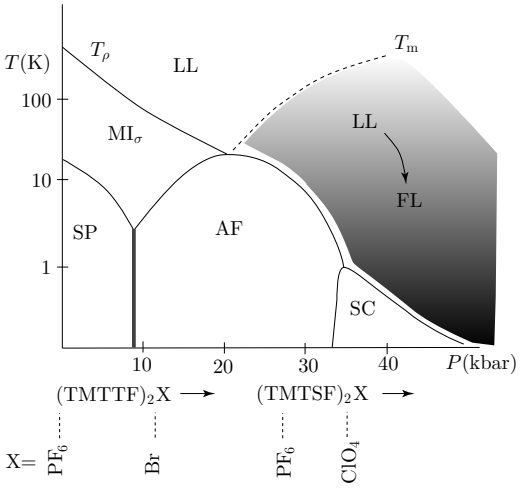

Figure 4.2: Unified experimental phase diagram for the TM compounds (from [69]). Either pressure or chemical changes (increasing pressure corresponds to going from the TMTTF to the TMTSF family and changing the anions) yields the same phases [MI: Mott insulator, LL: Luttinger liquid metal, FL: Fermi liquid metal, SP: spin-Peierls, AF: antiferromagnetic spin-density wave, SC: superconducting]. The TMTTF family is insulating at ambient pressure whereas the TMTSF family shows good metallic behaviour at room temperature.

.

magnetoresistance depends on the orientation of the field with respect to the crystal axis and not direction of current flow. Magic-angle effects had been predicted beforehand by Lebed [72, 73], but he predicted peaks in magnetoresistance at the magic angles rather than dips which are seen. Furthermore, the temperature dependence of the magnetoresistance is very curious. Without a magnetic field applied, the temperature dependence shows a conducting like behaviour ($dR/dT > 0$). As the magnetic field is applied, this turns to insulating like ($dR/dT < 0$), but at the magic angles, it returns to conducting like.

This led Chashechkina and Chaikin to propose [74] that such systems could be modelled as Mott-insulating chains which become conducting when inter-chain hopping is taken into account. A magnetic field acts to dephase this inter-chain coupling at all but the magic angles, and therefore we should obtain the metal-insulator transition as a function of angle as is seen in experiments.

To test this proposal, we choose a simple model of a one dimensional Mott Insulator [75] and treat the inter-chain coupling within the Random Phase Approximation (RPA). Although going beyond RPA as in the previous chapter would be nice, the difficulty of calculating multi-point correlation functions in the one dimensional Mott Insulator model relegate this as future work.

We start by introducing the model in the absence of the field, then show how the equations are modified when an external magnetic field is present. We then go on to calculate numerically the single particle density of states for certain choices of the parameters which are of physical interest. In the presence of interchain hopping, but the absence of the magnetic field, there is a coherent mode in the system. We show how Landau levels form in this coherent mode of the system, and see that the density of states depends strongly on the angle

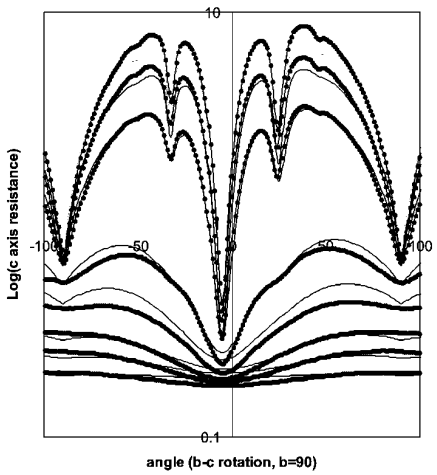

Figure 4.3: Magnetoresistance of$(TMTSF)_2PF_6$ at low temperature (T=1.2K) and high pressure (p=9.2kbar) as a function of angle of magnetic field. The c-axis is the least conducting axis, the graphs are similar for the magnetoresistance of the other axis. The different curves are for different magnetic fields, the strongest being the top curve at 7.8T. After [74].

of the applied magnetic field. However, we find that our simple model is not strong enough to reproduce the experimental results, even qualitatively. We suggest some reasons for this, and propose some additions to the model.

4.2 The Model and 1D Green's Function

The model we consider is the quasi-one-dimensional Hubbard model, a prototypical lattice model of correlated electrons:

$$\begin{aligned} H &= \sum_l H_{1D}^{(l)} + \sum_{l,m,j,\sigma} t_{lm}\, c_{j,\sigma}^{(l)\dagger} c_{j,\sigma}^{(m)} + \text{H.C.} \\ H_{1D}^{(l)} &= -t \sum_{j,\sigma} c_{j,\sigma}^{(l)\dagger} c_{j+1,\sigma}^{(l)} + \text{h.c.} + U \sum_j n_{j,\uparrow}^{(l)} n_{j,\downarrow}^{(l)} \,. \end{aligned} \tag{4.1}$$

Here l, m label chains, j labels the sites along a given chain, and we will assume we are at half filling so Umklapp processes are important. As usual, H_{1D} is the Hamiltonian of uncoupled chains and the full Hamiltonian involves adding an inter-chain hopping term to this.

The 1D retarded Green's function was calculated in the field-theory limit using the form factor method (see section 2.2.2) by Essler and Tsvelik [75]. Here, we reproduce the main points of their derivation.

The Hamiltonian 4.1 can be bosonised as in section 2.1, resulting in independent spin and charge sectors. In this case, the spin-sector is a described by a free boson and the charge sector by a sine-Gordon model (c.f. the opposite in the previous chapter):

$$\mathcal{L}_s = \frac{1}{2}\left[v_s^{-1}(\partial_\tau \Phi_s)^2 + v_s(\partial_x \Phi_s)^2\right],$$

$$\mathcal{L}_c = \frac{1}{2}[v_c^{-1}(\partial_\tau \Phi_c)^2 + v_c(\partial_x \Phi_s)^2] + \lambda \cos(\beta \Phi_c) \,, \tag{4.2}$$

where $v_s = v_F - Ua_0/2\pi$, $v_c = v_F + Ua_0/2\pi$ and $\beta^2 = 8\pi$. If we consider further density-density interactions (eg nearest neighbour repulsion) then we get the same form for the bosonised Lagrangian, but with $\beta^2 < 8\pi$.

The spin-sector is trivial as it is a free massless boson. In the charge sector, the first non-vanishing form-factor is between the vacuum and a scattering state of one spinon and one antiholon. Techniques of integrability require this form factor to be a constant [75]. Combining this with Lorentz invariance gives the first term in the form-factor expansion of the charge part of the single-particle Greens function to be (up to a numerical factor)

$$\begin{aligned} &\int_{-\infty}^{\infty} d\theta \; e^{\theta/2} \exp\left[-\Delta\tau \cosh\theta - \mathrm{i}\Delta \frac{x}{v_c} \sinh\theta\right] \\ &= \frac{\exp[-\Delta\sqrt{\tau^2 + x^2 v_c^{-2}}]}{\sqrt{v_c\tau + ix}}, \end{aligned} \tag{4.3}$$

where Δ is the single particle spectral gap which is half the gap seen in optical spectroscopy experiments. The leading corrections to this involve states containing one holon and two antiholons or vice versa and are thus of order $O(e^{-3\Delta r})$. Combining 4.3 with the free spin sector gives

$$\langle \bar{\Psi}_\sigma(x,\tau) \bar{\Psi}_\sigma^\dagger(0,0)\rangle \simeq \frac{Z_0}{2\pi} \frac{\exp[-m\sqrt{\tau^2 + x^2 v_c^{-2}}]}{\sqrt{(v_s\tau + ix)(v_c\tau + ix)}} \,, \tag{4.4}$$

where the constant $Z_0 = 0.9218$ is chosen so that the field operators satisfy the standard conformal normalisation.

This can then be Fourier-transformed to give the result for the retarded Green's function

$$\begin{aligned} G^{(R)}(\omega, q) &= -Z_0 \sqrt{\frac{2}{1+\alpha}} \frac{\omega + v_c q}{\sqrt{m^2 + v_c^2 q^2 - \omega^2}} \\ &\times \left[\left(m + \sqrt{m^2 + v_c^2 q^2 - \omega^2}\right)^2 - \frac{1-\alpha}{1+\alpha}(\omega + v_c q)^2\right]^{-\frac{1}{2}} \end{aligned} \tag{4.5}$$

where $\alpha = v_s/v_c$ and $Z_0 = 0.9218$. For spin velocity equal to charge velocity, it simplifies to

$$G_{1D}(q,\omega) = \frac{Z_0}{\omega - q}\left(1 - \frac{\Delta}{\sqrt{\Delta^2 + q^2 - \omega^2}}\right) \tag{4.6}$$

For the rest of this chapter we stick with $v_c = v_s$ for simplicity, and because the difference in charge and spin velocities is unlikely to significantly affect the properties we are interested in.

In the first approximation, we assume that the 1D Green's function in a magnetic field is not changed significantly from this.

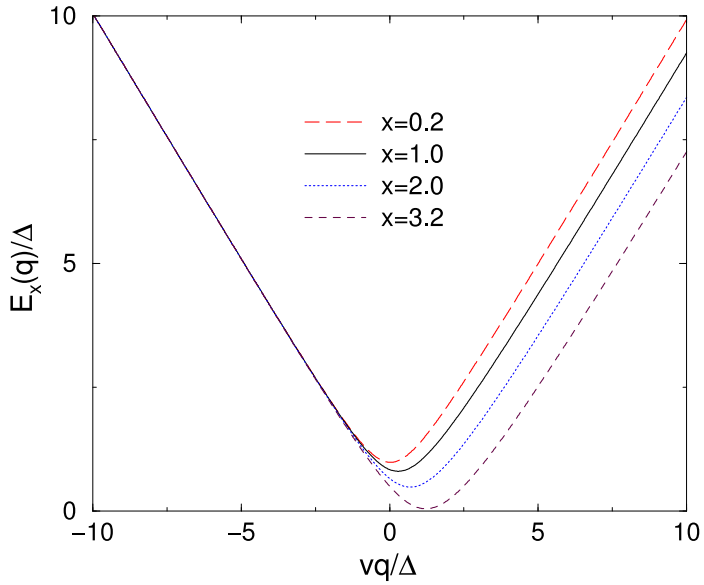

Figure 4.4: Dispersion of the coherent mode along the chain direction for several values of $x = -Z_0 t_\perp(\vec{k})$.

4.3 Inter-chain coupling and the magnetic field

4.3.1 RPA in the absence of a magnetic field

We use the usual RPA approximation (see section 3.3.2) to add our weak inter-chain hopping

$$G^{-1}(\omega; q, \vec{k}) = G_{1D}^{-1}(\omega, q) + t_\perp(\vec{k}). \tag{4.7}$$

The square-root singularity in the one-dimensional Green's function will give rise to a coherent mode in the full Greens function for arbitrarily small $t_\perp$ at

$$G_{1D}^{-1}(\omega, q) + t_\perp(\vec{k}) = 0. \tag{4.8}$$

For $t_\perp/\Delta > 3.61$, this equation has a solution for $\omega = 0$ so the coherent mode will be soft and the three-dimensional system will be a metal. This is shown in figure 4.4.

We also show in figure 4.5 the shape of the Fermi surface when the inter-chain hopping puts the Mott insulator into its metallic state. We see that we obtain little pockets of Fermi surface in this state. We should point out that there is another calculation for the same model using Dynamical Mean Field Theory (DMFT) rather than the RPA approximation [76]. This gives very different results, where the Fermi-surface ends up very close to the non-interacting system. There is no reason why one should expect these two approximations to give the same results, RPA is exact in the infinite connectivity limit, DMFT is exact in the infinite dimensional limit. It is not possible to say which result should be closer to that of a real three-dimensional system without further calculation which at this time has not been done.

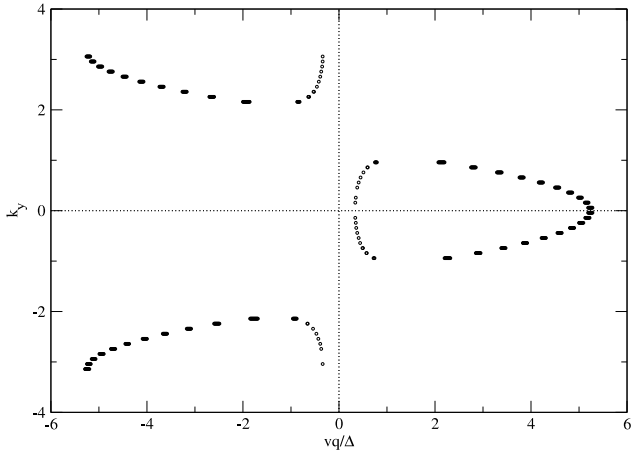

Figure 4.5: Fermi Surface from RPA calculation when the system is driven into a metallic state by the interchain coupling. We see that we get little pockets of Fermi-surface.

4.3.2 Magnetic field parallel to chain direction

The magnetic field will modify the hopping term by the Peierls factor $p \to \vec{p} - e\vec{A}/c$ [77]. We will use units where $e = c = 1$. This will give rise to an effective inter-chain hopping. Thus for an appropriate range of bare $t_\perp$, adding a magnetic field could cause a metal-insulator transition.

Choose the vector potential so that $A_x = Hy$, $A_y = 0$, $A_z = 0$. This changes $t_x \to t_x e^{\mathrm{i}Hy}$. The RPA equation thus becomes

$$\left(G_{1D}^{-1}(\omega, q) + t_x e^{\mathrm{i}H\hat{y}} + t_y\right) G(\omega; q, k_x, k_y) = 1, \tag{4.9}$$

where $\hat{y} = \partial/\partial k_y$. This is equivalent to the Hofstadter problem of an electron on a two dimensional lattice in a magnetic field. The $t_\perp$ in the denominator of the RPA equation is replaced by its eigenvalues in the Hofstatdter problem [78]. For $t_x \approx t_y$, these eigenvalues have a very intricate fractal like structure, however this rapidly disappears as the system becomes more anisotropic. The eigenvalues of the Hofstadter problem are plotted in figs 4.6, 4.7 and 4.8.

The properties of the coupled Mott insulators then depend on these eigenvalues. In particular, there will be a strong dependence on the largest eigenvalue: if this is above the single chain gap then the electron-like propagating mode in the chain direction, given by $G_{1D}^{-1}(\omega, q) = E_{\mathrm{Hofstadter}}$ will have low energy excitations. However as the strength of the magnetic field changes, the largest eigenvalue also changes, and if this falls below the gap, then the coherent electron-like mode will be gapped, which will drastically affect the transport properties.

The possibility of seeing any of this fractal structure within coupled Mott insulators is remote, as the eigenvalues will be smoothed out by dispersion in the chain direction, as well

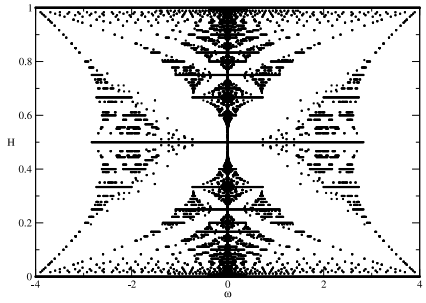

Figure 4.6: Eigenvalues against magnetic field, $t_x/t_y = 1$. There is an intricate fractal-like pattern.

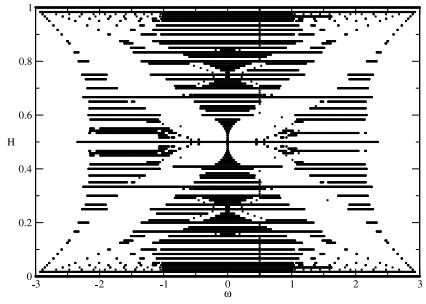

Figure 4.7: Eigenvalues against magnetic field, $t_x/t_y = 0.5$.

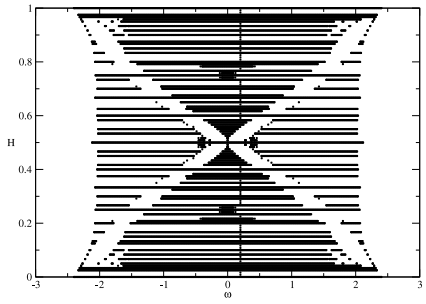

Figure 4.8: Eigenvalues against magnetic field, $t_x/t_y = 0.2$. Most of the fine structure has gone.

as by any anisotropy in two interchain hopping terms. This section is included mainly as a model curiosity than as any experimental predictions.

4.3.3 Magnetic field perpendicular to chain direction

In the experiments, the magnetic field was perpendicular to the chain direction. In this case, we pick the vector potential $A_x = H_y z$, $A_y = -H_x z$, $A_z = 0$. In an external magnetic field, momentum is no longer a good quantum number, so the Green's function becomes a matrix, $G(\omega, k_\perp; q, q')$.

The modified RPA equation is

$$\begin{aligned} & G_{1D}^{-1}(\omega, q) G(\omega, k_\perp; q, q') \\ - \; & t_y e^{\mathrm{i}k_y} G(\omega, k_\perp; q - H_x, q') \\ - \; & t_y e^{-\mathrm{i}k_y} G(\omega, k_\perp; q + H_x, q') \\ - \; & t_x e^{-\mathrm{i}k_x} G(\omega, k_\perp; q - H_y, q') \\ - \; & t_x e^{\mathrm{i}k_x} G(\omega, k_\perp; q + H_y, q') \\ & = \delta(q - q'). \end{aligned} \tag{4.10}$$

For H_x/H_y rational, this is a matrix equation and can be solved numerically. In order to control the singularities in numerics, the 1D Green's function is modified by

$$G_0^{-1} \to G_0^{-1} + \mathrm{i}\eta, \tag{4.11}$$

where it is understood that $\eta \to 0+$. At a qualitative level, we can think of η as a temperature like broadening parameter.

4.4 Density of states

The easiest physical quantity to investigate is the single particle density of states (DoS)

$$\rho(\omega) = -\Im \int dk_\perp dq G(\omega, k_\perp; q, q). \tag{4.12}$$

In the absence of inter-chain coupling, the density of states is zero below $\omega = \Delta$. In the presence of inter-chain coupling, a coherent mode forms in this region and the Mott gap is filled in. In the presence of a magnetic field, this coherent mode splits into Landau levels, as shown in figure 4.9.

The finite width of the Landau levels is due to the third dimension coupling. With a cosine dispersion, their shape is given by

$$\rho(\omega) = \sum_{\omega_{LL}} \frac{1}{\sqrt{t_z^2 - (\omega - \omega_{LL})^2}}, \tag{4.13}$$

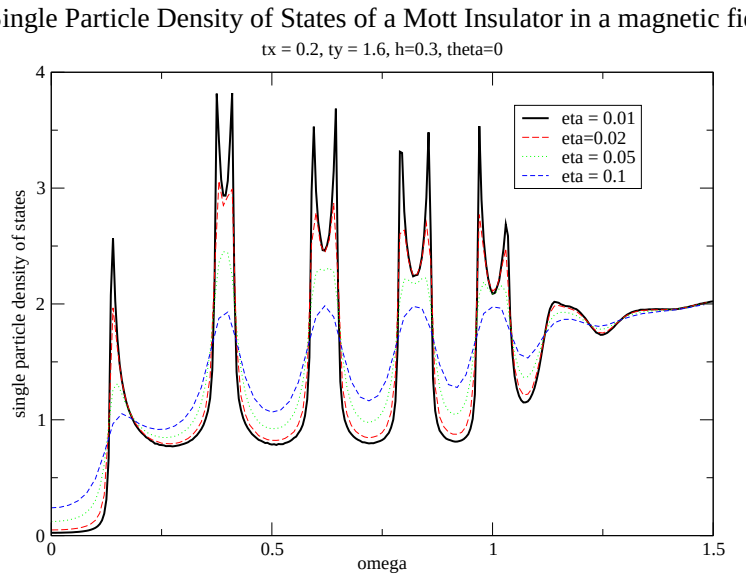

Figure 4.9: The variation of the density of states with the broadening parameter η.

where the sum is over the positions of the Landau levels ω_{LL}. This is clearly demonstrated in figure 4.10 where the third dimension hopping is less than the Landau level splitting.

We can now see how changing the angle of the magnetic field influences the relative width of each Landau level - figure 4.11. The hopping parameters t_x and t_y here are chosen to give an anisotropy similar to the experimental value, and have a total magnitude that puts the system just on the metallic side of the metal-insulator transition in the absence of the external field.

The question of low temperature DC transport depends on the density of states at the Fermi-level $\omega = 0$. This is plotted in figure 4.12 as a function of angle of the applied field. We see a very strong variation with the angle. We see that this variation becomes even stronger as the broadening variable $\eta \to 0$ in figure 4.13. We also see that for lower magnetic fields, the shape becomes more interesting. Some lower magnetic fields are plotted in figure 4.14.

In figure 4.16 we can how the DoS varies with η at lower magnetic fields. Where the density of states rises with decreasing η is a metal and where it decreases with decreasing η is an insulator. So on this figure we can clearly see metal-insulator transitions as the angle of the magnetic field is varied.

4.5 Interpretation and Extensions to the model

The results of this simplified model can be interpreted as follows:

- The one-dimensional chains are Mott insulators, with a single-particle gap, and no electron-like excitations.

- Adding interchain hopping to these chains generates a coherent mode. Depending on the strength of the interchain terms, this mode may be gapped, or it may become soft in

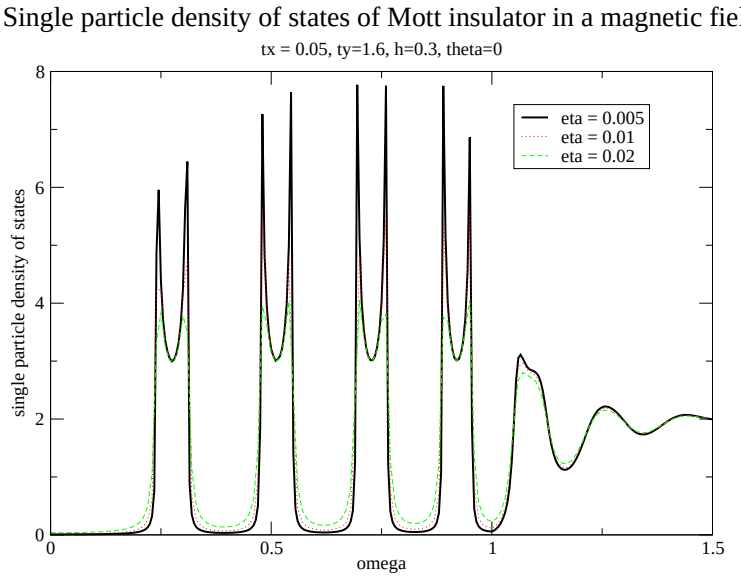

Figure 4.10: Demonstrating the shape of the density of states in the limit of Landau-level splitting greater than the third dimension coupling

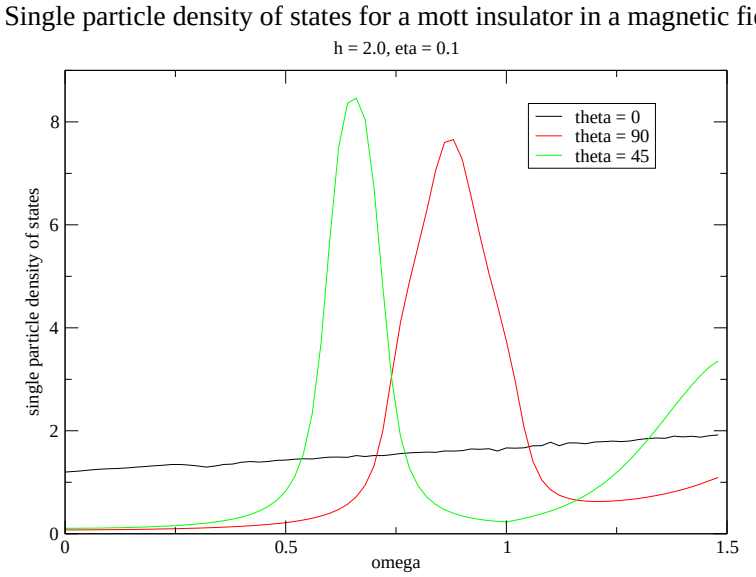

Figure 4.11: The variation of the density of states with angle of magnetic field in a large magnetic field.

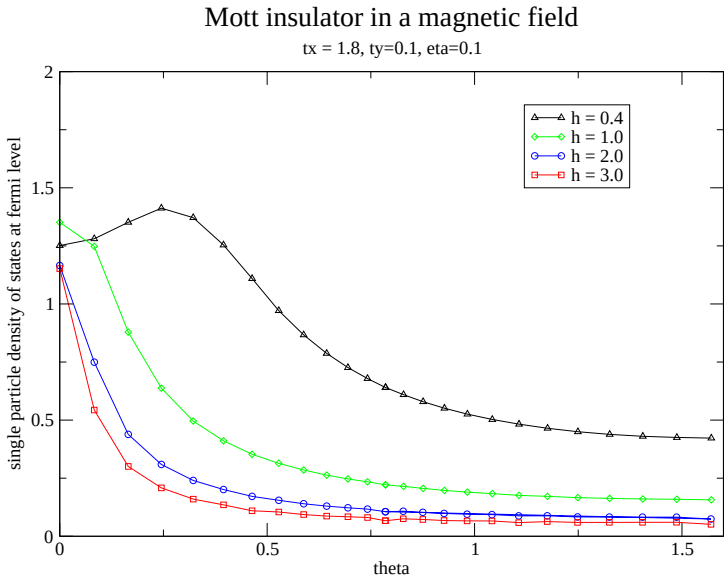

Figure 4.12: The variation of the density of states at the Fermi level with angle of magnetic field.

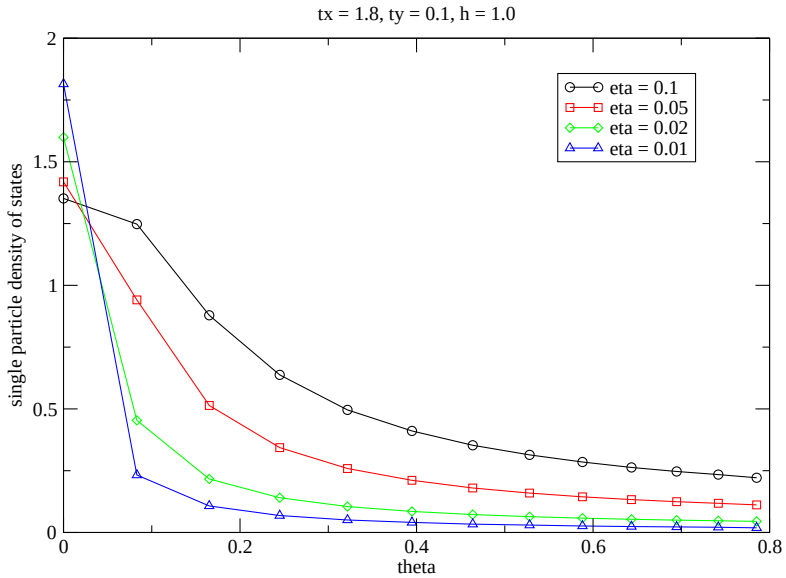

Figure 4.13: The variation of the density of states at the Fermi level with angle of magnetic field.

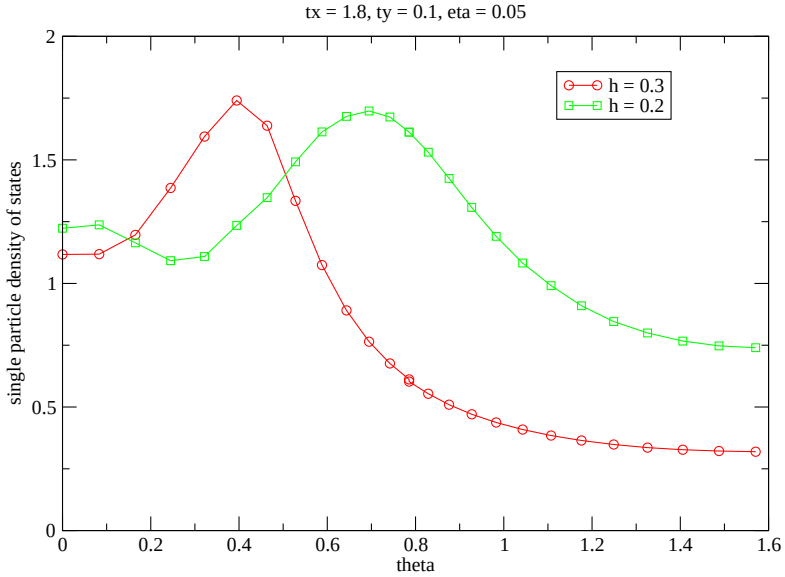

Figure 4.14: The variation of the density of states at the Fermi level with angle of magnetic field.

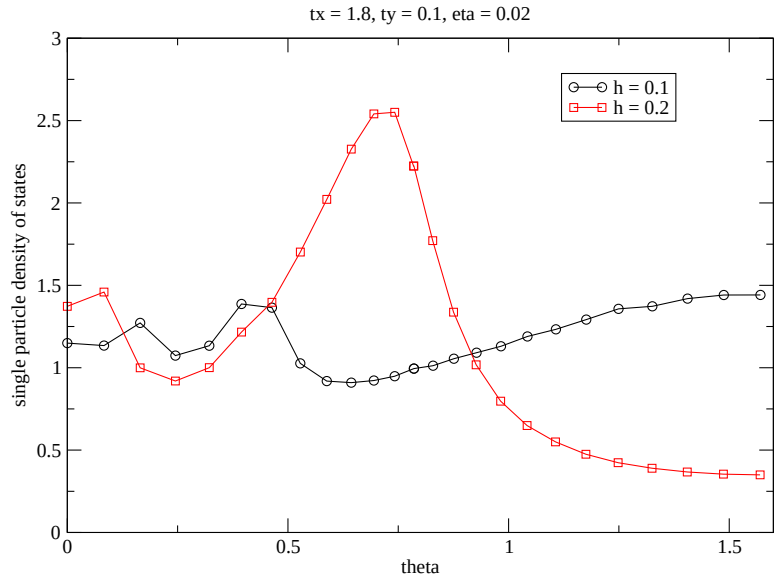

Figure 4.15: The variation of the density of states at the Fermi level with angle of magnetic field.

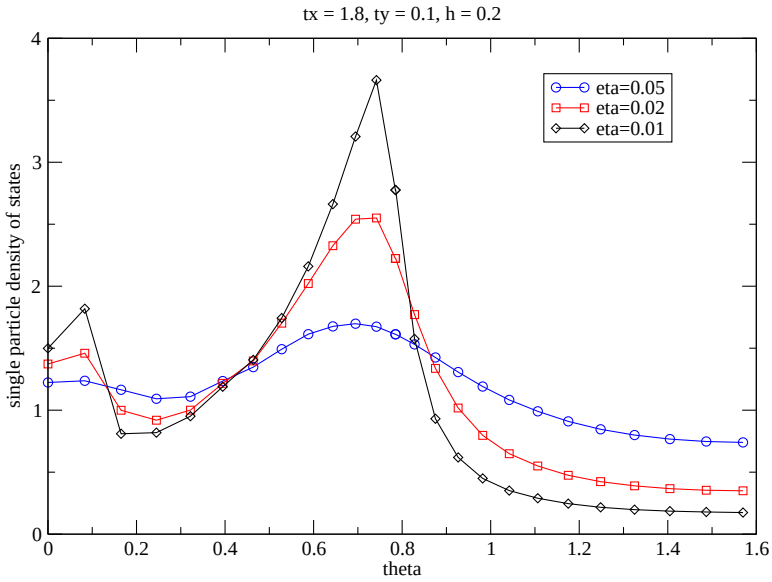

Figure 4.16: The variation of the density of states with magnetic field at different broadening parameters

which case we have a metal-insulator transition.

- Adding a strong magnetic field perpendicular to the chain direction causes this mode to split into Landau 'bands' (because we are in a 3D system, not 2D). When looking at simply the density of states and integrating over all momenta, the position of these bands depend both on the strength and the angle of the magnetic field. This can cause a metal-insulator transition as the angle varies.

- This metal-insulator transition however depends on the exact positions of the Landau levels which in turn depends on the strength of the magnetic field and so will not reproduce magic angle effects where the position of the dips depend only on the angle and not on the strength of the magnetic field.

It may be that looking at the single particle density of states is too simplistic a view and if we start looking at conductivity then the magic angle effects will occur. However, it is not obvious that one would be able to reproduce the experimental results with this model. The idea that the magnetic field dephases the interchain hopping and therefore affects a metal insulator transition is correct. However, the material has very strong anisotropy in the b and c directions and within the RPA approximation, this means there is very little effect of the third coupling as they are in some sense just summed together. Going beyond RPA takes account of hopping off a chain and back onto the same chain. So here, the changes in phase in hopping from the magnetic field become much more important so this may reproduce magic angle effects. However, the problems of calculating the multi-particle correlation functions in the 1D case along with the extra difficulty of applying interchain perturbation theory in a

magnetic field means that this is a difficult problem for future thought. The results of this chapter however show that the idea is promising, although we don't yet have the best way to tackle this problem.

Chapter 5

The quantum Ising model

The power of accurate observation is frequently called cynicism by those who don't have it.

–George Bernard Shaw

The Ising model is a generic model for many quantum and classical systems. Besides extensive applications to spin systems (here we refer the reader to [79, 80, 81]), the model is also used to describe interacting electric dipoles (like in systems with orbital degrees of freedom [82]) or arrays of interacting Josephson junctions (see, for example [83]). Reduced dimensions are the most interesting because here the model exhibits strongest correlations.

In one dimension the quantum Ising model (see equation 5.1 below) is exactly solvable by means of Jordan-Wigner transformation which converts the spin Hamiltonian into a Hamiltonian of non-interacting fermions. In general the spectrum has a gap which is closed when the transverse magnetic field is equal to the exchange integral ($g = 0$). There is also an exact solution when the magnetic field has a z-component, although only when the x-component is equal to J [84]. This solution predicts a rich spectrum with as many as eight particles and a hidden E_8 symmetry. An interesting question is whether some of this fascinating physics may survive in realistic systems which are almost never truly one-dimensional. In this chapter, we will introduce a quasi-one-dimensional quantum Ising model, and show that in certain regions of parameter space, one-dimensional effects are clearly visible [2].

We begin by reviewing the many fascinating properties of the one dimensional quantum Ising model. We then introduce the quasi-one-dimensional model and show how the interchain coupling as usual gives rise to a finite temperature ordered phase. We calculate the phase diagram within the RPA approximation and then go on to look at correlation functions in the ordered phase. We discover that deep in the ordered phase, the correlation functions are very one-dimensional in character, allowing the possibility of seeing some of the physics of the quantum Ising chain in real three dimensional materials. We show that Sodium Vanadate is a good candidate material for description by our model, and finish off by a brief aside linking our work to the three dimensional classical Ising model.

5.1 The one dimensional quantum Ising model

5.1.1 The model at $T = 0$

A full review of all the work done on the one-dimensional quantum Ising model is the subject of an entire book by itself, see for example [79, 80, 81]. Here we give a concise, self contained but by no means complete review of the model, concentrating in particular on the results that will be useful later.

The quantum Ising model was first introduced by De Gennes [85] to model the order-disorder transition in double-well ferroelectric materials, for example KH_2PO_4. Each proton of the hydrogen bond can occupy one of two minima of a double well created by the oxygen atoms. These two possibilities are are represented by a pseudo-spin at each site, with $\sigma^z = +1/2$ corresponding to one of the minima and $\sigma^z = -1/2$ the other. The operator σ^x is then a tunnelling term between the two minima; including also electrostatic dipolar interaction between neighbouring sites gives the effective low-energy pseudo-spin Hamiltonian

$$H_{1D} = -J \sum_n \left\{ \sigma_n^z \sigma_{n+1}^z + (1+g)\sigma_n^x \right\}. \tag{5.1}$$

The model shows competition between the ordering term J and the tunnelling term $J(1+g)$.

This model has a hidden symmetry, involving dual fields. Define a dual lattice $\{n+1/2\}$ with fields defined by

$$\begin{aligned} \mu_{n+1/2}^z &= \prod_{j=1}^{n} \sigma_j^x, \\ \sigma_n^z &= \prod_{j=1}^{n-1} \mu_{j+1/2}^x, \end{aligned} \tag{5.2}$$

so that

$$\begin{aligned} \mu_{n-1/2}^z \mu_{n+1/2}^z &= \sigma_n^x, \\ \sigma_n^z \sigma_{n+1}^z &= \mu_{n+1/2}^x. \end{aligned} \tag{5.3}$$

In terms of the new variables, the Hamiltonian preserves its form

$$H_{1D} = -J(1+g) \sum_n \left(\mu_{n-1/2}^z \mu_{n+1/2}^z + \frac{1}{1+g} \mu_{n+1/2}^x \right). \tag{5.4}$$

We see that the self-duality point is $g = 0$ - as we will show later this corresponds to a quantum phase transition. The μ fields are sometimes known as the disorder operators.

The model can be solved by a Jordan-Wigner transformation. We write

$$\sigma_n^x = 2a_n^\dagger a_n - 1,$$

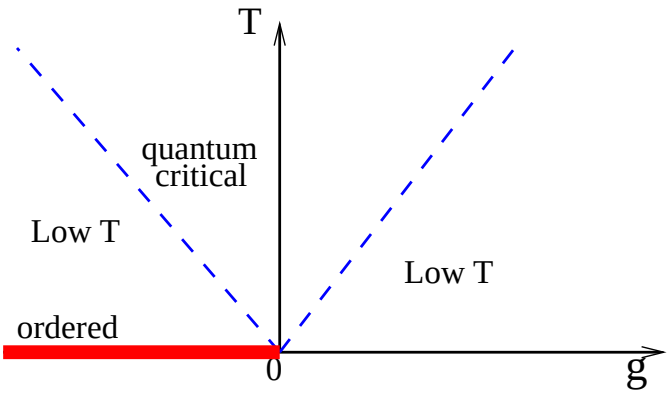

Figure 5.1: Phase Diagram of model (5.1). At $T = 0$ there is an ordered phase for $g < 0$ which has $\langle \sigma^z \rangle \neq 0$. For $T = 0$ and $g > 0$, the system is a quantum paramagnet, and by the duality 5.2, we have $\langle \mu^z \rangle \neq 0$ in this region. At finite temperature, long range order is forbidden by the Mermin Wagner theorem. There are crossovers (given by the dashed lines) where the single-particle energy gap $\Delta \sim T$ between the low-temperature behaviour and a universal quantum critical regime.

$$\sigma_n^z \;=\; (-1)^{n-1} \exp\left[\mathrm{i}\pi \sum_{j=1}^{n-1} a_j^\dagger a_j \right] (a_n^\dagger + a_n), \tag{5.5}$$

where the Fermi operators a satisfy the usual anti-commutation relations

$$\left\{ a_n, a_m^\dagger \right\} = \delta_{nm}, \quad \{a_n, a_m\} = 0. \tag{5.6}$$

The Hamiltonian becomes quadratic

$$H_{1D} = J \sum_n \left[-(a_n^\dagger - a_n)((a_{n+1}^\dagger + a_{n+1}) + (g+1)(a_n^\dagger - a_n)(a_n^\dagger + a_n) \right], \tag{5.7}$$

which can be easily diagonalised to give the spectrum

$$\epsilon(k) = 2J\sqrt{g^2 + 4(g+1)\sin^2(k/2)}. \tag{5.8}$$

We see that this is gapless at $g = 0$ where the model is critical. For $g < 0$ the model is an a 'quantum ordered' phase where $\langle \sigma^z \rangle \neq 0$ at $T = 0$. For $g > 0$ it is a 'quantum disordered phase' where in fact $\langle \mu^z \rangle \neq 0$ at $T = 0$. The phase diagram is shown in figure 5.1.

Although we have mapped the model on to free fermions and thereby solved it exactly, it is still not easy to extract spin-spin correlation functions because our transformation was non-local in space. The correlation functions are most easily calculated in terms of a form factor expansion - see section 2.2.2 and also [86].

The relevant minimal form factors were calculated in section 2.2.2:

$$F_{min}^{(n)}(\theta_1, \ldots, \theta_n) = \prod_{i<j} \tanh\left(\frac{\theta_i - \theta_j}{2} \right), \tag{5.9}$$

where n is odd for correlators of σ^z and even for correlators of μ^z (in the disordered phase).

To lowest order, the correlation function is

$$\chi_{1D}(\omega, k) = \frac{Z_0(ma_0/v)^{1/4}}{\omega^2 - (vk)^2 - m^2}, \tag{5.10}$$

where $Z_0 = 1.8437$ is fixed by the conformal normalisation 5.21 of the field operators. This is valid for small ω. In real space, it corresponds to long distance asymptotics

$$\chi_{1D}(r) = \frac{Z_0(ma_0/v)^{1/4}}{\pi} K_0(mr) + O(e^{-3r}) \tag{5.11}$$

The next term in the form factor expansion, the three particle contribution can be represented as

$$\begin{aligned} &\frac{\chi_3(s^2)}{\chi_1(s=0)} = \\ &\frac{1}{3}\int \frac{dx}{4\pi}\int \frac{dy}{4\pi}\frac{f(2x)f(y+x)f(y-x)}{(s/m)^2 - [1+4\cosh x(\cosh x + \cosh y)]}, \\ &f(x) = \tanh^2(x/2), \end{aligned} \tag{5.12}$$

where $s^2 = \omega^2 - (vk)^2$ and is plotted in Fig. 5.2. The imaginary part of this term (which is the contribution to the structure factor) and of all higher terms in the series is zero below $\omega = 3m$, however all terms in the expansion contribute towards the real part at $\omega = 0$. Fortunately the contribution from higher order terms[1] are negligible at small s (see e.g. [88]). We see explicitly in this case that $\chi_3(s=0)/\chi_1(s=0) = 0.0002$ so that 5.10 is indeed a very good approximation for small s.

5.1.2 The model at finite temperature - scaling behaviour

The correlation functions at finite but low temperature can be well approximated[79] by adding the quantum dephasing time, τ_ψ, into equation 5.10:

$$\chi_{1D}(\omega, k) = \frac{Z_0(ma_0/v)^{1/4}}{(\omega + \mathrm{i}/\tau_\psi)^2 - (vk)^2 - m^2}. \tag{5.15}$$

[1] In fact, for this model it turns out one can sum all the terms in the series and write the result exactly in terms of the solution of a Painleve equation [86]:

$$\langle\sigma(r)\sigma(0)\rangle = \sinh\frac{\chi(s)}{2}\exp\left\{-\frac{1}{4}\int_s^\infty duu\left[\left(\frac{d\chi}{du}\right)^2 - \sinh^2\chi\right]\right\} \tag{5.13}$$

where s is the scaling variable $s = mr/2$ and $\chi(s)$ is a solution of the radial sinh-Gordon equation

$$\frac{d^2\chi}{ds^2} + \frac{1}{s}\frac{d\chi}{ds} = 2\sinh(2\chi) \tag{5.14}$$

which under the transformation $\eta = e^{-\chi}$ is equivalent to the Painleve III equation [87]. The ability to write correlation functions in terms of non-linear differential equations seems to be specific to this model, and although a very nice result, is not that useful in terms of extracting low energy behaviour.

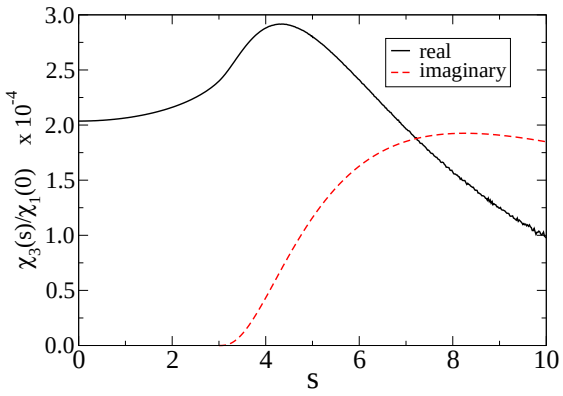

Figure 5.2: The three particle contribution to the dynamical susceptibility for a single chain normalised to the one-particle contribution at $s = 0$.

The quantum dephasing time can be estimated in a semi-classical approximation. For an excitation, the decay rate will be given by

$$\frac{1}{v_k \tau_k} \sim e^{-\epsilon_k/T}. \tag{5.16}$$

The dephasing time is given by summing over all of these

$$\begin{aligned} 1/\tau_\psi &= \frac{2}{\pi}\int_0^\infty dk \frac{d\epsilon_k}{dk} e^{-\epsilon_k/T} \\ &= \frac{2}{\pi}\int_m^\infty d\epsilon_k e^{-\epsilon_k/T} \\ &= (2T/\pi)\mathrm{e}^{-m/T}. \end{aligned} \tag{5.17}$$

See [79] for a more detailed calculation.

5.1.3 The critical model in a magnetic field

Adding an external field to the model 5.1 gives

$$H_{1D} = \sum_n \left\{ -J_\parallel \left[\sigma^z(n)\sigma^z(n+1) + (1+g)\sigma^x(n)\right] + h\sigma^z(n) \right\}, \tag{5.18}$$

which turns out to be integrable at $g = 0$ [84]. The details are messy, but it can be shown that the model has a hidden E_8 symmetry, and an infinite number of conserved charges. The solution has eight different particles, whose masses and weights were calculated in [89] and are listed in table 5.1.

m_i/m_1	Z_i	m_i/m_1	Z_i
1.000	0.247159	2.956	0.0021898
1.618	0.0690172	3.218	0.0011328
1.989	0.0209579	3.891	0.0001623
2.405	0.0122653	4.783	0.0000055

Table 5.1: The masses and weights of the particles of the one-dimensional quantum Ising model in a magnetic field (after [89]). The first three particles lie below the incoherent continuum which begins at $\omega = 2m_1$.

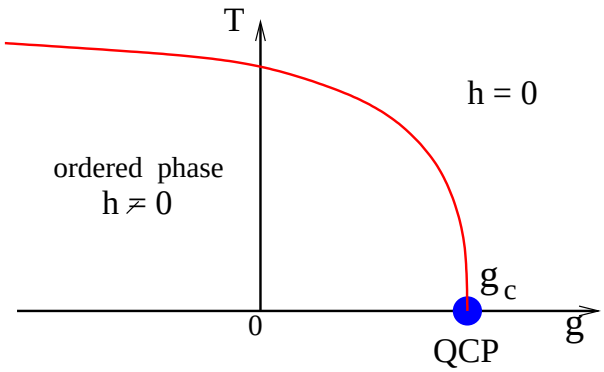

Figure 5.3: Expected Phase Diagram of model (5.20); the order parameter $h \sim \langle \sigma^z \rangle$. Estimates of g_c and $T_c(g = 0)$ are given by equation 5.27 and equation 5.26 respectively. In the vicinity of $g = 0, T = 0$ the physics is well described by model 5.18.

5.2 The quasi-one-dimensional model

Now we go on to consider the quasi-one-dimensional (meaning as usual weakly coupled one-dimensional chains) quantum Ising model described by the following Hamiltonian:

$$H = \sum_j H_{1D}^{(j)} + \sum_{i,j,n,m} J_{nm}(i-j)\sigma_i^z(n)\sigma_j^z(m), \tag{5.19}$$

$$H_{1D}^{(j)} = -J_{\parallel} \sum_n \left\{ \sigma_j^z(n)\sigma_j^z(n+1) + (1+g)\sigma_j^x(n) \right\}, \tag{5.20}$$

where i, j label the chains, n, m label the sites on the chain and σ are the Pauli spin operators. For simplicity we discuss the case where $J_{nm}(i-j) = J_{\perp}(i-j)$ if $n = m$ and 0 otherwise, although the extension to the more general case follows trivially.

We would expect a non-zero inter-chain coupling to extend the ordered region to finite temperatures and to shift the critical coupling to $g \neq 0$ as shown schematically in figure 5.3.

The spectrum and dynamics of the model close to the transition line are very well understood [90]. The transition itself falls into the 3D Ising model universality class and the Quantum Critical Point (QCP) falls into the 4D Ising model universality class. We concentrate our attention on the region of phase diagram well below the transition line where new non-universal physics can be found. We will demonstrate that non-trivial physical effects are possible in this region.

Although model 5.20 is a lattice model, we will be working in the field theoretic limit where we fix the normalisation of the magnetisation operator by the standard conformal field theory condition:

$$\chi_{1D}(\tau, x) = \langle \sigma(\tau, x)\sigma(0)\rangle = \frac{(a_0/v)^{1/4}}{|r|^{1/4}},\ |r| \to 0, \tag{5.21}$$

where $r^2 = \tau^2 + (x/v)^2$, τ is the Matsubara time, $v = J_\parallel a_0$ is the on-chain velocity and a_0 is the lattice spacing in the chain direction.

There are three energy scales in this problem: the on chain coupling $J_\parallel$, the spectral gap for a single chain $m = |g|J_\parallel$, and the inter-chain coupling $J_\perp$. In order to treat the model as weakly coupled chains we must have $J_\perp \ll J_\parallel$ and in order to apply the continuous limit field theoretic techniques to solve the uncoupled chains, we must have $m \ll J_\parallel$. However, m and $J_\perp$ can both be of the same order of magnitude.

5.2.1 The Phase Diagram

To estimate the critical temperature, we use the RPA to calculate the three dimensional susceptibility

$$\chi(\omega, k; \mathbf{k}_\perp) = [\chi_{1D}^{-1}(\omega, k) - J_\perp(\mathbf{k}_\perp)]^{-1}, \tag{5.22}$$

and then look for $\omega = 0$ divergences in the correlation function which signify a developing instability. In this expression, χ_{1D} is the susceptibility of a single chain:

$$\chi_{1D}(\omega, k) = -\mathrm{i}\sum_n \int_0^\infty dt \mathrm{e}^{\mathrm{i}\omega t - \mathrm{i}kn}\langle[\sigma^z(t, n), \sigma^z(0, 0)]\rangle. \tag{5.23}$$

We begin by considering the line $g = 0$ where the uncoupled chains are critical. We showed in section 2.3 that at finite temperature the spin-spin correlation function 5.21 becomes

$$\chi_{1D}(\tau, x) = \left[\frac{(\pi T a_0/v)^2}{\sinh(\pi T(x/v - \mathrm{i}\tau))\sinh(\pi T(x/v + \mathrm{i}\tau))}\right]^{1/8}. \tag{5.24}$$

The Fourier transform (5.23) gives the dynamic susceptibility [91]

$$\chi_{1D}(\omega = 0, k = 0) = \frac{a_0}{v}(2\pi T a_0/v)^{-7/4}\sin\frac{\pi}{8}B^2(1/16, 7/8), \tag{5.25}$$

where $B(x, y) = \Gamma(x)\Gamma(y)/\Gamma(x+y)$ is the Beta function[2]. From equation 5.22 we extract the transition temperature:

$$T_c/J_\parallel = 2.12\left[\frac{z_\perp J_\perp}{J_\parallel}\right]^{4/7}. \tag{5.26}$$

Now let us estimate the position of the Quantum Critical Point (QCP) on the g axis.

[2]Note that although the equation contains the rather ill-defined lattice spacing, a_0, it is always in the combination $v/a_0 = J$ meaning that this equation relates the static susceptibility to the bare parameters independent of any high energy cut-off as it must for a well defined theory.

Again we use the RPA equation (5.22) substituting in the expression for the dynamical spin susceptibility 5.10 of the off-critical Ising model. We can see that the QCP where $T_c \to 0$ is given by the condition

$$g_c \approx 1.42(z_\perp J_\perp/J_\parallel)^{4/7}. \tag{5.27}$$

The RPA expression for the susceptibility at the QCP is

$$\chi(\omega, k; \mathbf{k}_\perp) \sim \frac{1}{\omega^2 - (vk)^2 - (\mathbf{v}_\perp \mathbf{k}_\perp)^2}, \tag{5.28}$$

where $\mathbf{v}_\perp = (1/2) Z_0 g^{1/4} J_\parallel \left(\mathrm{d}^2 J_\perp(\mathbf{k}_\perp = 0)/\mathrm{d}\mathbf{k}_\perp^2 \right)$. In the vicinity of QCP the low-energy behaviour of the quantum Ising model is universal and falls in the universality class of the (d+2)-dimensional classical Ising model, where d is the number of transverse dimensions. Since $d = 2$ corresponds to the upper critical dimension of that model, the fluctuations give only logarithmic corrections to RPA in three dimensions.

Near the critical point, we can examine the shape of the phase boundary. For low temperature, the correlation functions at finite temperature can be well approximated by 5.15. The RPA then gives the condition for a singularity at $\omega = 0$, $k = 0$ as

$$m^2 + 1/\tau_\psi^2 = Z_0 J_\parallel J_\perp g^{1/4}, \tag{5.29}$$

so the transition temperature in the vicinity of the critical point is approximately

$$\begin{aligned} T_c &= \frac{m}{\ln(1/y) - \ln\ln(1/y)}, \\ y &= \frac{\pi}{2} \left(Z_0 (J_\perp/J_\parallel) g^{-7/4} - 1 \right)^{1/2}. \end{aligned} \tag{5.30}$$

For $g < 0$, uncoupled chains are completely ordered at $T = 0$, and at $T > 0$ and m not too small there is order on a length scale

$$\xi_c = v(2mT/\pi)^{-1/2} e^{m/T}. \tag{5.31}$$

A crude estimate for the transition temperature can be is given by

$$\frac{J_\perp}{T_c} \left(\frac{\xi_c(T_c)}{v/m} \right)^2 \sim 1, \tag{5.32}$$

which gives

$$T_c \approx \frac{2m}{\ln(m/J_\perp)}. \tag{5.33}$$

5.2.2 Dispersion in the ordered phase

In the ordered state expression 5.23 has to be modified. Namely, one has to replace χ_{1D} by the dynamical susceptibility calculated in the presence of an effective magnetic field generated by the neighbouring chains [92]. In other words, in calculating χ_{1D} one has to use the following

Hamiltonian:

$$H_{1D} = \sum_n \left\{ -J_\parallel \left[\sigma^z(n)\sigma^z(n+1) + (1+g)\sigma^x(n) \right] + h\sigma^z(n) \right\}, \tag{5.34}$$

with the self-consistency relation

$$h = J_\perp(q=0)\langle\sigma^z\rangle. \tag{5.35}$$

Now we go on to calculate the dispersion and spectrum within the ordered phase, where we have to consider $h \neq 0$. Model 5.34 is exactly solvable only at $g = 0$ [84]. As we have mentioned, the spectrum consists of eight particles which are listed in table 5.1. The contributions to the dynamical susceptibility for small ω decline quickly with the growth of the particle mass and the decrease in spectral weight of the mode. Therefore the magnetic susceptibility at $T = 0$ can be well approximated by keeping only the first three poles below the incoherent continuum

$$\chi_{1D}(s) = \left(\frac{4m_1^2}{15\pi J_\parallel h} \right)^2 \sum_{i=1}^{3} \frac{Z_i}{s^2 - m_i^2}, \tag{5.36}$$

with s defined as before. In this model, the mass scale is given by[93]

$$\begin{aligned} m_1(h)/J_\parallel &= \alpha_1 (h/J_\parallel)^{8/15}, \\ \alpha_1 &= 4.40490858, \end{aligned} \tag{5.37}$$

and the single-particle expectation value is

$$\begin{aligned} \langle\sigma^z(0)\rangle &= \alpha_2 (h/J_\parallel)^{1/15}, \\ \alpha_2 &= 1.07496. \end{aligned} \tag{5.38}$$

The self-consistency relations 5.35 therefore give

$$\begin{aligned} h/J_\parallel &= \left[\alpha_2 J_\perp(0)/J_| \right]^{15/14}, \\ m/J_\parallel &= \alpha_1 \left[\alpha_2 J_\perp(0)/J_\parallel \right]^{4/7}. \end{aligned} \tag{5.39}$$

In the RPA 5.22, the dispersion is given by the condition

$$\begin{aligned} \frac{1}{\tilde{J}_\perp} &= \sum_i \frac{Z_i}{s^2 - m_i^2}, \\ \tilde{J}_\perp &= \left(\frac{4m_1^2}{15\pi h} \right)^2 J_\perp = \alpha_3 m_1^2 \frac{J_\perp(\mathbf{k}_\perp)}{J_\perp(0)}, \end{aligned} \tag{5.40}$$

where the final relation is obtained from the self-consistent relations with $\alpha_3 = (4/15\pi)^2\alpha_1^2/\alpha_2 =$

0.130. To second order in $J_\perp$ this is solved to give

$$s^2/m_1^2 = m_i^2/m_1^2 + Z_i \tilde{J}_\perp \left[1 + \sum_{j\neq i} \frac{Z_j m_1^2 \tilde{J}_\perp}{m_i^2 - m_j^2}\right]. \tag{5.41}$$

In numerical values this gives for the first three modes

$$(s/m)^2 \approx \begin{cases} 1.0 + 0.032 J_\perp(\mathbf{k}_\perp)/J_\perp(0), \\ 2.618 + 0.009 J_\perp(\mathbf{k}_\perp)/J_\perp(0), \\ 3.956 + 0.003 J_\perp(\mathbf{k}_\perp)/J_\perp(0). \end{cases} \tag{5.42}$$

The relative weights of each mode are not significantly changed from those for the pure one-dimensional case.

It is remarkable how weak the dispersion in the perpendicular direction is, the ordered phase remains very one-dimensional in character even when $J_\perp/J_\parallel$ is not very small.

We can obtain some results slightly away from the integrable lines. In the neighbourhood of the QCP where h is small, the dynamic susceptibility is given by 5.10 with the mass replaced by [94]

$$m \to m[1 + (h/J_\parallel)^2 + O(h^4)]. \tag{5.43}$$

For small h, we must also have

$$\langle\sigma\rangle = \chi(\omega = 0, k = 0)h, \tag{5.44}$$

which combined with the mean-field condition (5.34) gives

$$\frac{h}{J_\parallel} = \sqrt{\frac{1}{g\left[J_\parallel/(Z_0 J_\perp(0))\right]^{4/7}} - 1}, \tag{5.45}$$

$$m/J_\parallel = \left(Z_0 J_\perp(0)/J_\parallel\right)^{4/7}. \tag{5.46}$$

Here, the dispersion in the perpendicular direction is much stronger than in 5.42. It is given by 5.28 at the QCP; in the vicinity of g_c the gap is given in the ordered phase by $m \sim (g_c - g)^2$, to be contrasted with $m \sim (g - g_c)$ at $g > g_c$.

Our results indicate that some of the beautiful physics of quantum Ising model in magnetic field with a hidden E_8 symmetry may be observed even in a realistic quasi-one-dimensional model in its ordered phase far from the transition line (in the vicinity of point 0 on figure 5.3). At this point it may be possible to observe at least three coherent peaks in the dynamical magnetic susceptibility whose relative strength is approximately $1 : 0.28 : 0.09$ (see equations 5.36 and Table 5.1). At this point the spectrum is extremely one-dimensional in character. We expect that when one moves along the g-axis of the phase diagram in figure 5.3 towards the QCP, the excitation gaps will decrease and the transverse dispersion will grow. At the QCP the spectrum is three-dimensional gapless and the spin-spin correlation function is given by

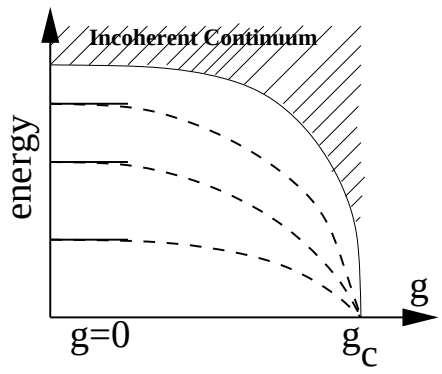

Figure 5.4: A schematic diagram showing what happens to the coherent modes as a function of g. To the left of the figure, we have three coherent modes with very one-dimensional dispersions. As we move to the right, the transverse dispersion grows and the overall mass scale decreases until all modes collapse at criticality.

equation 5.28 with logarithmic corrections. These corrections will convert the pole into a continuum; at criticality all excitation modes will collapse into it. This is illustrated schematically in figure 5.4.

5.3 Application to α' Sodium Vanadate

The layered oxide, α'-Sodium Vanadate (NaV_2O_5) was first studied back in the 1970's [95], but more recently there has been a lot of renewed interest in the material following the discovery of a phase transition at 34 Kelvin [96]. This phase transition shows a number of interesting properties:

- Below T_c, there is a simultaneous onset of charge ordering and opening of a spin gap [95].
- Below T_c, there is also a large increase in the unit cell, which doubles in two directions and increases by a factor of 4 in the direction perpendicular to the layers [97].
- This was initially thought to be a spin-Peierls transition, but the strong suppression of T_c with magnetic field characteristic of spin-Peierls materials was not seen in NaV_2O_5 [98].
- Also, the spin gap at low temperatures is of order $\delta = 100$K, [96, 99] which gives the value $2\Delta/T_c \approx 6$ which is very different from the canonical BCS-value of 3.5 typical of Spin-Peierls systems.
- X-ray studies [100, 101, 102] show that above T_c, all Vanadium sites are equivalent, $Va^{4.5+}$, whereas below T_c they are not, although the ordering is still controversial [103].

These all go to indicate that it is not the opening of the spin-gap that drives the transition. This is further corroborated by careful experiments [104, 105] which show there are actually two

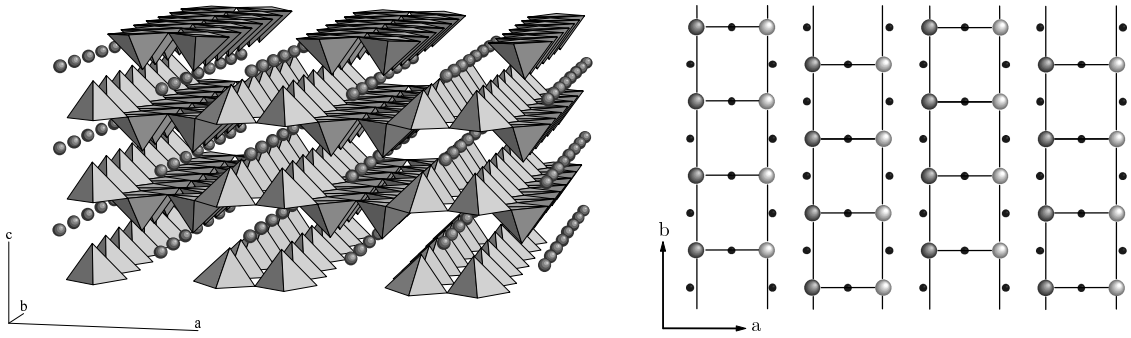

Figure 5.5: Structure of Sodium Vanadate (after [109]). The Vanadium ions for two-leg ladders in the ab plane, with lines of Sodium atoms between the layers.

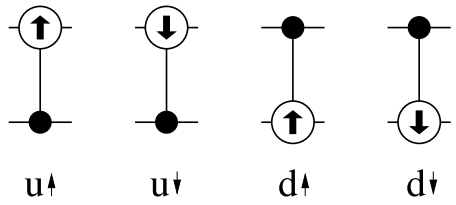

Figure 5.6: The pseudo-spin/charge ordering mapping (after [108]). The spin refers to the spin of the electrons, the pseudo-spin as to whether it sits on the upper or lower leg of the ladder.

second-order transitions, the first one at $T_{c1} \approx 34$K leads to charge ordering and the second about 0.3K lower opens the spin gap. Thus one wants a model in which charge ordering is the driving force and the opening of the spin gap a secondary effect.

Sodium Vanadate is made up of quarter filled ladders, see figure 5.5, with the coulomb repulsion between the legs of the ladders such that the low energy states all have one electron per rung. A number of authors [106, 107] proposed a spin-pseudospin model, where the spin refers to the real spin of the electrons, and the two eigenstates of the pseudospin refer to whether a particular electron is on the upper or lower leg of the ladder - see figure 5.6. The operator σ^x is then a hopping term between the legs, and $\sigma^z\sigma^z$ is the interaction between neighbouring electrons, which depends on whether they are both on the same leg or not. Once we have mapped the ladders to spins, the lattice becomes a quasi-one dimensional frustrated lattice - figure 5.7. The pseudo-spin Hamiltonian then simply becomes our Hamiltonian 5.20.

To try and quantitatively calculate anything of physical interest for this system, we would have to take into account not only the spin fluctuations, but also the change in lattice parameters accompanying the transitions. This is beyond the scope of the present work as there are many competing effects in this material. However, we can suggest that the low energy isospin excitations which should be experimentally observable with optical absorption [108] will be very one dimensional in character, and may show a number of distinct modes as given in section 5.2.2.

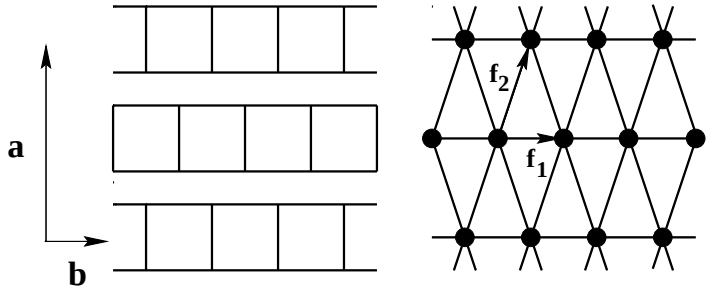

Figure 5.7: Showing the pseudo-spin lattice after the mapping (after [108]). When each rung of the ladders becomes a single site in our effective model, the underlying lattice is triangular.

5.4 Link to the 3D Ising Model

The one-dimensional quantum Ising model is equivalent (in the scaling limit) to the two dimensional classical Ising model [110] with the relation $g = (T - T_{c0})/T_{c0}$. Hence coupled chains in the quantum case corresponds to coupled planes in the classical case. Within RPA, the scaling exponents can be obtained easily from equation 5.28. They are $\gamma = 1$, $\nu = 1/2$ which are the mean-field values as expected in this approximation. In this approximation, we see that the critical temperature for the isotropic 3D Ising model (which is outside the range of applicability of RPA) can be read off equation 5.27

$$\frac{T_c - T_{c0}}{T_{c0}} = 1.42 z_\perp^{4/7} \tag{5.47}$$

where T_{c0} is the transition temperature for the 2D Ising model given by $\sinh(2J_{\text{inplane}}/T_c) = 1$, and $z_\perp = 2$ because we are coupling planes together. This gives $J/T_c = 0.228$ which is not far from the true numerical result $J/T_c = 0.222$. So as in previous work, we see that RPA actually gives a pretty good estimate of the transition temperature.

Another interesting thing is to look at the crossover from the 2D to the 3D Ising model, to which end we consider a 3D Ising model with interaction strength J in the xy plane and aJ in the z direction. The RPA then gives

$$\frac{T_c - T_{c0}}{T_{c0}} = 1.42 (2a)^{4/7}, \tag{5.48}$$

where all temperatures are measured in units of J. For small a, this should be fairly accurate although there is currently a complete lack of Monte Carlo data for the anisotropic Ising model to compare it to.

Chapter 6

Final remarks

Like Olympic medals and trophies, all it signifies is that the receiver has done something of no use to anybody a little better than everybody else.

–Joseph Heller (Catch 22)

In this thesis we were looking at selected models of strongly correlated electrons. The models were all quasi-one-dimensional so we could use a particular recipe to solve them; namely solving the one dimensional subsystem exactly by means of powerful non-perturbative techniques and then adding in some higher-dimensional coupling perturbatively.

- We first considered a model of unconventional superconductivity, introduced as a possible model for High-Tc materials in a stripe phase, but more easily applied to structurally one-dimensional compounds. Within the RPA approximation we calculated the transition temperature for general K_c. We calculated the ratio T_c/Δ_c where Δ_c is the zero temperature gap in the charge sector. We saw that this decreases below the BCS value as the coupling strength is increased. We also looked at the properties of our model in a magnetic field, noting in particular the extreme anisotropy of the phase diagram, and the possibility of SC-CDW transitions as you vary strength or even angle of magnetic field. We then went on to calculate the first corrections to T_c in the vicinity of the critical point which is decreased because of the interplay between the two interactions. We finally showed that in two dimensions where RPA breaks down completely, we get a transition of the Kosterlitz-Thouless type which has the same energy scales as the ordering transition in higher dimensions.

- We then went on to consider unusual magneto-resistance properties measured in Bechgaard salts, namely large dips in the magneto-resistance at 'magic angles', with a corresponding insulator-metal transition in the temperature dependence at these points. Our model consisted of one-dimensional Mott insulating chains with enough interchain hopping to drive the system to a metallic state. We concentrated on calculating the density of states as a function of the strength and angle of the magnetic field. We showed that although our model had some of the properties needed to explain the measured results, it was oversimplified and although promising in some respects, did not reproduce the

magic angle effects seen in experiments. We suggested several extensions to the model which may be necessary to explain this phenomena.

- We finished by considered a model of coupled quantum Ising chains. We saw that within the RPA approximation, we could calculate the phase diagram of the model and the dispersion in the ordered phase. The most interesting thing is how one dimensional the excitations are in the three dimensional ordered phase.

Throughout this work, we have tried to motivate much of our theory from real materials. As real materials are always far more complicated than our simplified models, the application of the models to the materials has been mostly only at the qualitative level. However we see the solution of these models as a starting point to make more detailed calculations on individual materials. Executing these more specific calculations, as well as attempting to refine our general solutions by going beyond RPA are obvious future directions for research. The overall message from this thesis is that the world of many electrons still has many unexplored possibilities. And starting from somewhere different than simply turning the e-e interactions off can give a lot of insight into the strange and wonderful world of strongly correlated systems.

Bibliography

[1] S.T.Carr and A.M.Tsvelik, Phys. Rev. B **65**, 195121 (2002).

[2] S.T.Carr and A.M.Tsvelik, Phys. Rev. Lett. **90**, 177206 (2003).

[3] L.D.Landau, Soviet Physics JETP **3**, 920 (1957).

[4] A.A.Abrikosov, L.P.Gorkov, and I.E.Dzyaloshinski, *Methods of Quantum Field Theory in Statistical Physics* (Dover, New York, 1963).

[5] D.Senechal, cond-mat/9908262 (1999).

[6] S.Tomonaga, Prog. Theor. Phys. (Kyoto) **5**, 544 (1950).

[7] J.M.Luttinger, J.Math. Phys. **4**, 1154 (1963).

[8] D.C.Mattis and E.H.Lieb, J. Math. Phys. **6**, 304 (1965).

[9] R.Heidenreich, B.Schroer, R.Seiler, and D.Uhlenbrock, Phys. Lett. **54**, 119 (1975).

[10] A.Luther and I.Peschel, Phys. Rev. B **9**, 2911 (1974).

[11] S.Coleman, Phys. Rev. D **11**, 2088 (1975).

[12] S.Mandelstam, Phys. Rev. D **11**, 3026 (1975).

[13] A.O.Gogolin, A.A.Nersesyan, and A.M.Tsvelik, *Bosonization and Strongly Correlated Systems* (Cambridge University Press, Cambridge, UK, 1998).

[14] V.J.Emery, in *Highly Conducting One-Dimensional Solids*, edited by R. J.T.Devreese and V. Doren (Plenum, New York, 1979), p. 327.

[15] J. Delft and H.Schoeller, Annalen der Physik **4**, 225 (1998).

[16] K.Huang, *Quantum Field Theory* (John Wiley and Sons, New York, New York, 1998).

[17] F.D.M.Haldane, J. Phys. C **12**, 4791 (1979).

[18] F.D.M.Haldane, J. Phys. C **14**, 2585 (1981).

[19] A.Luther and V.Emery, Phys. Rev. Lett. **33**, 589 (1974).

[20] F.A.Smirnov, *Form Factors in Completely Integrable Models of Quantum Field Theories* (World Scientific, New York, 1992).

[21] M.Jimbo, *Yang Baxter equation in Integrable Systems* (World Scientific, Singapore, 1990).

[22] A.B.Zamolodchikov and Al.B.Zamolodchikov, Annals of Phys. (NY) **120**, 253 (1979).

[23] D.Iagolnitzer, Saclay, preprint DPh-T/77-130 (1977).

[24] H.Bethe, ZPhys **71**, (1931).

[25] V.E.Korepin, N.M.Bogoliubov, and A.G.Izergin, *Quantum Inverse Scattering Method and Correlation Functions* (Cambridge University Press, Cambridge, UK, 1993).

[26] H. Babujian and M. Karowski, in *From Integrable Models to Gauge Theories,* edited by V.G.Gurzadyan and A.G.Sedrakian (World Scientific, New York, 2001).

[27] H. Babujian, A. Fring, M. Karowski, and A. Zapletal, Nucl. Phys. B **538**, 535 (1999).

[28] H. Babujian and M. Karowski, Nucl. Phys. B **620**, 407 (2001).

[29] M.Karowski and P.Weisz, Nucl. Phys. B **139**, 455 (1978).

[30] B.Berg, M.Karowski, and P.Weisz, Phys. Rev. D **19**, 2477 (1979).

[31] A.Leclair, F.Lesage, S.Sachdev, and H.Saleur, Nucl. Phys. B **482**, 579 (1996).

[32] A.M.Polyakov, JETP Lett **12**, 381 (1970).

[33] A.A.Belavin, A.M.Polyakov, and A.B.Zamolodchikov, Nucl. Phys. B **241**, 333 (1984).

[34] P. Francesco, P.Mathieu, and D.Senechal, *Conformal Field Theory* (Springer, New York, 1997).

[35] C.Itzykson and J-M.Drouffe, *Statistical Field Theory* (Cambridge University Press, Cambridge, UK, 1989), Vol. 2.

[36] D.J.Scalapino, Y.Imry, and P.Pincus, Phys. Rev. B **11**, 2042 (1975).

[37] E.Arrigoni, Phys. Rev. Lett. **83**, 128 (1999).

[38] V. Irkhin and A. Katanin, Phys. Rev. B **61**, 6757 (2000).

[39] M. Bocquet, cond-mat/0110429 (2001).

[40] P.W.Anderson, Phys. Rev. Lett. **67**, 3844 (1991).

[41] J.G.Bednorz and K.A.Muller, Z. Phys. B **64**, 189 (1986).

[42] V. Emery, S. Kivelson, and J. Tranquada, Proc. Natl. Acad. Sci. **96**, 8814 (1999).

[43] E. Carlson, D. Orgad, S. Kivelson, and V. Emery, Phys. Rev. B **62**, 3422 (2000).

[44] V. Emery, S. Kivelson, and O. Zachar, Phys. Rev. B **59**, 15641 (1999).

[45] E.Arrigoni, E.Fradkin, and S.A.Kivelson, cond-mat/0309572 (2003).

[46] K. Efetov and A. Larkin, Soviet Physics JETP **42**, 390 (1975).

[47] A.V.Rozhkov and A.J.Millis, Phys. Rev. B **66**, 134509 (2002).

[48] V. Emery and S. Kivelson, Nature **397**, 410 (1995).

[49] F.D.M.Haldane, Phys. Lett. A **93**, 464 (1983).

[50] I.Affleck, J. Phys.: Condens. Matter **1**, 3047 (1989).

[51] D.G.Shelton, A.A.Nersesyan, and A.M.Tsvelik, Phys. Rev. B **53**, 8521 (1996).

[52] E.Witten, Commun. Math. Phys. **92**, 455 (1984).

[53] S.Lukyanov and A.B.Zamolodchikov, Nucl. Phys. B **493**, 571 (1996).

[54] W.H.Press, S.A.Teukolsky, W.T.Vetterling, and B.P.Flannery, *Numerical Recipes in C* (Cambridge University Press, Cambridge, UK, 1992).

[55] F. Essler and A. Tsvelik, cond-mat/0205294 (2002).

[56] D. Orgad, Philos Mag B **81**, 375 (2001).

[57] H.Takayama, Y.Lin-Lui, and K.Maki, Phys. Rev. B **21**, 2388 (1980).

[58] V. Berezinskii, Soviet Physics JETP **32**, 493 (1970).

[59] J.M.Kosterlitz and D.J.Thouless, J. Phys. C **6**, 1181 (1973).

[60] Y.Piskunov, D.Jerome, P.Auban-Senzier, P.Wzietek, C.Bourbonnais, U.Ammerhal, G.Dhalenne, and A.Revcolevschi, cond-mat/0110559 (2001).

[61] M.Takigawa, N.Motoyama, H.Eisaki, and S.Uchida, Phys. Rev. B **57**, 1124 (1998).

[62] M. Uehara, T. Nagata, J. Akimitsu, H. Takahashi, N. Mori, and K. Kinoshita, Phys. Soc. Jpn. **65**, 2764 (1996).

[63] T.Nagata, M.Uehara, J.Goto, J.Akimitsu, N.Motoyama, H.Eisaki, S.Uchida, H.Takahashi, T.Nakanishi, and N.Mori, Phys. Rev. Lett. **81**, 1090 (1998).

[64] B. Gorshunov, P. Haas, M. Dressel, T. Vuletic, B. Hamzic, S. Tomic, J. Akimitsu, and T. Nagata, cond-mat/0201413 (2002).

[65] T.Vuletic, B.Korin-Hamzic, S.Tomic, B.Gorshunov, P.Haas, T.Room, M.Dressel, J.Akimitsu, T.Sasaki, and T.Nagata, cond-mat/0305159 (2003).

[66] C.Presura, M.Popinciuc, P. Loosdrecht, D. der Marcel, M.Mostovoy, T.Yamauchi, and Y.Ueda, Phys. Rev. Lett. (2002).

[67] T.Yamauchi, Y.Ueda, and N.Mori, Phys. Rev. B **89**, 57002 (2002).

[68] K.Okazaki, A.Fujimori, T.Yamauchi, and Y.Ueda, cond-mat/0308368 (2003).

[69] C.Bourbonnais and D.Jerome, in *Advances in Synthetic Metals, Twent years of Progress in Science and Technology*, edited by P. amd S.Lefrant and G.Bidan (New York, ADDRESS, 1999), p. 206.

[70] D.Jerome, in *Organic Superconductors: From (TMTSF)$_2PF_6$ to Fullerenes* (Marcel Dekker, Inc, New York, 1994), p. 405.

[71] E. Chashechkina and P. Chaikin, Phys. Rev. Lett. **80**, 2181 (1998).

[72] A.G.Lebed, Pis'ma Zh. Eksp. Teor. Fiz. **43**, 137 (1986).

[73] A.G.Lebed and P.Bak, Phys. Rev. Lett. **63**, 1315 (1989).

[74] E. Chashechkina and P. Chaikin, Phys. Rev. B **65**, 12405 (2001).

[75] F. Essler and A. Tsvelik, Phys. Rev. B **65**, 115117 (2002).

[76] S.Biermann, A.Georges, T.Giamarchi, and A.Lichtenstein, in *Proceedings of NATO ASI "Field Theory of Strongly Correlated Fermions and Bosons in Low-Dimensional Systems"* (Windsor, England, 2001).

[77] R.E.Peierls, Z. Phys. B **80**, 763 (1933).

[78] D. Hofstadter, Phys. Rev. B **14**, 2239 (1976).

[79] S.Sachdev, *Quantum phase transitions* (Cambridge University Press, Cambridge, UK, 1999).

[80] B.K.Chakrabarti, A.Dutta, and P.Sen, *Quantum Ising Phases and Transitions in Transverse Ising Models*, Vol. m 41 of *Lecture Notes in Physics* (Springer-Verlag, Berlin, 1996).

[81] D.C.Mattis, *The Theory of Magnetism II: Thermodynamics and Statistical Mechanics*, Vol. 55 of *Springer Series in Solid-State Sciences* (Springer-Verlag, Berlin, Heidelberg, New York, Tokyo, 1985), p. 109.

[82] K.I.Kugel and D.I.Khomskii, Sov. Phys. Usp. **25**, 231 (1982).

[83] B.Doucot, M.V.Feigelman, and L.B.Ioffe, cond-mat/0211146 (2002).

[84] A.B.Zamolodchikov, Int. J. Mod. Phys. A **3**, 743 (1988).

[85] P. G. de Gennes, Solid State Commun. **1**, 132 (1963).

[86] O.Babelon and D.Bernard, Phys. Lett. B **288**, 113 (1992).

[87] T.T.Wu, B.M.McCoy, C.A.Tracy, and E.Barouch, Phys. Rev. B **13**, 316 (1976).

[88] J.Balog and M.Niedermaier, Nucl. Phys. B **500**, 421 (1997).

[89] G.Delfino and G.Mussardo, Nucl. Phys. B **455**, 724 (1995).

[90] C.Itzykson and J-M.Drouffe, *Statistical Field Theory* (Cambridge University Press, Cambridge, UK, 1989), Vol. 1.

[91] H.J.Schulz and C.Bourbonnais, Phys. Rev. B **27**, 5856 (1983).

[92] H.J.Schulz, Phys. Rev. Lett. **77**, 2790 (1996).

[93] V. Fateev, Phys. Lett. B **324**, 45 (1994).

[94] G. Delfino, G. Mussardo, and P. Simonetti, Nucl. Phys. B **473**, 469 (1996).

[95] A.Carpy and J.Galy, Acta Crystallogr. Sect B: Struct. Crystallogr. Cryst. Chem. **31**, 1481 (1975).

[96] M.Isobe and Y.Ueda, J. Phys. Soc. Jpn. **65**, 1178 (1996).

[97] Y.Fujii, H.Nakao, T.Yoshihama, M.Nishi, K.Nakajima, K.Kakurai, M.Isobe, Y.Ueda, and H.Sawa, J. Phys. Soc. Jpn. **66**, 326 (1997).

[98] W.Schnelle, Y.Grin, and R.Kremer, Phys. Rev. B **59**, 73 (1999).

[99] T.Yosihama, M.Nishi, K.Nakajima, K.Kakurai, Y.Fujii, M.Isobe, C.Kagami, and Y.Ueda, J. Phys. Soc. Jpn. **67**, 744 (1998).

[100] A.Meetsma, J. Boer, A.Damascelli, T.T.M.Palstra, J.Jegoudes, and A.Revcolevschi, Acta. Crysallogr. Sect. C: Cryst. Struct. Commun **54**, 1558 (1998).

[101] H.Smolinski, C.Gros, W.Weber, U.Peuchert, G.Roth, M.Weiden, and C.Geibel, Phys. Rev. Lett. **80**, 5164 (1998).

[102] H.Schnering, Y.Grin, M.Kaupp, M.Somer, R.K.Kremer, O.Jepsen, T.Chatterji, and M.Weiden, Z.Kristallogr. **213**, 246 (1998).

[103] A.Bernert, T.Chatterji, P.Thalmeier, and P.Fulde, Euro. Phys. J. B **21**, 535 (2001).

[104] M.Koppen, D.Pankert, R.Hauptmann, M.Lang, M.weiden, C.Geibel, and F.Steglich, Phys. Rev. B **57**, 8466 (1998).

[105] Y.Fagot-Revurat, M.Mehring, and R.Kremer, Phys. Rev. Lett. **84**, 4176 (2000).

[106] M.V.Mostovoy and D.I.Khomskii, Solid State Commun. **113**, 159 (2000).

[107] A.Bernert, P.Thalmeier, and P.Fulde, cond-mat/0108008 (2001).

[108] M.V.Mostovoy, D.I.Khomskii, and J.Knoester, Phys. Rev. B **65**, 64412 (2002).

[109] A.Damascelli, C.Presura, D. der Marel, J.Jegoudez, and A.Revcolevschi, Phys. Rev. B **61**, 2535 (2000).

[110] T.D.Schultz, D.C.Mattis, and E.H.Lieb, Rev. Mod. Phys. **36**, 856 (1964).